PEROXISOMAL RETROGRADE SIGNALING IN *Caenorhabditis elegans*

Dissertation der Fakultät für Biologie

der Ludwig–Maximilians–Universität München

Elisabeth Rackles

München, 2021

Diese Dissertation wurde angefertigt
unter der Leitung von Dr. Stéphane Rolland
im Bereich der Zell- und Entwicklungsbiologie
an der Ludwig-Maximilans-Universität München

Erstgutachterin: Prof. Dr. Barbara Conradt

Zweitgutachter: Prof. Dr. Christof Osman

Tag der Abgabe: 27.08.2020

Tag der mündlichen Prüfung: 12.03.2021

Eidesstattliche Erklärung:

Ich versichere hiermit an Eides statt, dass die vorgelegte Dissertation von mir selbstständig und ohne unerlaubte Hilfe angefertigt wurde.

München, 26.08.2020

_____

Elisabeth Rackles

Erklärung:

Hiermit erkläre ich, dass die Dissertation weder ganz noch in wesentlichen Teilen einer anderen Prüfungskommission vorgelegt worden ist und dass ich mich nicht anderweitig einer Doktorprüfung ohne Erfolg unterzogen habe.

München, 26.08.2020

_____

Elisabeth Rackles

ACKNOWLEDGEMENTS

First, I would like to thank Dr. Stéphane Rolland for supervising this thesis and inspiring me with his dedication and enthusiasm for science. Many thanks, Stéphane, for the great working atmosphere and for your constant support during my PhD studies. Thank you for the time that you invested in my project, for the scientific discussions and for your patience in answering all my questions. Moreover, I greatly appreciate the scientific freedom you gave me during my PhD, which essentially contributed to my development as a scientist.

I would like to thank my principal supervisor, Prof. Dr. Barbara Conradt, for providing me with the opportunity to realize the PhD in her laboratory, for her helpful professional advice and useful comments on my project. Moreover, I would like to thank all the other members of my doctoral thesis committee, especially Prof. Christof Osman, who kindly agreed to co-referee this thesis. I am thankful for his valuable scientific and professional advice.

I am grateful for being part of the graduate school Life Science Munich and the kind support given by the coordinators Francisca Mende and Nadine Hamze. In this line, I would also like to thank my thesis advisory committee Prof. Dr. Dario Leister, Prof. Dr. Ida van der Klei and PD Dr. Eric Lambie for their guidance, constructive criticism and discussions.

To all my past and present colleagues: Thank you for your help and advice as well as the friendly working atmosphere in the laboratory. Special thanks to our coffee group for keeping me well caffeinated. Marion, Carina, Jenny, Anna, Laura, Lisa, Adi, Sandra and Fritzi: I really enjoyed our daily breaks! Thanks to Nikhil for his ”Guten Morgen, Frau Rackles” which made me smile every morning. To Jeffrey and Eric for introducing me to Eisbach surfing. Finally, many thanks to Laura, Adi, Fabi, Simon and the rest of the PPPP crew for all the unforgettable moments and the great time we had.

And to my friends and family: Thank you for your never-ending support and encouragement. I am beyond grateful.

ABSTRACT

Peroxisomes are essential metabolic organelles. One of their functions is the degradation of very long chain and long chain fatty acids by beta-oxidation. During this process, toxic hydrogen peroxide is produced, which is degraded by the peroxisomal catalase. Due to its ability to produce and degrade hydrogen peroxide, the organelle was named 'peroxisome'.

The importance of functional peroxisomes is highlighted by the existence of severe human diseases that are caused by mutated peroxisomal genes. Therefore, the maintenance of functional peroxisomes is essential for the cell. One important part of organellar quality control is the maintenance of protein homeostasis. In mammals and yeast, the peroxisomal Lon protease has protease and chaperone functions and plays a role in the quality control of peroxisomes. The *Caenorhabditis elegans* homolog of the peroxisomal Lon protease (LONP-2) has not been characterized so far. To study the function of LONP-2, I generated a reporter strain expressing an unfolded protein targeted to peroxisomes. The unfolded protein can be stabilized in a folded state by the addition of a small molecule ligand. Using this assay, I show that LONP-2 is like its homologs required to degrade unfolded proteins targeted to peroxisomes.

While this represents some evidence that LONP-2 participates in the quality control of peroxisomal matrix proteins, it remains elusive how peroxisomal quality control is regulated. Quality control of other organelles has been shown to involve a retrograde signaling from the organelle to the nucleus to activate the production of organelle-specific proteases and chaperones in response to organelle-specific stress. In my thesis, I present evidence of the existence of such a retrograde signaling for peroxisomes in *C. elegans*, which we define as peroxisomal retrograde signaling (PRS). Specifically, I show that perturbing peroxisomal biogenesis by inactivating genes encoding peroxisomal biogenesis factors leads to the transcriptional activation of the peroxisomal Lon protease *lonp-2*. Furthermore, the peroxisomal catalase (*ctl-2*) is also up-regulated upon peroxisomal biogenesis stress. The transcriptional activation of *lonp-2* and *ctl-2* is dependent on the nuclear hormone recep-

tor NHR-49, a functional homolog of the mammalian peroxisome proliferator-activated receptor alpha (PPARalpha), and its co-activator MDT-15. Perturbation of peroxisomal biogenesis might lead to impaired peroxisomal lipid metabolism. We hypothesized that the resulting change in lipid composition could act as a signal for the induction of the PRS. Consistent with our hypothesis, knock-down of peroxisomal beta-oxidation enzymes also induced the PRS. Proteomic analysis revealed that the activation of the PRS leads to the up-regulation of peroxisomal beta-oxidation enzymes and proteins involved in the innate immune response. This could represent a compensatory mechanism to maintain the peroxisomal function in response to peroxisomal biogenesis stress.

Peroxisomes and mitochondria are known to physically and functionally interact in the cell. For example, metabolic pathways are shared between the two organelles. It is conceivable that peroxisomal dysfunction also affects mitochondrial function and, hence, induces the mitochondrial unfolded protein response. The mitochondrial unfolded protein response is a quality control pathway that induces the up-regulation of mitochondria-specific proteases and chaperones in response to mitochondrial dysfunction. In support of this notion, I found that knock-down of specific peroxisome biogenesis factors induces the up-regulation of the mitochondrial chaperone *hsp-6*, which is a target gene of the mitochondrial unfolded protein response. This suggests the existence of a cross-talk between the peroxisomal and mitochondrial stress responses, which could play a role in the maintenance of the cellular function.

CONTENTS

1

INTRODUCTION

1.1 The model organism *Caenorhabditis elegans*

In 1974, the soil nematode *Caenorhabditis elegans* was introduced by Sydney Brenner as a model to study development and neurobiology [Brenner, 1974]. Since then, studying *C. elegans* has contributed to our knowledge about a large variety of biological processes. It has been shown that there is a strong conservation of cellular pathways between *C. elegans* and mammals. Moreover, about 38% of the predicted protein-coding genes are conserved between worms and humans [Shaye and Greenwald, 2011].

C. elegans has several advantages as a model organism. It is easy to maintain in the laboratory: it is small (about 1 mm in length) and grows on *Escherichia coli* as a food source. Moreover, *C. elegans* has a rapid life cycle of about three days and a short life span of about two weeks. The developmental rate of the animals can be controlled by growth at different temperatures (low temperatures lead to a slower development). *C. elegans* animals mainly exists as self-fertilizing hermaphrodites, which produce hundreds of offspring per animal. Inside the hermaphrodite, oocytes are fertilized by the sperm and the resulting zygote starts to develop. After egg laying, the embryo further develops outside the hermaphrodite (Figure 1.1). Then, the larva hatches and the animal develops through four larval stages (L1-L4) into an adult hermaphrodite. Under unfavorable conditions, L2 larvae can molt into an alternative L3 larval stage, called the ”dauer” larva. In this stage, the animals can survive several months without food. As soon as the conditions improve and food is available, they continue their development as L4 larvae. This feature of their life cycle is very advantageous to keep stocks of worm strains in the laboratory. Furthermore, for long-term storage, worm stocks can be frozen at -80°C [Corsi et al., 2015].

Apart from its easy maintenance in the laboratory, *C. elegans* has several advantages for experimental procedures. For example, the animals are transparent throughout their life, which makes them very suitable for fluorescent microscopy analysis [Corsi et al., 2015]. Another advantage is that they can be genetically modified very easily. Knockdown of genes by RNA interference (RNAi) can be done by feeding *E. coli* expressing the corresponding double-stranded RNA of a gene [Timmons and Fire, 1998]. RNAi

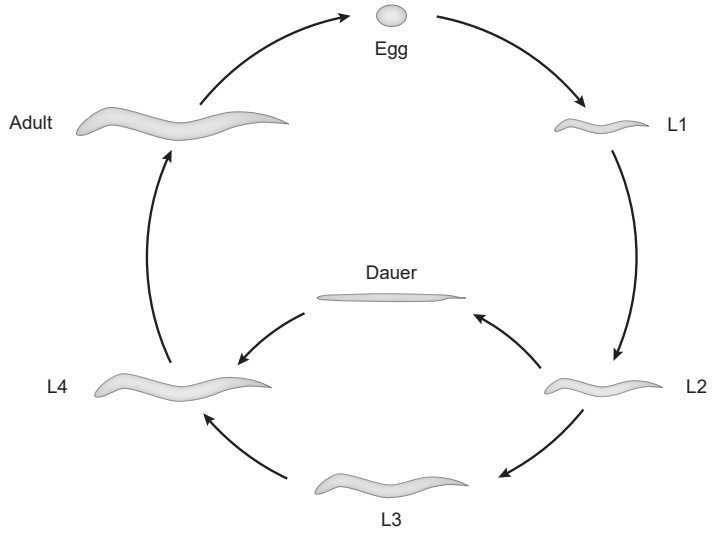

Figure 1.1: The *C. elegans* life cycle. The embryo develops first within and then outside the adult hermaphrodite. After hatching, the animals develop through four larval stages (L1-L4) into adult hermaphrodites. Under unfavorable conditions, L2 larvae can molt into a stress-resistant "dauer" larva. (Figure adapted from [Altun et al., 2020]).

libraries containing bacterial strains targeting almost all predicted genes in *C. elegans* enable genome-wide RNAi screens [Kamath and Ahringer, 2003, Rual et al., 2004]. Moreover, a large number of *C. elegans* strains containing mutations of specific genes are available. Male animals can be generated, which enables the generation of strains with new genotypes by crosses [Corsi et al., 2015]. Taken together, all the mentioned features (and many others) make *C. elegans* a powerfull model organism to study biological processes.

1.2 Peroxisomes

Peroxisomes were first discovered in mouse kidney cells in 1954. Due to their morphology as small cytoplasmic bodies surrounded by a single membrane, they were initially named 'microbodies' [Rhodin, 1954]. In the 1960's, it was demonstrated that microbodies contain enzymes required for the production and degradation of hydrogen peroxide and, therefore, the term 'peroxisome' was established [De Duve and Baudhuin, 1966]. Peroxisomes have tissue-specific sizes (0.1-1 μm in diameter) and enzyme compositions to adapt to the metabolic functions of each tissue [Novikoff and Novikoff, 1973].

Although *C. elegans* is a relatively simple organism, many of its genes have functional counterparts in humans. In particular, several *C. elegans* homologs of mammalian peroxisomal proteins have been identified, like for example proteins required for peroxisomal biogenesis (see chapter 1.3.3) or peroxisomal beta-oxidation (see chapter 1.4.2) [Petriv et al., 2002, Gurvitz et al., 2000]. In *C. elegans*, peroxisomes are mainly present in hypodermal cells, the intestine and in the pharyngeal gland [Yokota et al., 2002, Petriv et al., 2002]. Their size (0.1-0.3 μm in diameter) is similar to the size of the smaller type of mammalian peroxisomes, which are present in the mammalian epithelial cells of the digestive tract [Yokota et al., 2002, Novikoff and Novikoff, 1973]. All in all, the knowledge about peroxisomes in *C. elegans* is limited. Several peroxisomal proteins were identified in large scale RNAi screens. However, the phenotype caused by the knock-down of the peroxisomal gene was only minimally described and has mostly not been investigated further (reviewed in [Van Veldhoven and Baes, 2013]). Recently, *C. elegans* peroxisomes have mainly been studied in the context of their function in the biogenesis of nematode-specific pheromones (see chapter 1.4.2).

1.3 Peroxisome biogenesis

1.3.1 *De novo* peroxisome biogenesis

Peroxisomes can be formed *de novo* or they arise from pre-existing peroxisomes by fission (see chapter 1.3.4). The proteins involved in peroxisomal biogenesis are called peroxins and are encoded by the *PEX* genes [Distel et al., 1996]. During *de novo* peroxisomal biogenesis in mammals, pre-peroxisomal vesicles containing distinct peroxins are formed (Figure 1.2). Recently, it has been shown that vesicles budding from the outer mitochondrial membrane contain the membrane proteins PEX3 and PEX14. Additionally, pre-peroxisomal vesicles containing PEX16 bud from the endoplasmic reticulum. The two populations of vesicles fuse to form peroxisomes that can import other peroxisomal membrane proteins (PMPs) (see chapter 1.3.2). Finally, they become import-competent for peroxisomal matrix proteins (see chapter 1.3.3) and mature peroxisomes are formed [Sugiura et al., 2017].

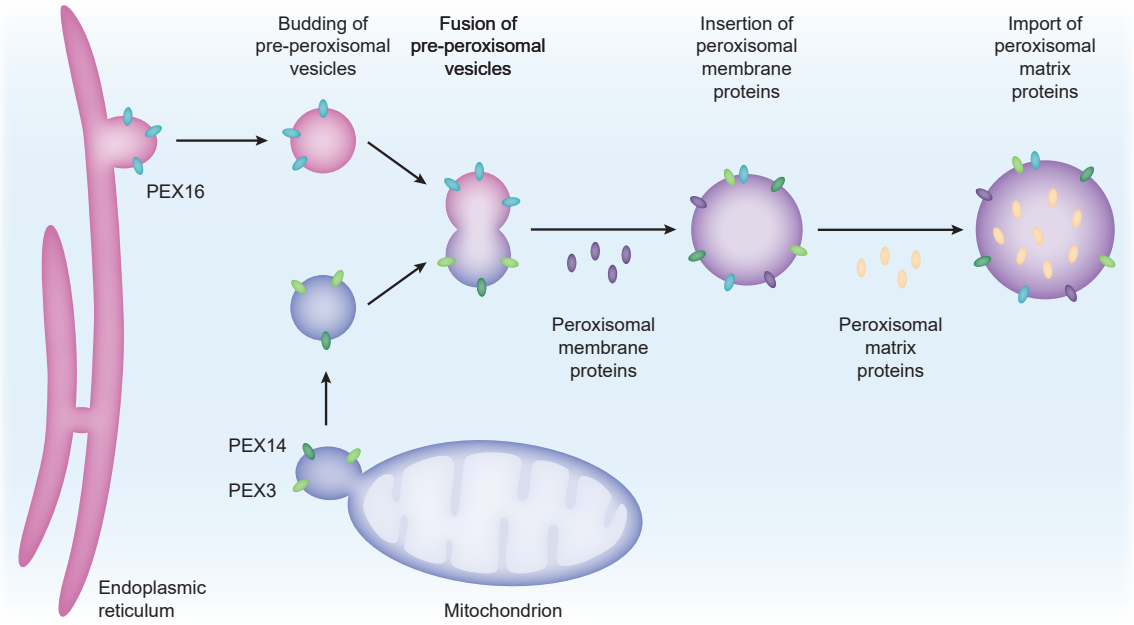

Figure 1.2: *De novo* peroxisome biogenesis in mammals. Pre-peroxisomal vesicles containing specific peroxisomal proteins bud from the endoplasmic reticulum and mitochondria. The vesicles fuse to form pre-peroxisomes. Next, further peroxisomal membrane proteins are inserted. Finally, peroxisomal matrix proteins are imported leading to the formation of mature peroxisomes. (Figure adapted from [Kim, 2017]).

1.3.2 Insertion of peroxisomal membrane proteins

While the pre-peroxisomal vesicle contains certain PMPs, other PMPs are subsequently inserted in the peroxisomal membrane. These PMPs contain multiple membrane peroxisomal targeting sequences [Jones et al., 2004]. To sort PMPs to peroxisomes, they are bound by the cytosolic chaperone and import receptor PEX19 (Figure 1.3A) [Jones et al., 2004]. The receptor-cargo complex docks to PEX3 at the peroxisomal membrane [Fang et al., 2004]. The mechanism of how the PMPs are inserted into the peroxisomal membrane is still unknown (reviewed in [Jansen and van der Klei, 2019]). PEX3 can be targeted to peroxisomes indirectly via mitochondria (see chapter 1.3.1) [Sugiura et al., 2017] or directly in an PEX19-dependent manner [Matsuzaki and Fujiki, 2008]. In this case, PEX19 docks to PEX16 at the peroxisomal membrane [Matsuzaki and Fujiki, 2008].

The *C. elegans* genome encodes 11 homologs of the 16 human peroxins (Table 1.1) [Thieringer et al., 2003, Petriv et al., 2002]. Since the gene class PEX was already used

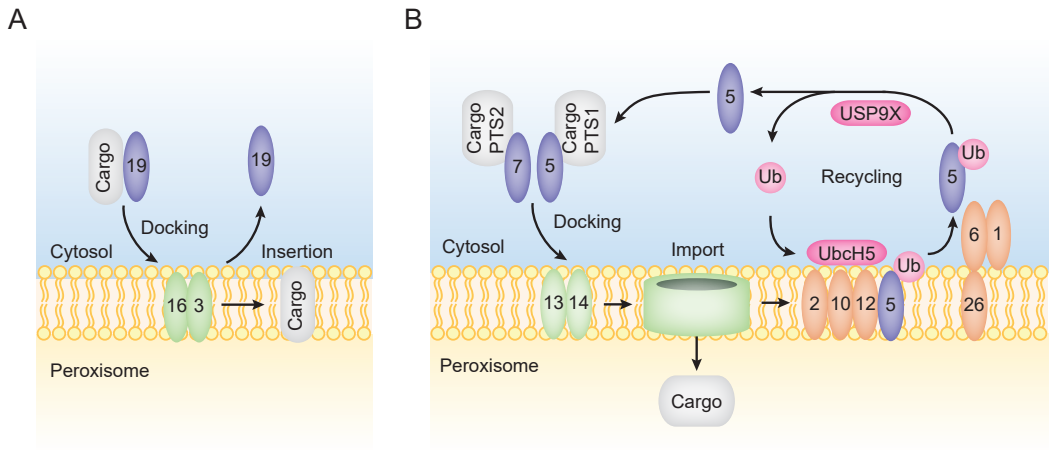

Figure 1.3: Import of peroxisomal proteins in mammals. (A) Insertion of peroxisomal membrane proteins. PEX19 binds peroxisomal membrane proteins and brings them to the membrane. PEX19 binds PEX3/PEX16 and the cargo is inserted in the peroxisomal membrane by an unknown mechanism. The numbers represent the PEX proteins. (B) Peroxisomal matrix protein import. The import receptors PEX5 or PEX7 bind peroxisomal matrix proteins containing a peroxisomal targeting sequence. The complex docks to the peroxisomal membrane via PEX13/14. The cargo is translocated to the peroxisomal matrix. Finally, the receptor gets monoubiquitinated (Ub=ubiquitin) and recycled. (Figure adapted from [Kim and Hettema, 2015]).

for other genes (pachytene exit defect), the gene class for peroxins in *C. elegans* is PRX. Homologs of PEX3 and PEX19, but not of PEX16 have been identified [Thieringer et al., 2003]. The insertion of membrane proteins has not been studied in *C. elegans*. However, it has been shown that the knock-down of *prx-19* leads to the block of the import of peroxisomal matrix proteins presumably indirectly by preventing the insertion of PMPs required for peroxisomal matrix protein import [Petriv et al., 2002].

1.3.3 Peroxisomal matrix protein import

In mammals, peroxisomal matrix proteins can be imported as monomers but also as oligomers [Freitas et al., 2011, Otera and Fujiki, 2012]. Peroxisomal matrix proteins are synthesized in the cytosol and recognized by the receptor PEX5, which interacts with the C-terminal peroxisomal targeting signal 1 (PTS1) [Fransen et al., 1995] (Figure 1.3B). The PTS1 is a tripeptide with the sequence SKL or conservative variants [Gould et al., 1989]. Additionally, the residues upstream of the tripeptide influence the binding of PEX5 [Lametschwandtner et al., 1998]. Some peroxisomal matrix proteins contain an N-terminal PTS2 signal, which is recognized by the receptor PEX7 [Braverman et al.,

Table 1.1: Effect of knock-down of peroxins in *C. elegans*.

Human peroxin	*C. elegans* homolog	Effect of knock-down in *C. elegans*	Reference
PEX1	*prx-1*	No import defect	[Petriv et al., 2002]
		Slow growth	[Simmer et al., 2003]
PEX2	*prx-2*	No import defect	[Petriv et al., 2002]
		Slow growth	[Simmer et al., 2003]
PEX3	*prx-3*	Slow growth	[Simmer et al., 2003]
PEX5	*prx-5*	Import defect	[Petriv et al., 2002]
		Larval arrest	[Thieringer et al., 2003]
PEX6	*prx-6*	Larval arrest	[Thieringer et al., 2003]
PEX7	Absent		[Motley et al., 2000] [Thieringer et al., 2003]
PEX10	*prx-10*	Slow growth	[Simmer et al., 2003]
PEX11α	?		No reference found
PEX11β	?		No reference found
PEX11γ	*prx-11*		[Thieringer et al., 2003]
PEX12	*prx-12*	Fewer and larger peroxisomes	[Petriv et al., 2002]
		Slow growth	[Simmer et al., 2003]
PEX13	*prx-13*	Import defect	[Petriv et al., 2002]
		Larval arrest	[Simmer et al., 2003]
PEX14	*prx-14*	Larval arrest	[Simmer et al., 2003]
PEX16	Absent		[Thieringer et al., 2003]
PEX19	*prx-19*	Import defect	[Petriv et al., 2002]
		Larval arrest	[Simmer et al., 2003]
PEX26	?		No reference found

1997]. The PTS2 consists of nine amino acids and is cleaved after the import of the protein [Swinkels et al., 1991]. PEX7 interacts with a long isoform of PEX5 (PEX5L), which acts as a co-receptor to form the receptor-cargo complex [Braverman et al., 1998]. The complex of PEX5 with a PTS1 protein or of PEX5L-PEX7 with a PTS2 protein docks at the peroxisomal membrane via PEX13 and PEX14 [Gouveia et al., 2000, Fransen et al., 1998, Mukai and Fujiki, 2006]. Next, the cargo is released to the peroxisomal matrix and the receptor is recycled for another round of import [Francisco et al., 2013]. For recycling, PEX5 is monoubiquitinated at a conserved cysteine residue [Okumoto et al., 2011]. This step requires the E2 ubiquitin-conjugating enzymes UbcH5a/b/c [Grou et al., 2008] and the RING domain proteins PEX2, PEX10 and PEX12, which have E3 ligase activities [Okumoto et al., 2014]. The ubiquitinated receptor is exported via PEX1 and PEX6 in an ATP-dependent manner [Miyata and Fujiki, 2005]. Finally, the receptor is deubiquitinated by USP9X and can be used for another round of import [Grou et al., 2012].

The *C. elegans* genome encodes homologs for all except one peroxin required for peroxisomal matrix protein import (Table 1.1) [Thieringer et al., 2003]. No homolog of the receptor PEX7 has been identified and peroxisomal matrix proteins in *C. elegans* only contain a PTS1 and no PTS2 is present [Motley et al., 2000]. To study if some of the identified peroxins also represent functional homologs, the localization of CFP tagged at its C-terminus with a PTS1 was analyzed. The knock-down of *prx-5* and *prx-13* led to a redistribution of the CFP signal to the cytosol [Petriv et al., 2002, Thieringer et al., 2003]. Additionally, the interaction of PRX-5 with the peroxisomal targeting sequence SKL has been shown by a two-hybrid assay [Gurvitz et al., 2000]. Taken together, PRX-5 likely represents a functional homolog of the mammalian import receptor PEX5 and is required for the import of peroxisomal matrix proteins in *C. elegans*.

1.3.4 Peroxisome biogenesis by growth and division

Peroxisome are not only formed *de novo* (see chapter 1.3.1), but peroxisomal biogenesis can also occur by growth and division. In mammals, this pathway requires peroxins of the PEX11 family. First, peroxisomes are elongated in a PEX11β-dependent manner [Delille et al., 2010]. Next, PEX11β and PEX11γ recruit the dynamin-related protein

DRP1, MFF1 and FIS1, which are required for both mitochondrial and peroxisomal fission [Kobayashi et al., 2007, Koch and Brocard, 2012]. Finally, the newly formed peroxisomes import peroxisomal membrane and matrix proteins [Kobayashi et al., 2007].

The two mechanisms of peroxisome biogenesis have not been studied in *C. elegans*. However, the genome encodes a homolog of the mammalian PEX11γ [Li et al., 2002]. Moreover, it has been shown that peroxisomes are more fused in *C. elegans* carrying a double mutation in the genes coding for the DRP1 and MFN1/2 homologs [Weir et al., 2017a].

1.4 Functions of peroxisomes

1.4.1 Overview of metabolic pathways in peroxisomes

Peroxisomes are sites for various metabolic pathways (Figure 1.4). For example, fatty acids are degraded by peroxisomal alpha- and beta-oxidation (see chapter 1.4.2). The products of the beta-oxidation pathway either exit the peroxisome for final degradation in mitochondria or they serve as substrates for various biosynthesis pathways (reviewed in [Wanders et al., 2016]). These pathways include the synthesis of bile acids from cholesterol. Bile acids participate in the digestion and adsorption of fat [Pedersen and Gustafsson, 1980]. Another anabolic pathway taking place in peroxisomes is the synthesis of etherphospholipids, which are found in most mammalian cellular membranes [Heymans et al., 1983]. The major class of etherphospholipids in mammals are plasmalogens, which are especially enriched in the myelin sheath in the nervous tissue and are required for normal nervous system function [Macala et al., 1983, Brites et al., 2009]. Furthermore, plasmalogens are required for the storage of polyunsaturated fatty acids, which are also synthesized in peroxisomes [Ferdinandusse et al., 2003]. Additionally, peroxisomes are required for the metabolism of some amino acids [Van Veldhoven et al., 1991, De Duve and Baudhuin, 1966, Wanders et al., 1989] and the detoxification of glyoxylate, which is formed in the intermediary metabolism of glycine [Danpure and Jennings, 1986]. Furthermore, purines are degraded in peroxisomes [Angermüller et al., 1987].

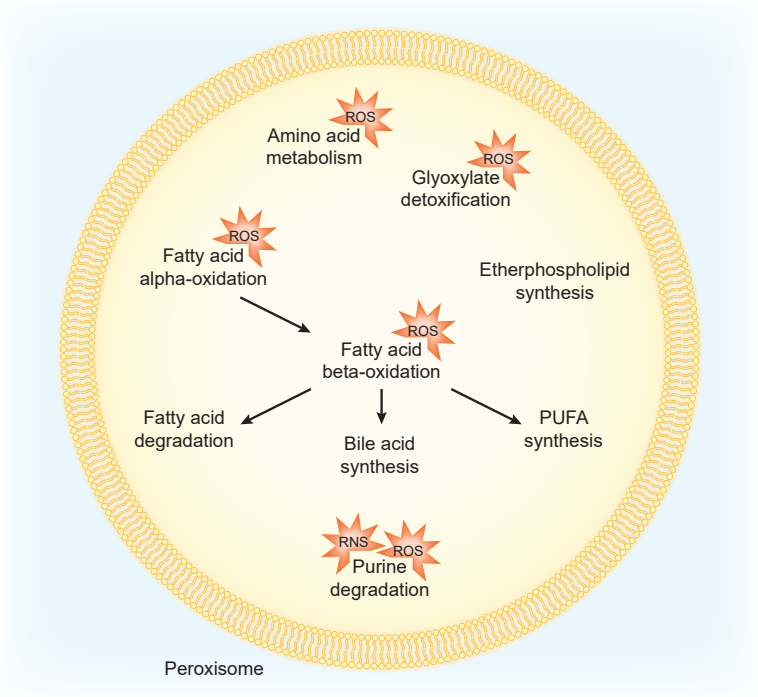

Figure 1.4: Selected metabolic pathways in peroxisomes. Peroxisomal beta-oxidation is required for the degradation of fatty acids or to generate substrates for other metabolic pathways. Reactive oxygen species (ROS) or reactive nitrogen species (RNS) are produced as byproducts of the metabolic pathways. Therefore, peroxisomes contain several antioxidant systems. (PUFA=Polyunsaturated fatty acid).

Many metabolic pathways in peroxisomes produce hydrogen peroxide, superoxide or nitric oxide as byproducts (Figure 1.4). Therefore, peroxisomes contain several antioxidant enzymes. One example is the peroxisomal catalase, which catalyzes the reaction of hydrogen peroxide to water and oxygen. It protects the cell from toxic peroxides generated in peroxisomes [Siraki et al., 2002]. The inhibition of catalase in rats leads to an accumulation of hydrogen peroxide in peroxisomes and thus to a reduction of the activity of thiolase, which is an peroxisomal beta-oxidation enzyme [Hashimoto and Hayashi, 1987]. In contrast, analysis of a *C. elegans* strain harboring a deletion of the peroxisomal catalase gene *ctl-2* showed that the size of lipid droplets accumulated in the cells is not changed compared to wild-type cells. From these observations, the authors conclude that fat metabolism is not changed in the *ctl-2* mutants. However, the mutation leads to a change in peroxisomal morphology and a decreased life span of the animals [Petriv and Rachubinski, 2004]. Another enzyme that degrades hydrogen peroxide in mammalian peroxisomes is the peroxiredoxin 5 [Walbrecq et al., 2015]. To degrade superoxide, per-

oxisomes contain a Cu,Zn superoxide dismutase [Keller et al., 1991]. Furthermore, the glutathione S-transferase kappa 1 contributes to lipid peroxide detoxification in mammalian cells [Wang et al., 2013]. *C. elegans* expresses several ROS metabolizing enzymes and among them also homologs of superoxide dismutases and peroxiredoxins. However, the catalase CTL-2 is the only enzyme that has been shown to localize to peroxisomes (reviewed in [Miranda-Vizuete and Veal, 2017]).

1.4.2 The peroxisomal beta-oxidation pathway

Peroxisomal beta-oxidation in mammals

One important metabolic function of peroxisomes is the degradation of very long-chain and long-chain fatty acids by peroxisomal beta-oxidation. Prior to their degradation, the fatty acids are activated by the attachment of coenzyme A (CoA). The reaction is catalyzed by various acyl-CoA synthetases, which are localized outside and also inside peroxisomes [Steinberg et al., 1999, Watkins et al., 2007] (Figure 1.5). The fatty acids are transported into peroxisomes by ABC class D transporters. It is still under debate if free fatty acids or the activated CoA esters are transported [van Roermund et al., 2011, van Roermund et al., 2014]. 3-methyl-branched fatty acids first have to undergo one cycle of alpha-oxidation before they can enter the peroxisomal beta-oxidation pathway (reviewed in [Jansen and Wanders, 2006]). One cycle of peroxisomal beta-oxidation reduces the fatty acid chain by two (or three) carbon atoms and leads to the release of one acetyl-CoA (or propionyl-CoA) molecule in a four step enzymatic reaction. During the first, rate-limiting step acyl-CoA is dehydrogenated to 2-trans-enoyl-CoA thereby producing hydrogen peroxide, which is subsequently degraded by the peroxisomal catalase. This reaction is catalyzed by acyl-CoA oxidases (ACOX). In humans, ACOX1 is required for the oxidation of straight-chain fatty acids, whereas ACOX2 and ACOX3 are involved in the degradation of 2-methyl-branched-chain fatty acids [Vanhove et al., 1993, Ferdinandusse et al., 2018]. The next two steps of hydratation and dehydrogenation of the substrate are catalyzed by one of the two so-called bifunctional enzymes (MFP1 and MFP2). Both enzymes can act on straight-chain compounds but only MFP2 accepts substrates with a 2-methyl-branch. Moreover,

the two enzymes show different stereospecificity [Palosaari and Hiltunen, 1990, Jiang et al., 1997]. The final step of peroxisomal beta-oxidation involves a thiolytic cleavage of the substrate by either the straight-chain specific 3-oxo-acyl thiolase (ACAA1) [Bout et al., 1991] or the branched-chain specific sterol carrier protein X (SCPx) [Wanders et al., 1997].

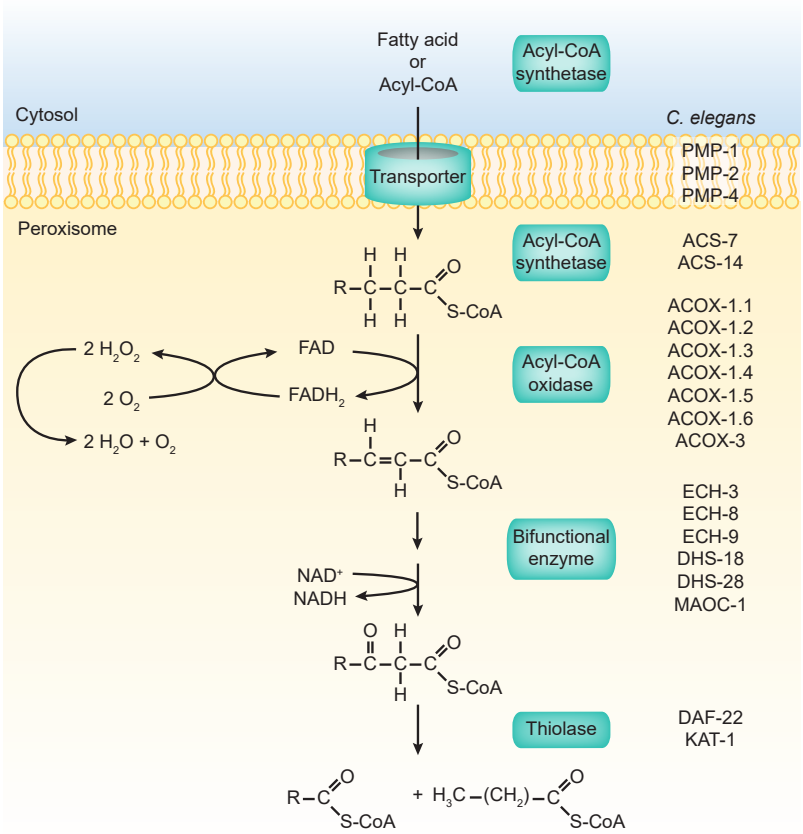

Figure 1.5: The peroxisomal beta-oxidation pathway. Very long chain fatty acids are imported into peroxisomes and degraded by a four step reaction. First, the activated fatty acids are oxidized by acyl-CoA oxidases. The next two steps are catalyzed by the bifunctional enzyme. Finally, the substrate is cleaved by a thiolase. Potential *C. elegans* homologs of the enzymes are shown. However, only for a subset of these homologs the function in peroxisomal beta-oxidation has been shown experimentally.

Peroxisomal beta-oxidation in *C. elegans*

Studies using computer-based and experimental approaches revealed that the peroxisomal beta-oxidation enzymes are conserved from yeast and human to *C. elegans* [Petriv et al., 2002, Gurvitz et al., 2000]. The function of the *C. elegans* beta-oxidation enzymes has mainly been studied in the context of the biosynthesis of a class of pheromones called

'ascarosides'. These pheromones regulate various behaviors such as the induction of the stress-resistant *dauer* larval stage, aggregation and mating behavior [Butcher et al., 2007, Golden and Riddle, 1982, Srinivasan et al., 2012, Srinivasan et al., 2008a]. The different biological activities of ascarosides are associated with various chemical modifications of the molecules. Ascarosides are derivatives of the 3,6-dideoxysugar-ascarylose attached to a fatty acid side chain at the (ω-1)- or ω-position. Moreover, additional modifications can occur at the sugar (head groups) or at the end of the side chain (terminal group) [Hollister et al., 2013]. A variety of ascarosides with different side-chain lengths can be produced by the shortening of long-chain precursors by peroxisomal beta-oxidation (Figure 1.5). Homologs of the human ABC class D transporters are encoded by five *pmp* genes. However, only PMP-1, PMP-2 and PMP-4 have been shown to localize to peroxisomes [Lee et al., 2014]. The first step of peroxisomal beta-oxidation is catalyzed by acyl-CoA oxidases (ACOX-1.1 to ACOX-1.6 and ACOX-3), which show preferences in the processing of different ascarosides [Joo et al., 2010, von Reuss et al., 2012, Zhang et al., 2016, Zhang et al., 2018]. MAOC-1 and DHS-28 are functional homologs of the mammalian bifunctional enzyme MFP2 and catalyze the next two steps of the beta-oxidation cycle [Zhang et al., 2010, von Reuss et al., 2012, Butcher et al., 2009]. Finally, the substrate is cleaved by DAF-22, which encodes a homolog of the thiolase domain of human SCPx [Butcher et al., 2009]. Three ORFs have been predicted to represent orthologs of the human peroxisomal thiolase ACAA1 [Petriv et al., 2002]. However, only KAT-1 has a functional peroxisomal targeting sequence and additionally a mitochondrial targeting sequence [Mak et al., 2006]. The described DHS-28/MAOC-1/DAF-22 beta-oxidation pathway has not only been implicated in the biosynthesis of ascarosides, but also in the degradation of triacylglyerols [Zhang et al., 2010, von Reuss et al., 2012, Artyukhin et al., 2018]. Additionally to the described enzymes, the *C. elegans* genome comprises further genes predicted by sequence homology to code for peroxisomal beta-oxidation enzymes [Gilst et al., 2005]. However, their function has not yet been tested experimentally.

Transcriptional regulation of the peroxisomal beta-oxidation

In mammals, metabolic pathways in peroxisomes are regulated by a subfamily of nuclear receptors: the peroxisome proliferator activated receptors (PPARs). The peroxisomal and mitochondrial beta-oxidation is regulated by the member PPARα [Aoyama et al., 1998]. PPARs act as a ligand-activated transcription factors, which form heterodimers with retinoid X receptors (RXR) and bind to PPAR response elements, which are specific DNA regions located 5' of the target genes (Figure 1.6) [Keller et al., 1993, Tugwood et al., 1992]. The receptors can be activated by a broad spectrum of ligands, which can be natural compounds like fatty acids, eicosanoids or phospholipids. Furthermore, there is also a broad range of synthetic ligands, so called peroxisome proliferators [Keller et al., 1993, Forman et al., 1997, Kliewer et al., 1997]. The ligands are transported to the nucleus by fatty acid binding proteins [Hostetler et al., 2009]. The transcriptional regulation of PPAR target genes depends on the binding of co-factors. More than 300 co-activators and co-repressors have been identified so far (reviewed in [Viswakarma et al., 2010]). Ligand binding to the PPAR-RXR heterodimer leads to a conformational change, which promotes the release of co-repressor proteins and the binding of co-activator proteins [Dowell et al., 1999].

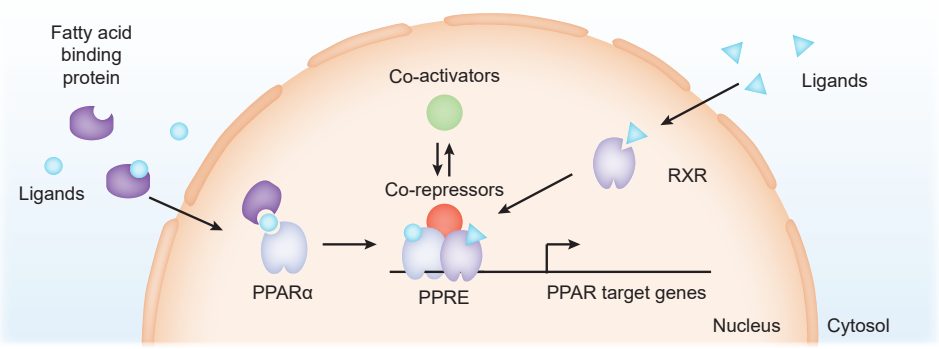

Figure 1.6: Transcriptional regulation by the peroxisome proliferator activated receptor alpha (PPARα). Fatty acid binding proteins bring the ligands to PPARα. It forms a heterodimer with the retinoid X receptor (RXR) and binds to the PPAR response element (PPRE), which is located up-stream of the PPARα target genes. Ligand binding to the PPARα-RXR heterodimer leads to a conformational change, which promotes the release of co-repressor proteins and the binding of co-activator proteins. (Figure adapted from [Ehrenborg and Krook, 2009]).

In *C. elegans*, the nuclear hormone receptor NHR-49 is required for the regulation of lipid metabolism. Therefore, it was suggested that it is a functional homolog of PPARα, although it is a sequence homolog to the hepatocyte nuclear factor 4 [Gilst et al., 2005]. Similar to PPARα, NHR-49 interacts with different co-factors to regulate specific metabolic pathways. The nuclear hormone receptors NHR-13, NHR-22, NHR-66 and NHR-105 as well as the Mediator subunit MDT-15 were identified as NHR-49 co-factors in yeast-two hybrid screens. Additionally, the nuclear hormone receptors NHR-66 and NHR-80 show a physical interaction with NHR-49 *in vitro*. The physical interaction was also reflected in functional studies. The interaction of NHR-49 and NHR-66 is required for the regulation of sphingolipid metabolism and lipid remodeling, whereas the NHR-49/NHR-80 and NHR-49/NHR-13 heterodimers regulate fatty acid desaturation [Pathare et al., 2012]. Additionally, an interaction of NHR-49 with MDT-15 is also implicated the regulation of the expression of fatty acid desaturases. Furthermore, the NHR-49/MDT-15 heterodimer is controlling genes involved in the fasting response [Taubert et al., 2006]. Similar to the mammalian fatty acid binding proteins, the *C. elegans* lipid binding proteins LBP-5 and LBP-8 have been shown to bind fatty acids and to regulate NHR-49 target genes [Xu et al., 2011, Folick et al., 2015].

1.4.3 The role of peroxisomes in the immune response

Peroxisomal metabolism is also required for the regulation of inflammation and immune functions. For example, peroxisomes play a role in the anti-inflammatory response in mammalian macrophages. The knock-down of the peroxin PEX14 or the peroxisomal beta-oxidation enzyme MFP2 leads to an enhanced inflammatory response due to an increase of pro-inflammatory proteins [Vijayan et al., 2017]. Moreover, the anti-inflammatory response in mammalian macrophages is dependent of peroxisome proliferator activated receptors (PPARs) [Chang et al., 2015, Devchand et al., 1996]. Di Cara *et al.* analyzed the effect of the loss of the peroxisomal import receptors PEX5 and PEX7 on phagocytosis in murine and *Drosophila* macrophages. Disruption of peroxisomal import leads to a decreased phagocytosis of bacteria upon infection. However, phagocytosis can be rescued by treatment of the cells with lipids that are normally synthesized in perox-

isomes. Moreover, infection leads to a transcriptional up-regulation of genes encoding enzymes for lipid metabolism in *Drosphila* [Di Cara et al., 2017].

Several known human pathogens can also infect the intestine of *C. elegans*. Therefore, it is a good model organism to study host-pathogen interactions. For example the Gram-negative bacterium *Pseudomonas aeruginosa* is pathogenic to *C. elegans* and humans [Tan et al., 1999]. However, the *C. elegans* immune system is less complex than the immune system of other invertebrates or mammals. *C. elegans* lacks an adaptive immune system and specialized immune cells. Furthermore, only the most ancestral signaling networks of the innate immunity are conserved. For instance, the role of the p38 MAP kinase pathway in the innate immune response is conserved between *C. elegans* and humans [Kim et al., 2002]. In contrast, no *C. elegans* homologs of the NF-κB family of transcription factors have been identified and homologs of the *Drosophila* Toll pathway are not required for the resistance to pathogens [Pujol et al., 2001]. The *C. elegans* innate immune system induces the secretion of several antimicrobial proteins upon pathogen infection. These proteins include C-type lectins, DUF274 proteins, lysozymes, collagens and UDP-glucosyltransferases [Simonsen et al., 2012]. Furthermore, extracellular reactive oxygen species are produced in the intestinal lumen to fight infection by the pathogenic bacterium *Enterococcus faecalis* [Chávez et al., 2007, Chávez et al., 2009, Hoeven et al., 2011]. The peroxisomal catalase CTL-2 and the mitochondrial Cu/Zn superoxide dismutase SOD-3 are required for the resistance to the pathogen infection, presumably to protect the intestinal cells from the cytotoxic ROS [Chávez et al., 2007]. The requirement of CTL-2 for the resistance to *E. faecalis* infection shows that peroxisomes are involved in the innate immune response in *C. elegans*. Moreover, the PPARα homolog NHR-49 is required for the survival on *E. faecalis* [Sim and Hibberd, 2016]. Since NHR-49 is an important regulator of fat metabolism, it is conceivable that, similar to mammals and *Drosophila*, peroxisomal lipid metabolism also plays a role in the *C. elegans* innate immunity.

1.5 Peroxisomal disorders

The importance of peroxisomes in human metabolism is highlighted by the existence of severe genetic diseases called peroxisomal disorders. These rare diseases either lead to a perturbation of peroxisomal function because peroxisomes lack a specific enzyme (single peroxisomal enzyme deficiencies) or they interfere with peroxisomal biogenesis (peroxisome biogenesis disorders) (reviewed in [Wanders, 2018]). To get a more comprehensive picture of peroxisomal disorders, various peroxisome deficient model organisms have been studied [Hiebler et al., 2014, Baes et al., 1997, Fan et al., 1996, Mast et al., 2011]. The model organism *C. elegans* also has been proposed to be suitable to study peroxisomal biogenesis disorders [Thieringer et al., 2003, Coppa et al., 2020].

While peroxisome biogenesis disorders cause abnormalities in many peroxisomal metabolic pathways, single peroxisomal enzyme deficiencies affect only one specific pathway [Wangler et al., 2018]. Therefore, they are classified according to the metabolic pathway that is affected. The X-linked adrenoleukodystrophy is with a prevalence of 1:20,000 to 1:30,000 incidences the most common peroxisomal disorder [Wiesinger et al., 2015]. X-linked adrenoleukodystrophy leads to an accumulation of very long chain fatty acids due to a mutation in the gene ABCD1, which is coding for a peroxisomal half-ABC transporter [Igarashi et al., 1976, Mosser et al., 1993]. Five other diseases caused by mutations in enzymes or transporters required for peroxisomal beta-oxidation have been described so far [Ferdinandusse et al., 2000, Ferdinandusse et al., 2006a, Ferdinandusse et al., 2006b, Ferdinandusse et al., 2007, Ferdinandusse et al., 2017]. Furthermore, single peroxisomal enzyme deficiencies affect peroxisomal alpha-oxidation [Jansen et al., 1997], etherphospholipid biosynthesis [Ofman et al., 1998, Buchert et al., 2014], glyoxylate metabolism [Danpure et al., 1994, Frishberg et al., 2014], bile acid synthesis [Vilarinho et al., 2016, Ferdinandusse et al., 2014, Hadžić et al., 2012] and hydrogen peroxide metabolism [Takahara, 1952].

Peroxisome biogenesis disorders occur due to mutations in one of the 13 PEX genes (Zellweger spectrum disorders (reviewed in [Waterham and Ebberink, 2012]), Rhizomelic chondrodysplasia punctata type 1 [Motley et al., 1997] and type 5 [Baroy et al., 2015])

or due to deficiencies of proteins required for peroxisomal fission [Waterham et al., 2007, Koch et al., 2016]. The severity of the disorders correlates with the predicted consequence of the mutation on the protein function and its effect on peroxisomal matrix protein import and peroxisome number [Rosewich et al., 2005, Matsumoto et al., 2003]. The Zellweger spectrum disorders display a broad clinical heterogeneity. Some patients present severe phenotypes like neuronal migration defects and liver dysfunction leading to a high mortality within the first years of life [Govaerts et al., 1982], whereas patients with a mild form of Zellweger spectrum disorder survive until adulthood [Berendse et al., 2016].

1.6 Protein quality control of different organelles

1.6.1 Protein quality control mechanisms

The maintenance of proteostasis is essential for the cell. The accumulation of misfolded proteins or protein aggregates often leads to neurodegenerative diseases like Alzheimer's disease or Parkinson's disease. To maintain proteostasis, chaperones assist the refolding of proteins and prevent their aggregation. Moreover, misfolded proteins can be degraded by proteases or by the proteasome. If proteins form aggregates or escape the surveillance of the proteasome system, they are degraded by the lysosome via the autophagy pathway (reviewed in [Chen et al., 2011]). Specific stress response pathways exist for the different organelles. For example, the endoplasmic reticulum or mitochondria induce unfolded protein response pathways upon the accumulation of misfolded proteins or protein aggregates. These pathways induce a retrograde signal from the organelle to the nucleus. The signal leads to the up-regulation of effector genes (among others organelle-specific chaperones or proteases), which contribute to restore the organelle's function (reviewed in [Almanza et al., 2019, Melber and Haynes, 2018]). In this chapter, I will focus on the peroxisomal and mitochondrial protein quality control mechanisms.

1.6.2 Peroxisomal protein quality control

Peroxisomal protein quality control includes the removal of non-functional proteins by the AAA+ ATPases Msp1 and the peroxisomal Lon protease. In *S. cerevisiae*, quality control of peroxisomal membrane proteins depends on Msp1, which is localized to peroxisomes and mitochondria. Weir *et al.* analyzed the effect of the over-expression of the peroxisomal membrane protein Pex15. A fraction of Pex15 mislocalized to mitochondria, where it was rapidly degraded in an Msp1-dependent manner. Additionally, over-expressed Pex15 that localized to the peroxisomal membrane was first also degraded by Msp1. However, Pex15 rapidly adapted an Msp1-insensitive state. The authors suggested that at the peroxisomal membrane Pex15 is stoichiometrically protected by Pex3 [Weir et al., 2017b]. Although Msp1 is conserved between the species, its function in peroxisomal quality control has only been studied in *S. cerevisiae*.

Quality control of peroxisomal matrix proteins requires the peroxisomal Lon protease. It was first identified in rat liver cells and shows structural and functional similarities to the mitochondrial Lon protease [Kikuchi et al., 2004, Bartoszewska et al., 2012]. Analysis of the peroxisomal Lon protease in several model organisms suggests that it is required for the degradation of peroxisomal metabolic enzymes [Aksam et al., 2007, Yokota et al., 2008, Bartoszewska et al., 2012, Goto-Yamada et al., 2014]. Furthermore, the degradation of an artificially over-expressed unfolded protein targeted to peroxisomes also requires the peroxisomal Lon protease [Aksam et al., 2007]. In line with these observations, *in vitro* studies revealed that the peroxisomal Lon protease has chaperone and ATP dependent protease activity [Bartoszewska et al., 2012, Aksam et al., 2007, Omi et al., 2008]. Additionally, the peroxisomal Lon protease cooperates with autophagy in the degradation of non-functional peroxisomes in some organisms. In the plant *Arabidopsis thaliana*, knock-out mutants of the peroxisomal Lon protease show increased autophagy [Goto-Yamada et al., 2014, Farmer et al., 2013]. Furthermore, in mammalian cells that were pre-treated by a peroxisome proliferator two observations were made: peroxisomal beta-oxidation enzymes were degraded by the peroxisomal Lon protease [Yokota et al., 2008] and peroxisomes were degraded by autophagy [Iwata et al., 2006]. In contrast, in the

yeast *Hansenula polymorpha* and in the filamentous fungus *Penicillium chrysogenum*, the peroxisomal number is not changed in peroxisomal Lon protease mutants indicating that autophagy is not induced [Aksam et al., 2007, Bartoszewska et al., 2012]. All in all, the different studies suggest that some functions of the peroxisomal Lon protease are conserved, whereas other are organism-specific. The *C. elegans* gene *lonp-2* encodes a homolog of the peroxisomal Lon protease. However, its function has not been characterized so far.

1.6.3 The mitochondrial unfolded protein response

Mitochondria synthesize ATP by oxidative phosphorylation, are involved in programmed cell death and are sites for various metabolic pathways. Recently, it has been shown that perturbation of many (but not all) mitochondrial functions can induce the mitochondrial unfolded protein response (UPR^{mt}) [Rolland et al., 2019]. This stress response pathway induces the up-regulation of mitochondrial chaperones and proteases to restore the organelle's function. While the UPR^{mt} was discovered in mammalian cells [Martinus et al., 1996], many of the components of the pathway were identified in *C. elegans*. The induction of UPR^{mt} in *C. elegans* is regulated by the bZip transcription factor ATFS-1, which has a nuclear localization signal and a mitochondrial targeting sequence [Haynes et al., 2010]. Under physiological conditions, ATFS-1 is imported into mitochondria, where it is degraded by the mitochondrial Lon protease (Figure 1.7) [Nargund et al., 2012]. In case of mitochondrial dysfunction, non-functional proteins are cleaved by the protease CLPP-1 and exported to the cytosol by the ABC transporter HAF-1 [Haynes et al., 2007, Haynes et al., 2010]. It has been proposed that HAF-1 modulates mitochondrial import and thus the import of ATFS-1 [Nargund et al., 2012]. Additionally, most inducers of UPR^{mt} directly or indirectly perturb mitochondrial import [Nargund et al., 2012, Rolland et al., 2019]. Thus, ATFS-1 can no longer enter mitochondria, where it is degraded, but translocates to the nucleus, where it activates the transcription of genes required for among others mitochondrial quality control, detoxification, immunity or metabolism [Haynes et al., 2010, Nargund et al., 2012]. Additionally to ATFS-1, the induction of UPR^{mt} requires the transcription factor DVE-1 and its co-factor UBL-5 [Benedetti et al., 2006, Haynes

et al., 2007]. Furthermore, a complementary pathway that regulates cytosolic protein synthesis in response to mitochondrial stress exists. Mitochondrial dysfunction leads to the production of ROS, which activates the kinase GCN-2. The translation initiation factor eIF2α is phosphorylated by GCN-2, which leads to translational attenuation and, thus, to a reduction of the influx of proteins into mitochondria [Baker et al., 2012].

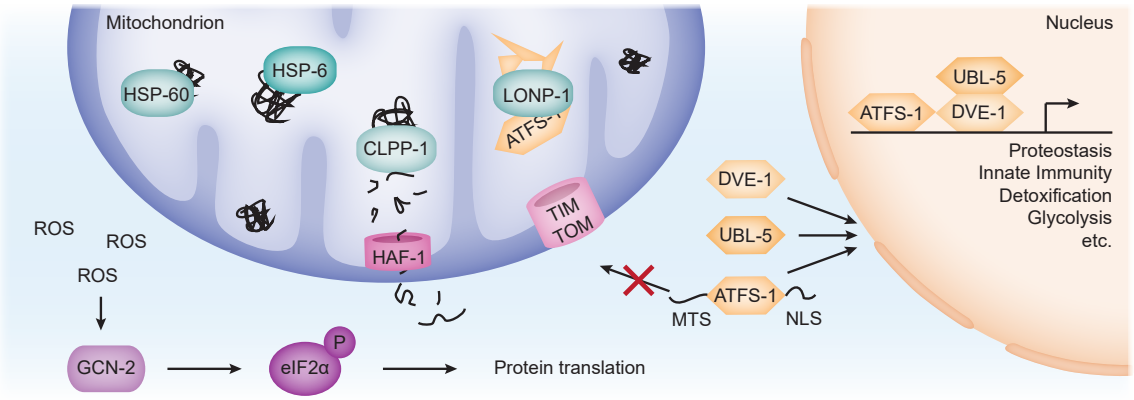

Figure 1.7: The mitochondrial unfolded protein response in *C. elegans*. The transcription factor ATFS-1 has a nuclear localization signal (NLS) and a mitochondrial targeting sequence (MTS). Upon activation of UPR^{mt}, ATFS-1 is no longer degraded by the mitochondrial Lon protease. Together with UBL-5 and DVE-1, it translocates to the nucleus, where they activate various stress response genes. As a complementary pathway, reactive oxygen species (ROS) produced by dysfunctional mitochondria activate the kinase GCN-2. This leads to the phosphorylation of eIF2α and by this to a change in protein translation. (Figure adapted from [Jovaisaite et al., 2014]).

The UPR^{mt} pathway is partially conserved from *C. elegans* to humans. In contrast to *C. elegans*, translational control by phosphorylated eIF2α is a prerequisite for the induction of mammalian UPR^{mt}. This results in an increased expression of ATF5, which is the functional homolog of the *C. elegans* transcription factor ATFS-1 and also harbors a nuclear localization signal and a mitochondrial targeting sequence [Zhou et al., 2008, Fiorese et al., 2016]. The up-regulation of ATF5 requires the transcription factors ATF4 and CHOP, which both are also targets of eIF2α phosphorylation [Zhou et al., 2008, Teske et al., 2013]. However, the functional interaction of ATF4, ATF5 and CHOP in the regulation of UPR^{mt} is not known. It has been shown that, similar to ATFS-1, ATF5 translocates to the nucleus upon mitochondrial dysfunction and activates mitochondria-specific stress response genes encoding for example chaperones like HSP60 or mitochondrial HSP70 [Fiorese et al., 2016].

1.7 Aim of this study

The importance of functional peroxisomal biogenesis is highlighted by the existence of severe human disorders caused by mutations in the PEX genes. Studying these diseases has significantly contributed to our understanding of the biology of peroxisomes. In general, these studies focus on peroxisomal defects caused by mutations. However, like for other organelles, the function of initially healthy peroxisomes can also get disrupted during the life of an organism. If the defect is not too severe one can speculate that a peroxisome-specific stress response pathway could be activated to restore the peroxisome's function like it has been shown for other organelles. Such a peroxisomal stress response pathway has not been described so far. However, it has been shown that the peroxisomal Lon protease can contribute to protein homeostasis by degrading misfolded proteins. Furthermore, it can act as a chaperone and contribute to the folding of proteins. This indicates that the peroxisomal Lon protease is part of a peroxisomal quality control system. Thus, it may be also part of a peroxisomal stress response pathway.

C. elegans is a suitable organism to study organellar stress response pathways. For example, the mitochondrial unfolded protein response has extensively been studied in *C. elegans*. Although it was first discovered in mammals, subsequent work was mostly done in *C. elegans* identifying several components of the pathway. Later, it has been shown that many of these components are conserved in humans. Therefore, we used *C. elegans* as a model organism to study the peroxisomal stress response. In contrast to mitochondria, the knowledge about peroxisomes in this organism is limited. However, it has been shown that many components of the peroxisomal biogenesis are conserved from humans to *C. elegans*. Furthermore, the peroxisomal beta-oxidation, which is an important function of peroxisomes, is also conserved between the species.

The first aim is to characterize the peroxisomal Lon protease LONP-2 in *C. elegans*. So far, it has not been studied if LONP-2 also has protease and chaperone functions, like it was shown for other organisms. Therefore, I will analyze if the *C. elegans* peroxisomal Lon protease is required for the degradation of an unfolded protein and might therefore be required for the peroxisomal stress response pathway.

Stress response pathways induce a retrograde signaling from the organelle to the nucleus to up-regulate specific target genes to restore the organelle's function. A similar pathway may exist in peroxisomes and the peroxisomal Lon protease might be a target gene for a peroxisomal retrograde signaling. The main aim of my study is to analyze if a peroxisomal retrograde signaling exists in *C. elegans* and to characterize the different components of the pathway.

Peroxisomes and mitochondria are known to physically and functionally interact in the cell. For example, metabolic pathways are shared between the two organelles. Moreover, it has been shown in mammals that perturbation of peroxisomal function also affects mitochondrial function. Therefore, the third aim of my thesis is to analyze if a perturbation of peroxisomal biogenesis also induces the mitochondrial unfolded protein response.

2

Materials and Methods

2.1 Strains and general maintenance of *C. elegans*

C. elegans strains were cultured as previously described [Brenner, 1974]. Animals were maintained at 15°C, 20°C or 25°C on nematode growth medium (NGM) plates with *Escherichia coli* OP50 bacterial lawns [Stiernagle, 2006]. Bristol N2 was used as the wild-type strain. The *prx-5(tm4948)* allele was obtained from the National BioResource Project (https://shigen.nig.ac.jp/c.elegans/). The *daf-22(m130)* [Golden and Riddle, 1985] and *ctl-2(ua90)* [Petriv and Rachubinski, 2004] alleles were obtained from the Caenorhabditis Genetics Center (https://cgc.umn.edu/). The strains used in this study are summarized in Table 2.1.

Table 2.1: *C. elegans* strains used in the study.

Strain	Genotype	Transgene description	Reference
MD4272	*bcIs140* V; *n765ts* X	$P_{vha\text{-}7}$*GFP::PTS1* (pBC1578) + $P_{vha\text{-}7}$*mKate2::pxmp-4* (pBC1699) + pL15.EK	This study
MD4635	*bcSi117*	$P_{daf\text{-}22}$*mKate2::daf-22* (pBC1918)	This study
MD4667	*bcSi118* IV; *bcSi119* X	$P_{daf\text{-}22}$*mKate2::daf-22* (pBC1918) + $P_{daf\text{-}22}$*GFP::pxmp-4* (pBC1945)	This study
-	*bcEx1316; bcEx1305*	$P_{vha\text{-}7}$*GFP::lonp-2* (pBC1711) + $P_{vha\text{-}7}$*mKate2::pxmp-4* (pBC1699)	This study
MD4601	*bcSi112* IV	$P_{daf\text{-}22}$*YFP::dhfr*^{mut}*::PTS1* (pBC1907)	This study
MD4651	*bcSi112* IV; *bcEx1375*	$P_{daf\text{-}22}$*YFP::dhfr*^{mut}*::PTS1* (pBC1907) + $P_{vha\text{-}7}$*mCherry::PTS1* (pBC1627)	This study
MD3919	*bcIs126* I	$P_{lonp\text{-}2}$*GFP* (pBC1503)	Generated for my Master thesis
MD3920	*bcIs128* I	$P_{lonp\text{-}2}$*GFP* (pBC1503)	Generated for my Master thesis
MD4247	*bcSi75* IV	$P_{lonp\text{-}2}$*GFP* (pBC1743)	This study
MD4253	*bcSi76* IV	$P_{ctl\text{-}2}$*GFP* (pBC1744)	This study

Table 2.1 continued from previous page

Strain	Genotype	Transgene description	Reference
MD4581	*bcSi110*	$P_{daf\text{-}22}GFP$ (pBC1905)	This study
SJ4100	*zcIs13* V	$P_{hsp\text{-}6}GFP$	[Yoneda et al., 2004]
SJ4058	*zcIs9* V	$P_{hsp\text{-}60}GFP$	[Yoneda et al., 2004]
MD4202	*tm4948* II	*prx-5(tm4948)*	This study
MD4211	*bcIs126* I; *tm4948* II	$P_{lonp\text{-}2}GFP$ carrying *prx-5(tm4948)*	This study
MD4212	*bcIs126* I	$P_{lonp\text{-}2}GFP$	This study
MD4292	*tm4948* II; *bcSi76* IV	$P_{ctl\text{-}2}GFP$ carrying *prx-5(tm4948)*	This study
MD4293	*bcSi76* IV	$P_{ctl\text{-}2}GFP$	This study
MD4304	*gk405* I	*nhr-49(gk405)*	This study
MD4464	*m130* II; *bcSi76* IV	$P_{ctl\text{-}2}GFP$ carrying *daf-22(m130)*	This study
MD4465	*bcSi76* IV	$P_{ctl\text{-}2}GFP$	This study
MD4475	*bcIs126* I; *m130* II	$P_{lonp\text{-}2}GFP$ carrying *daf-22(m130)*	This study
MD4381	*bcIs126* I; *ua90* II	$P_{lonp\text{-}2}GFP$ carrying *ctl-2(ua90)*	This study
MD4665	*ua90* II; *bcSi76* IV	$P_{ctl\text{-}2}GFP$ carrying *ctl-2(ua90)*	This study
MD4664	*bcSi76* IV	$P_{ctl\text{-}2}GFP$	This study

2.2 Generation of transgenic animals

2.2.1 Reporters to visualize peroxisomes by fluorescent microscopy

The membrane of peroxisomes in hypodermal cells was labeled by a fusion construct of mKate2 with the peroxisomal membrane protein PXMP-4. To this end, *mKate2* was am-

plified by PCR using the primers mkate2PTS1FNheI1 and mkate2-linker-R (Table 2.2). The fusion construct *linker::pxmp-4* was amplified from the plasmid pBC1574 using the primers mkate2-linker-F and PMP24R-KpnI. The *mKate2* and *linker::pxmp-4* fragments were fused by overlap extension PCR using the primers mkate2PTS1FNheI1 and PMP24R-KpnI. To generate the plasmid pBC1699, the obtained PCR product was first cloned into the EcoRV site of pBluescript KS(+) (Stratagene) and then sub-cloned into the NheI and KpnI sites of pBC1666, which contains the *vha-7* promoter and an *unc-54* 3'UTR.

The matrix of peroxisomes in hypodermal cells was labeled by a *GFP::PTS1* construct. The primers GFPPTS1F-KpnI and gftpts1R-new were used to amplify *GFP* from the plasmid pPD118.60 (a gift from Andrew Fire; Addgene plasmid no. 1598) and thereby to fuse the PTS1 SKL to *GFP*. The PCR product was cloned into the EcoRV site of pBluescript KS(+) (Stratagene), generating the plasmid pBC1572. The *GFP::PTS1* construct was sub-cloned into the KpnI and SacI sites of the plasmid pBC970, which contained the *vha-7* promoter and an *unc-54* 3'UTR. The final plasmid was named pBC1578.

The plasmids pBC1699 (1 ng/μl) and pBC1578 (1 ng/μl) were co-injected into MT1642(*lin-15(n765ts)*), using the *lin-15* rescue plasmid pL15.EK (50 ng/μl) as a co-injection marker. The obtained extrachromosomal array *bcEx1310* was integrated by UV treatment. The $P_{vha\text{-}7}$*GFP::PTS1* and $P_{vha\text{-}7}$*mKate2::pxmp-4* (*bcIs140; lin-15(n765ts)*) reporter strain was back-crossed five times with MT1642.

Table 2.2: Primers used in the study.

Name	Sequence (5'-3')
mkate2PTS1FNheI1	GCT AGC ATG TCC GAG CTC ATC AAG GAG
mkate2-linker-R	GGG AGC GCA GGC CGG AAC GGT GTC CGA GCT TG
mkate2-linker-F	CAA GCT CGG ACA CCG TTC CGG CCT GCG CTC CC
PMP24R-KpnI	GGT ACC CTA TGG ATG GAA TTC GAA TAG CC
GFPPTS1F-KpnI	GGT ACC ATG AGT AAA GGA GAA GAA CTT TTC
gftpts1R-new	GAA TTC TTA AAG TTT GGA ATG AAG AGG TTT G
Pdaf22-F	AAG CTA CGT AAT ACG ACT CAA TGG CTT TAC CAC CAA TTG
Pdaf22-mKate2-R	GAG CTC GGA CAT TTT TCT GGA ACA ATA TTT TTT TTT CGA AG
Pdaf22-mKate2-F	TTG TTC CAG AAA AAT GTC CGA GCT CAT CAA GGA G
mKate2-UTR-R	TGG TTG GCG TCA TGG AGT TGG ACG CCT GCG C
mKate2-UTR-F	GCG TCC AAC TCC ATG ACG CCA ACC AAG CCA AAG
Pdaf22-GFP-F	AAA AAT ATT GTT CCA GAA AAA TGA GTA AAG GAG AAG AAC
PXMP4-UTR-R	TTA AAT TAT TCC GTT TTT ATT TGG ATG GAA TTC GAA TAG
daf22-UTR-R	CGC GAT GCA TTC GAA GAT CTG CCC AAG TTA GTT TTT TAC TAG AAG CTG CC
Pdaf22-DHFR-R	TGC TCA CCA TTT TTC TGG AAC AAT ATT TTT TTT TC
Pdaf22-DHFR-F	TTC CAG AAA AAT GGT GAG CAA GGG CGA G
PLP-1p5'SphI	GCA TGC TTG AGC AGA AAA ATT GAG GC
PLP-1p3'KpnI	GGT ACC TTC ATT TCG GGC AAA ACT G
Plonp2GFP-F	ACG TCA CCG GTT CTA GAT ACT TGA GCA GAA C
unc54-R	TAG AGG GTA CCA GAG CTC ACA AAC AGT TAT GG
Pctl-2FSphI	GCA TGC ACT TTT GTA TAT AGA ATC TCG
Pctl-2RAgeI	ACC GGT TTT GGT TCT GAA ATT TTA GTT AGG

Table 2.2 continued from previous page

Name	Sequence (5'-3')
Pctl2GFP-F	ACG TCA CCG GTT CTA GAT ACA CTT TTG TAT ATA GAA TCT CGT TAT TTA TAA AC
Pctl2GFP-R	TAG AGG GTA CCA GAG CTC ACA AAC AGT TAT GG
Pdaf22-R	CTT TAC TCA TTT TTC TGG AAC AAT ATT TTT TTT TC
GFP-unc54-F	TTC CAG AAA AAT GAG TAA AGG AGA AGA AC
GFP-unc54-R	TTC GAA GAT CTG CCC ACT AGA AAC AGT TAT GTT TGG TAT ATT G
YFPDHFR-F-KpnI	GGT ACC ATG GTG AGC AAG GGC GAG
YFPDHFRPTS-R-SacI	GAG CTC TTA GAG CTT GGA GTG GAG TGG TCG CCG CTC CAG AAT CTC
acox-1.6-F	ATC ATC GAT GAA TTC GAG CTC ATG AGT CGA TGG ATT CAG C
acox-1.6-R	CTA TAG GGC GAA TTG GGT ACC TTG AAG TGT TGG AAT AAA CAT AAC

The $P_{daf\text{-}22}$*mKate2::daf-22* reporter was generated by amplifying the *daf-22* promoter from the plasmid pBC1905 using the primers Pdaf22-F and Pdaf22-mKate2-R. *daf-22* and its 3'UTR was amplified from *C. elegans* genomic DNA using the primers mKate2-UTR-F and daf22-UTR-R. The primer design for these two constructs was based on a previously published $P_{daf\text{-}22}$*GFP::daf-22* construct [Butcher et al., 2009]. The *mKate2::linker* fragment was amplified from pBC1699 using the primers Pdaf22-mKate2-F and mKate2-UTR-R. The three PCR products were ligated by Gibson assembly into the SpeI site of the MiniMos vector pCFJ909 (a gift from Erik Jorgensen; Addgene plasmid no. 44480), which harbors the *cb-unc-119(+)* rescue fragment. The obtained plasmid was named pBC1918. Microinjection of the plasmid pBC1918 (10 ng/μl) into the strain HT1593(*unc-119(ed3)*) using MiniMos [Frøkjaer-Jensen et al., 2014] generated the single-copy insertion allele *bcSi117*.

To label the peroxisomal membrane by GFP in cells that express *daf-22*, a P$_{daf\text{-}22}$*GFP::linker::pxmp-4* reporter was generated. To this end, the *GFP::linker::pxmp-4* fusion construct was amplified from the plasmid pBC1577 using the primers Pdaf22-GFP-F and PXMP4-UTR-R. The PCR product was used to replace the *mKate2::linker::daf-22* fragment of the plasmid pBC1918 by Gibson assembly. Microinjection of the obtained plasmid pBC1945 (10 ng/µl) into the strain HT1593(*unc-119(ed3)*) using MiniMos [Frøkjaer-Jensen et al., 2014] generated the single-copy insertion allele *bcSi119*. To generate a reporter strain expressing P$_{daf\text{-}22}$*mKate2::linker::daf-22* and P$_{daf\text{-}22}$*GFP::linker::pxmp-4*, the strains MD4636(*bcSi118*) and MD4666(*bcSi119*) were crossed.

2.2.2 Reporter to determine the sub-cellular localization of LONP-2

To analyze the sub-cellular localization of LONP-2, Emin Rizovic generated during his master thesis a P$_{vha\text{-}7}$*GFP::lonp-2* (*bcEx1316*) reporter, which expresses a GFP::LONP-2 fusion construct in hypodermal cells. To confirm the peroxisomal localization, I crossed this reporter with the P$_{vha\text{-}7}$*mKate2::pxmp-4* (*bcEx1305*) reporter, which labels peroxisomal membranes in hypodermal cells, and analyzed male animals of the F1 progeny.

2.2.3 Reporter expressing DHFR^{mut} in peroxisomes

To generate the P$_{daf\text{-}22}$*YFP::dhfr^{mut}::PTS1* reporter, the *YFP::DHFR^{mut}* fusion construct was amplified from the plasmid pBMN YFP-DHFR(DD) (a gift from Thomas Wandless; Addgene plasmid no. 29326) using the primers YFPDHFR-F-KpnI and YFPDHFRPTS-R-SacI, which contained the PTS1 (Table 2.2). To generate the plasmid pBC1635, the obtained PCR product was first cloned into the EcoRV site of pBluescript KS(+) (Stratagene) and then sub-cloned into the SacI and KpnI sites of pBC970. The *YFP::dhfr^{mut}::PTS1::unc-54 3' UTR* construct was amplified from the plasmid pBC1635 using the primers Pdaf22-DHFR-F and GFP-unc54-R. The *daf-22* promoter was amplified from the plasmid pBC1905 using the primers Pdaf22-F and Pdaf22-DHFR-R. To generate the plasmid pBC1907, the two PCR products were inserted by Gibson assembly into the SpeI site of the MiniMos vector pCFJ909 (a gift from Erik Jorgensen; Addgene

plasmid no. 44480), which harbors the *cb-unc-119(+)* rescue fragment. Microinjection of the plasmid pBC1907 (10 ng/μl) into the strain HT1593(*unc-119(ed3)*) using MiniMos [Frøkjaer-Jensen et al., 2014] generated the single-copy insertion allele *bcSi112*.

To confirm the peroxisomal localization of the $P_{daf\text{-}22}$*YFP::dhfr*^{mut}*::PTS1* construct, the plasmid pBC1627 ($P_{vha\text{-}7}$*mCherry::PTS1*) (5 ng/μl) was injected into the $P_{daf\text{-}22}$*YFP::dhfr*^{mut}*::PTS1* (*bcSi112*) reporter. The plasmid pRF4 (80 ng/μl), which contains the *rol-6(su1006dm)* allele [Mello et al., 1991], was used as a co-injection marker. The transgenic line *bcSi112* carrying the multi-copy extrachromosomal array *bcEx1375* was obtained.

2.2.4 Transcriptional reporters to analyze the peroxisomal retrograde signaling

The $P_{lonp\text{-}2}$*GFP* multi-copy reporters were generated by Stéphane Rolland and me during my master thesis. Since the reporters are essential for this project, I summarize their generation in this paragraph. A 1 kb fragment immediately 5' of the predicted start codon of *lonp-2* was amplified from *C. elegans* genomic DNA using the primers PLP-1p5'SphI and PLP-1p3'KpnI (Table 2.2). The fragment was sub-cloned in front of *GFP* in the plasmid pPD95_75 (a gift from Andrew Fire; Addgene plasmid no. 1494) to generate the plasmid pBC1503. Co-injection of the plasmid pBC1503 (5 ng/μl) with pRF4 (80 ng/μl), which contains the *rol-6(su1006dm)* allele [Mello et al., 1991], generated a transgenic line containing the multi-copy extrachromosomal array *bcEx1228*. The extrachromosomal array was integrated by UV treatment generating two independent lines (*bcIs126* and *bcIs128*). Both $P_{lonp\text{-}2}$*GFP* reporters were back-crossed five times with N2. The insertion of the *bcIs126* allele was mapped by snip-SNP mapping to LGI [Wicks et al., 2001].

To generate the $P_{lonp\text{-}2}$*GFP* single-copy reporter, the $P_{lonp\text{-}2}$*GFP::unc-54 3'UTR* construct was amplified from the plasmid pBC1503 using the primers Plonp2GFP-F and unc54-R. The PCR product was ligated by Gibson assembly into the AvrII site of the MosSCI vector pCFJ350 (a gift from Erik Jorgensen; Addgene plasmid no. 34866) [Frøkjaer-Jensen et al., 2012], which harbors the *cb-unc-119(+)* rescue fragment. Microinjection of the obtained plasmid pBC1743 (25 ng/μl) into the strain EG8081(*oxTi177; unc-119(ed3)*) using MosSCI [Frøkjaer-Jensen et al., 2012] generated the single-copy in-

sertion allele *bcSi75* on LGIV.

To construct the $P_{ctl\text{-}2}GFP$ reporter, a 1.6 kb fragment immediately 5' of the predicted start codon of *ctl-2* was amplified from *C. elegans* genomic DNA using the primers Pctl-2FSphI and Pctl-2RAgeI. The *lonp-2* promoter of the plasmid pBC1503 was replaced by the PCR product using the SphI and AgeI restriction sites, generating the plasmid pBC1690. The $P_{ctl\text{-}2}GFP$ fusion construct was amplified from the plasmid pBC1690 with the primers Pctl2GFP-F and Pctl2GFP-R. Using Gibson assembly, the PCR product was inserted into the AvrII site of the MosSCI vector pCFJ350 (a gift from Erik Jorgensen; Addgene plasmid no. 34866) [Frøkjaer-Jensen et al., 2012], which harbors the *cb-unc-119(+)* rescue fragment. The obtained plasmid was named pBC1744. Microinjection of the plasmid pBC1744 (25 ng/μl) into the strain EG8081(*oxTi177; unc-119(ed3)*) using MosSCI [Frøkjaer-Jensen et al., 2012] generated the single-copy insertion allele *bcSi76* on LGIV.

The $P_{daf\text{-}22}GFP$ reporter was generated by amplifying a 2.3 kb fragment immediately 5' of the predicted start codon of *daf-22* from *C. elegans* genomic DNA using the primers Pdaf22-F and Pdaf22-R. The *GFP::unc-54 3'UTR* fusion construct was amplified from the plasmid pBC1744 using the primers GFP-unc54-F and GFP-unc54-R. The two PCR products were ligated by Gibson assembly into the SpeI site of the MiniMos vector pCFJ909 (a gift from Erik Jorgensen; Addgene plasmid no. 44480), which harbors the *cb-unc-119(+)* rescue fragment. The obtained plasmid was named pBC1905. Microinjection of the plasmid pBC1905 (10 ng/μl) into the strain HT1593(*unc-119(ed3)*) using MiniMos [Frøkjaer-Jensen et al., 2014] generated the single-copy insertion allele *bcSi110*.

2.3 Analysis of peroxisomes by fluorescent microscopy

To analyze the tissue-specific localization of peroxisomes and the peroxisomal Lon protease, young adults of the reporter strains were mounted on 2% agarose pads and immobilized with M9 buffer (Table 2.3) containing 1 mM Levamisol. The slides were imaged using a Zeiss Axioskop 2 (100x, NA 1.3) equipped with a charge-coupled device camera (1300; Micromax) and the MetaMorph software 7.1.0.0 (Molecular De-

vices). For the analysis of peroxisomes in hypodermal cells, the $P_{vha\text{-}7}$*GFP::PTS1* and $P_{vha\text{-}7}$*mKate2::pxmp-4* reporter strain was imaged with the alae in focus and 1000 ms exposure time using a GFP and mCherry filter, respectively. To analyze the sub-cellular localization of LONP-2 in hypodermal cells, the $P_{vha\text{-}7}$*lonp-2::GFP* and $P_{vha\text{-}7}$*mKate2::pxmp-4* reporter strain was analyzed under the same conditions. To analyze the sub-cellular localization of DAF-22, the $P_{daf\text{-}22}$*mKate2::daf-22* reporter was imaged with 100 ms exposure time using a mCherry filter. Single plane images of the anterior part of the intestine (nuclei in focus) or of the head (hypodermal and head muscle cells in focus) were taken. To analyze the sub-cellular localization of the peroxisomal Lon protease, single plane images of the $P_{vha\text{-}7}$*GFP::lonp-2* and $P_{vha\text{-}7}$*mKate2::pxmp-4* reporter strain were taken with 1000 ms exposure time using a GFP and mCherry filter, respectively.

Table 2.3: M9 buffer.

Component	Amount
Na_2HPO_4	5.8 g
KH_2PO_4	3.0 g
NaCl	0.5 g
NH_4Cl	1.0 g
MilliQ H_2O	to 1 l

2.4 RNA interference experiments

The bacterial clones for RNAi by feeding were obtained from the Ahringer library [Kamath and Ahringer, 2003]. The *acox-1.1(RNAi)* clone was taken from the Vidal library [Rual et al., 2004] and the *tag-208(RNAi)* clone was previously generated in the laboratory [Rolland et al., 2019]. The control *mock(RNAi)* contains HT115 RNAi bacteria transformed with the empty RNAi vector pPD129.36. The *acox-1.6(RNAi)* clone was generated by amplifying the first three exons of *acox-1.6* from genomic DNA using the primers acox-1.6-F and acox-1.6-R (Table 2.2). The PCR product was ligated into the

SacI and KpnI site of pPD129.36 (a gift from Andrew Fire; Addgene plasmid no. 1654) by Gibson assembly and the obtained plasmid was transformed into HT115 RNAi bacteria.

On day one, the RNAi clones were inoculated into 2 ml of LB carbenicillin (100 μg/ml) tetracycline (12.5 μg/ml) (Table 2.4) and cultured overnight at 37°C and 200 rpm. The next day, 2 ml of LB carbenicillin (100 μg/ml) was inoculated with 20 μl of the overnight culture and was grown at 37°C and 200 rpm for 6 h. The RNAi cultures were then adjusted to 0.5 OD and 50 μl was used to seed a first set of 30 mm RNAi plates containing 6 mM IPTG [Rolland et al., 2019]. In the case of double RNAi experiments, each RNAi culture was diluted 1:2 (vol/vol). After seeding, the plates were protected from light and incubated at room temperature until the next day. On day three, a second set of RNAi plates were seeded (following the same protocol as for the first set of RNAi plates). Furthermore, four to eight L4 larvae of the transcriptional reporter strains were inoculated onto the seeded RNAi plates and incubated at 20°C for 22 h. During this incubation, the L4 larvae developed into adults and were transferred onto the second set of RNAi plates. The adults were let to lay eggs for 4 h at 20°C and then removed (hereafter referred to as 'lay-off'). The synchronized progeny was incubated for three days at 20°C. For imaging, about 10-15 F1 gravid adults per RNAi condition were mounted on 2% agarose pads and immobilized with M9 buffer containing 1 mM Levamisol. The slides were imaged using a Leica GFP dissecting microscope (M205 FA, Planapo 1× objective, 35x zoom, NA 0.07) with a GFP filter and the software Leica Application Suite (3.2.0.9652). The exposure time was set to 200 ms for all images to be able to compare the different fluorescence intensities.

In the case of the RNAi experiment to analyze peroxisomal import (see chapters 3.1.3, 3.1.4), the population was not synchronized by a lay-off. Instead, the stage of the F1 animals was determined by DIC microscopy and only young adults carrying not more than three eggs were mounted on 2% agarose pads and immobilized with M9 buffer containing 1 mM Levamisol. The anterior part of the intestine (nuclei in focus) or the hypodermis of the same region (alae in focus) of the $P_{daf\text{-}22}$*mKate2::daf-22* and $P_{daf\text{-}22}$*GFP::pxmp-4* reporter strain was imaged using a Leica SP5 confocal microscope (HCX PL APO

Table 2.4: LB-broth.

Component	Amount
Tryptone	10.0 g
Yeast extract	5.0 g
NaCl	10.0 g
MilliQ H_2O	0.8 l

Lambda Blue 63x oil objective, NA 1.4, 488 nm and 561 nm lasers) and the LAS AF software (Leica). At the anterior part of the $P_{vha\text{-}7}$*GFP::PTS1* and $P_{vha\text{-}7}$*mKate2::pxmp-4* reporter strain, the hypodermal cells were imaged with the alae in focus with 1000 ms exposure time and GFP and mCherry filters using a Zeiss Axioskop 2 (100x, NA 1.3) equipped with a charge-coupled device camera (1300; Micromax) and the MetaMorph software 7.1.0.0 (Molecular Devices).

The RNAi by feeding protocol was also modified for the preparation of the samples for the proteomic analysis (see chapter 3.3.10). On day one, the RNAi clones were streaked out on LB carbenicillin (100 μg/ml) tetracycline (12.5 μg/ml) plates and the plates were incubated overnight at 37°C. On day two, the RNAi bacteria were resuspended in LB and a first set of 100 mm RNAi plates containing 6 mM IPTG (two plates per condition) were seeded with 600 μl of RNAi suspension OD 0.5. In order to reduce the slow-growth phenotype, the *prx-5(RNAi)* and *prx-19(RNAi)* cultures were diluted 1:2 (vol/vol) with *mock(RNAi)*. After seeding, the plates were protected from light and incubated at room temperature until the next day. On day three, a second set of RNAi plates were seeded (following the same protocol as for the first set of RNAi plates). Furthermore, ∼200 N2 L4 larvae were pipetted onto each RNAi plate that was seeded the previous day. After incubation at 20°C for 22 h, the gravid adults were pipetted onto the second set of RNAi plates, let to lay eggs for four hours at 20°C and then removed. The synchronized progeny was incubated for three days (*mock(RNAi)* and *tag-208(RNAi)*) or four days (*prx-5(RNAi)* and *prx-19(RNAi)*) at 20°C to reach the adult stage and then collected in a tube. The worm pellet was washed four times with 10 ml of 1x PBS (Table 2.5). The samples were flash

frozen in liquid nitrogen and stored at -80°C until they were analyzed by LC-MS (see chapter 2.9).

Table 2.5: Phosphate-buffered saline (PBS) (10x).

Component	Amount
Na_2HPO_4	25.6 g
KH_2PO_4	2.0 g
NaCl	80.0 g
KCl	2.0 g
MilliQ H_2O	to 1 l

I developed a large scale protocol for the the preparation of the samples for the RNA-seq analysis (see chapter 3.3.9). The samples for the analysis were prepared by Judith Zacherl. On day one, the RNAi clones were inoculated into 2 ml of LB carbenicillin (100 μg/ml) tetracycline (12.5 μg/ml) and cultured overnight at 37°C and 200 rpm. The next day, 2 ml of LB carbenicillin (100 μg/ml) was inoculated with 20 μl of the overnight culture and was grown at 37°C and 200 rpm for 6 h. The RNAi cultures were then adjusted to 0.5 OD and 600 μl was used to seed a first set of 100 mm RNAi plates containing 6 mM IPTG (2 plates per condition). In order to reduce the slow-growth phenotype, the *prx-5(RNAi)* culture was diluted 1:2 (vol/vol) with *mock(RNAi)*. After seeding, the plates were protected from light and incubated at room temperature until the next day. On day three, a second set of RNAi plates (8 large plates per condition) were seeded following the same protocol as for the first set of RNAi plates. Furthermore, ∼160 N2 L4 larvae were pipetted onto each RNAi plate that was seeded the previous day. After incubation at 20°C for 22 h, the gravid adults were pipetted onto the second set of RNAi plates, let to lay eggs for 2 hours at 20°C and then removed. The synchronized progeny was incubated for three days (*mock(RNAi)* and *tag-208(RNAi)*) or four days (*prx-5(RNAi)*) at 20°C to reach the adult stage and then collected in a tube. The worm pellet was first washed with 50 ml MPEG (M9 + 0.1% Polyethylene glycol 8000 (Carl Roth)). The pellet was transferred into a smaller tube and washed two times with 1 ml of MPEG and two times with 1 ml of

M9. The samples were flash frozen in liquid nitrogen and stored at -80°C until they were analyzed by RNA-seq (see chapter 2.8).

2.5 Trimethoprim treatment

Trimethoprim (TMP) plates (30 mm) were prepared by adding TMP (Sigma) (100 mM in DMSO stock solution) to standard NGM media [Stiernagle, 2006] that was autoclaved and had cooled down to 55°C. The final concentration of TMP or DMSO (for control plates) was 1 mM. The plates were let to dry overnight at room temperature. *E. coli* OP50 was cultured in 4 ml LB overnight at 37°C and 200 rpm. The culture was pelleted and resuspended in 400 μl LB. The plates were seeded with 50 μl OP50 culture and let to dry for 30 min.

To analyze the effect of the knock-down of *lonp-2* (see chapter 3.2.2), the RNAi protocol (see chapter 2.4) was modified. The L4 larvae were not treated by RNAi, but adults that were grown on NGM plates were transferred onto RNAi plates and let to lay eggs for 4 h at 20°C and then removed. The synchronized progeny was incubated for four days at 15°C. The L4 larvae were then transferred onto NGM plates containing TMP or DMSO and incubated for 24 h at 20°C. The worms were mounted on 2% agarose pads and immobilized with M9 buffer containing 1 mM Levamisol. The anterior part of the intestine (nuclei in focus) or the hypodermis (alae in focus) of the same region were imaged using a Zeiss Axioskop 2 (100x, NA 1.3) equipped with a charge-coupled device camera (1300; Micromax) and the MetaMorph software 7.1.0.0 (Molecular Devices). The $P_{daf\text{-}22}$*YFP::dhfr*^{mut}*::PTS1* reporter was imaged with a YFP filter and 1000 ms exposure time and and $P_{vha\text{-}7}$*mCherry::PTS1* reporter was imaged with a mCherry filter and 200 ms exposure time. Furthermore, samples were collected for Western analysis (see chapter 2.6).

For the time course experiment (see chapter 3.2.3), transgenic animals expressing DHFR^{mut} were synchronized by lay-off (4 h at 20°C). L4 larvae were placed on the plates containing TMP or DMSO and incubated at 20°C. After 6 h and 24 h of treatment, the worms were mounted on 2% agarose pads and immobilized with M9 buffer containing

1 mM Levamisol. The hypodermal cells of the anterior part of the worms were imaged with the alae in focus with a YFP filter and 1000 ms exposure time using a Zeiss Axioskop 2 (100x, NA 1.3) equipped with a charge-coupled device camera (1300; Micromax) and the MetaMorph software 7.1.0.0 (Molecular Devices). After 24 h of treatment with TMP, the worms were transferred onto DMSO plates. 3 h and 6 h after the start of the washout period, they were again imaged and collected for Western analysis.

2.6 Analysis of protein levels by Western blotting

Synchronized *C. elegans* adult populations were either obtained by lay-offs or L4 larvae were picked onto a new NGM plate seeded with *E. coli* OP50 and incubated at 20°C for one day. The population was collected in a tube and washed three times with 1 ml MPEG. The *C. elegans* pellet was resuspended in 1 volume of Laemmli buffer 2x (Table 2.6). The samples were incubated for 5 min at 95°C and stored at -20°C.

Table 2.6: Laemmli Buffer (2x).

Component	Amount
Tris	0.12 g
HCl (1 M)	0.77 ml (to pH 6.8)
SDS	8.00 mg
MilliQ H_2O	1.23 ml
10% SDS	4.00 ml
Beta-Mercaptoethanol	0.14 ml
50% Glycerol	4.00 ml
Saturated Bromophenol blue	0.10 ml

The samples were centrifuged at 13,000 rpm for 1 min and the supernatant was used for SDS-PAGE (10% acrylamide). After separation by electrophoresis, the proteins were transferred to a PVDF membrane (Immobilon-P, Millipore). The membrane was blocked using 5% milk powder in TBS-T (Table 2.7) for 1 h at room temperature. The membrane was incubated with the primary antibodies overnight at 4°C and with the sec-

ondary antibodies for 45 min at room temperature. To detect Tubulin, monoclonal anti-Tubulin (1:10,000; Sigma) and horseradish peroxidase conjugated goat anti-mouse antibodies (1:7,500; BioRad #1706516) were used. HSP-6 was detected by a polyclonal anti-HSP-6 (1:5,000; [Köhler et al., 2015]) and horseradish peroxidase conjugated goat anti-rabbit antibodies (1:30,000; BioRad #1706515). To detect GFP, polyclonal anti-GFP (1:6,000; abcam ab290) and GAR-HRP antibodies (1:10,000) were used. The rabbit polyclonal anti-LONP-2 antibodies were generated using the antigenic peptide CDKFS-REIYSLIDEKEYGKLAD (LONP-2 C-terminal sequence) and subsequently affinity purified by Davids Biotechnologie and used at 1:3,000 for Western analysis. As secondary antibodies, horseradish peroxidase conjugated goat anti-rabbit antibodies (1:5,000; Bio-Rad #1706515) were used. The chemiluminescence was detected using the Amersham ECL (Prime) Western Blotting Detection Reagent (GE Healthcare) and the Chemi Doc XRS+ (BioRad). The band intensities were quantified using the Image Lab software 5.2.1.

Table 2.7: TBS-T.

Component	Amount
NaCl	8.0 g
KCl	0.2 g
Tris	3.0 g
HCl	adjust pH to 7.4
Tween 100 (Carl Roth)	0.1 ml
MilliQ H_2O	to 1 l

2.7 Lipid staining by Oil Red O

Lipid staining using the fixative dye Oil Red O (Sigma) was conducted as previously described [Escorcia et al., 2018]. Briefly, L4 larvae were picked onto a new NGM plate seeded with *E. coli* OP50 and incubated at 20°C for one day. The Oil Red O stock solution (500 mg/100 ml isopropanol) was diluted in water to 60% isopropanol and rocked

overnight. The next day, the worms were collected in a tube and washed three times with 1 ml PBST (1x PBS + 0.01% Triton X-100). The supernatant was removed, 600 μl of 40% isopropanol was added to the worm pellet and it was rocked for 3 min. The worms were centrifuged and the supernatant was removed. The Oil Red O working solution was filtered with a 22 μm PVDF filter and 600 μl of the filtered Oil Red O solution was added to the worm pellet. The samples were rocked for 2 h. The dye was removed and the worm pellet was resuspended in 600 μl PBST and rocked for 30 min to remove excess dye. The PBST was removed, the worms were resuspended in the remaining supernatant and were mounted on a microscope slide. The samples were imaged with 60 ms exposure time using a Leica MZ FLIII microscope (10x, NA 0.125) with a color-capable Nikon Digital Sight DS-Fi1 camera and the software NIS-Elements BR 3.10.

2.8 Gene expression analysis by RNA-seq

The frozen worm pellets of the RNAi experiment (see chapter 2.4) were send to Eurofins Genomics Europe Shared Services GmbH. Total RNA was extracted by the company using commercial kits with modified and optimized protocols. The library was prepared with an optimized protocol and standard Illumina adapter sequences have been used. Sequencing was performed with Illumina technology, HiSeq 4000 (read mode 1 x 50bp). The bioinformatics analysis by the company included the alignment of the RNA-Seq reads to the reference genome using Bowtie [Langmead et al., 2009]. Cufflinks, Cuffmerge and Cuffdiff was used to determine the differential expression levels. Genes were considered as significantly changed if the p-value was greater than the FDR after Benjamini-Hochberg correction for multiple testing. The data has been deposited in NCBI's Gene Expression Omnibus [Edgar et al., 2002] and is accessible through GEO Series accession number GSE156318 (https://www.ncbi.nlm.nih.gov/geo/query/acc.cgi?acc=GSE156318).

2.9 Protein quantification by LC-MS

The worm pellets of the RNAi experiment (see chapter 2.4) were treated by an initial step of sonication with glass beads (Bioruptor, Diagenode) and subsequently proteins were extracted and digested using the iST Preomics Kit (Germany). The analysis by LC-MS was conducted by our collaborator Ignasi Forné (Axel Imhoff lab; BMC Munich). The samples were injected in an RSLCnano system (Thermo) and separated in a 25-cm analytical Aurora C18 nanocolumn (75μm ID 120 Å, 1.6 μm, Ion Opticks). The effluent was directly electrosprayed into a Q Exactive HF (Thermo). MaxQuant 1.5.2.8 was used to identify proteins and quantify by LFQ. If the log2 value was >1 or $<$-1 and the p-value was $<$ 0.05 in a limma moderated t-test adjusted for multiple comparisons when compared to the control *tag-208(RNAi)*, the level of the identified protein was considered as significantly changed. The data set has been deposited to the ProteomeXchange Consortium via the PRIDE [Perez-Riverol et al., 2019] partner repository with the dataset identifier PXD014720.

2.10 Image analysis

The image analysis of the transcriptional reporter strains was performed as previously described [Rolland et al., 2019]. For the analysis of the peroxisomal number (see chapter 3.1.4) and the Oil Red O staining (see chapter 3.3.6), two-dimensional images were analyzed using Fiji/ImageJ2 [Rueden et al., 2017, Schindelin et al., 2012] with Fiji-implemented macros using the IJ1 Macro language, which were programmed by Christian Fischer (Barabra Conradt lab; LMU Munich).

To analyze the peroxisomal number, signal intensity and surface, the background of the fluorescent images was subtracted with a rolling ball radius and a binary mask of the image was generated using the Otsu automated threshold. Next, noise was removed by applying the Particle Analyzer with a minimum size of four pixels to the inverted mask. The original image was multiplied with the mask and the number of peroxisomes was measured by the 3D Objects counter plug-in for ImageJ.

The macro to analyze the Oil Red O staining was based on the image quantification performed by O'Rourke *et al.* [O'Rourke et al., 2009]. However, to improve the accuracy of the IsoData autothresholding to generate the whole worm mask, a maximum filter of five pixels was applied prior to top-hat filtering.

2.11 Statistical analysis

Statistical analysis was performed using the software R version 3.6.1 [R Core Team, 2019] with the packages *Rmisc* [Hope, Ryan M., 2013], *car* [Fox, John and Weisberg, Sanford, 2019], *userfriendlyscience* [Peters, Gjalt-Jorn Ygram, 2017] and *PMCMR* [Pohlert, Thorsten, 2014]. Normal distribution of the data was analyzed by diagnostic plots and additionally by a Shapiro-Wilk test. If two independent groups were compared, an F-test was used to test for equal variance. In the case of normal distribution and equal variance, a two sample t-test was applied to compare two independent groups. In the case of not normally distributed data, a Mann-Whitney-U test was used and in the case of heteroscedasticity, a Welch two sample t-test was used. If more than two independent groups were compared, a Brown-Forsythe test was used to test for equal variance. Data showing a normal distribution and equal variance was analyzed using a one-way ANOVA with Tukey's multiple comparison. Non-parametric data was analyzed using a Kruskal-Wallis test with Dunns's multiple comparison and Holm's p-value adjustment. In the case of heteroscedasticity, a Welch's ANOVA with Games-Howell post hoc test was used.

3

RESULTS

3.1 Analysis of peroxisomes in *C. elegans* by fluorescent microscopy

3.1.1 Peroxisomes are present in hypodermal cells in *C. elegans*

Previous studies have shown that peroxisomes are mostly present in hypodermal and intestinal cells in *C. elegans* [Yokota et al., 2002, Petriv et al., 2002]. To confirm the hypodermal localization of peroxisomes, I generated a reporter strain expressing GFP fused to the tripeptide SKL, which acts as a peroxisomal targeting sequence (PTS1) in *C. elegans* [Petriv et al., 2002]. The GFP::PTS1 fusion construct labels the peroxisomal matrix with GFP. Furthermore, the strain expressed the fusion construct mKate2::PXMP-4 to label the peroxisomal membrane with mKate2. The mammalian homolog of PXMP-4 has been shown to localize to the peroxisomal membrane [Pinto et al., 2006]. The constructs were placed under the control of the *vha-7* promoter, which is expressed in hypodermal cells. Fluorescent microscopy analysis of adult animals of the reporter strain showed a punctate signal in both channels, which is characteristic of peroxisomes (Figure 3.1). This also shows that PXMP-4 localizes to peroxisomes like its mammalian homolog. The GFP and mKate2 signals mostly co-localized. However, sometimes the peroxisomes were only labeled by mKate2, but not by GFP (Figure 3.1, arrowheads). These peroxisomes might represent pre-peroxisomes that are not yet import competent. Taken together, I confirmed that peroxisomes are present in hypodermal cells in *C. elegans*.

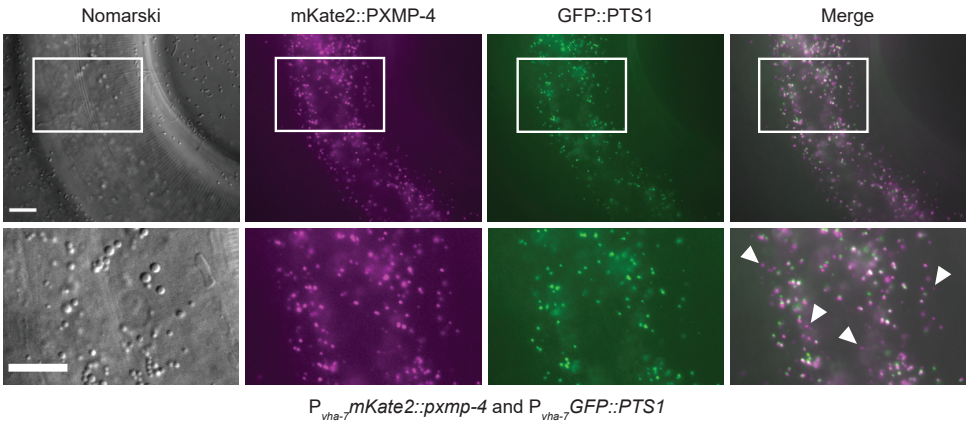

Figure 3.1: Labeling of peroxisomes in hypodermal cells. Analysis of adult animals carrying the $P_{vha\text{-}7}$*GFP::PTS1* and $P_{vha\text{-}7}$*mKate2::pxmp-4* (*bcIs140*) reporters by DIC and fluorescent microscopy. Arrowheads show peroxisomes only labeled by mKate2 and not by GFP. The scale bar represents 10 μm.

3.1.2 The peroxisomal matrix protein DAF-22 localizes to hypodermal cells and the intestine

To determine the tissue-specific localization of peroxisomes, I generated a reporter expressing the peroxisomal matrix protein DAF-22 fused to mKate2 under its endogenous promoter and 3'UTR. A similar construct has previously been used to label peroxisomes [Butcher et al., 2009]. Analysis of adult animals of the $P_{daf\text{-}22}$*mKate2::daf-22* (*bcSi117*) reporter by fluorescent microscopy revealed that peroxisomes that contain DAF-22 were mainly present in hypodermal and intestinal cells (Figure 3.2). This confirms the results of the analysis of the $P_{vha\text{-}7}$*GFP::PTS1* and $P_{vha\text{-}7}$*mKate2::pxmp-4* (*bcIs140*) reporter (Figure 3.1) and the observations made in previous studies [Yokota et al., 2002, Petriv et al., 2002, Butcher et al., 2007]. The number of peroxisomes was higher in the intestine than in hypodermal cells (Figure 3.2). In both tissues, the peroxisomes showed some variation in size and signal intensity. Interestingly, in head muscle cells, only very few peroxisomes with weak signal intensity were present (Figure 3.2, arrowhead). Due to the expression of the reporter in the hypodermal cells, it was not possible to determine if middle body muscle cells also contain peroxisomes. Similarly, it was difficult to determine the exact location of the neurons. However, it seems that head neurons do not contain peroxisomes. To label the different tissues by a fluorescent marker would help to identify the right tissue and thus could give a more reliable result. The results suggest that, like previously reported, peroxisomes are mostly present in the intestinal and hypodermal cells of *C. elegans* adult animals.

3.1.3 Knock-down of *prx-5* leads to a reduction of peroxisomal matrix protein import in the intestine

PRX-5 is required for the import of peroxisomal matrix proteins [Petriv et al., 2002]. To examine the effect of the knock-down of *prx-5* on peroxisomal matrix protein import, I generated a reporter strain expressing mKate2::DAF-22 and GFP::PXMP-4 under the control of the *daf-22* promoter (Figure 3.3A). L4 larvae carrying the $P_{daf\text{-}22}$*mKate2::daf-22* and $P_{daf\text{-}22}$*GFP::pxmp-4* reporters were subjected to *prx-5(RNAi)* or the negative con-

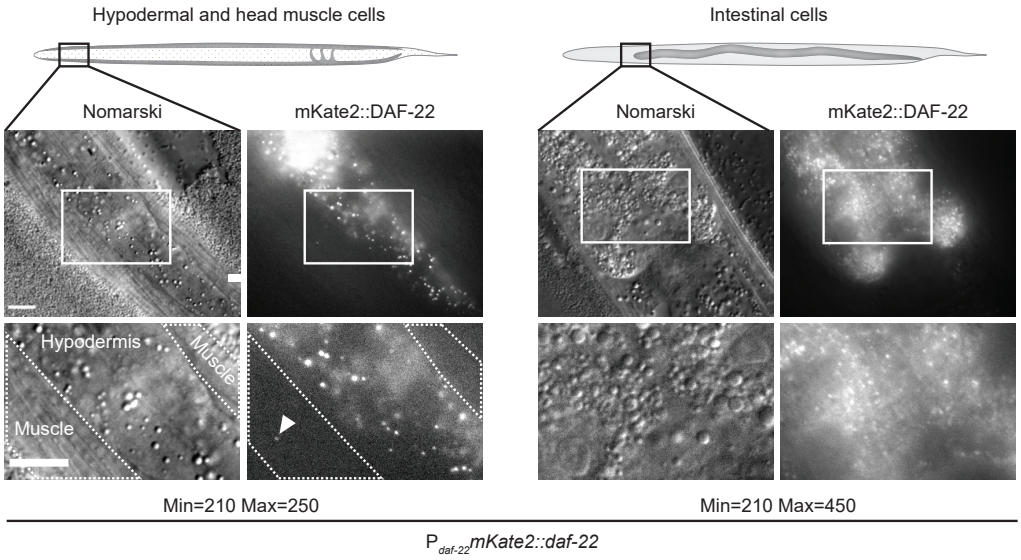

Figure 3.2: Tissue-specific localization of the peroxisomal matrix protein DAF-22. Analysis of adult animals carrying the $P_{daf\text{-}22}$*mKate2::daf-22* (*bcSi117*) reporter by DIC and fluorescent microscopy. In the left schematic, hypodermal cells are highlighted with dots and muscle cells in grey. Both cell types are present in the same microscopy image. The arrowhead points at a peroxisome in a muscle cell. In the right schematic, the intestine is highlighted in grey. The different intensity values (Min and Max) are indicated and the scale bar represents 10 μm.

trol *tag-208(RNAi)*, which encodes the *C. elegans* homolog of human Sorbin. To reduce the slow-growth phenotype, *prx-5(RNAi)* was diluted with *tag-208(RNAi)*, which results in a ∼60% reduction of PRX-5 protein (see proteomic analysis in chapter 3.3.10). The adults of the next generation were analyzed by confocal microscopy. In intestinal cells, the knock-down of *prx-5* led in the majority of analyzed animals (77%) to a partial block of the import of mKate2::DAF-22 (Figure 3.3B, C). The remaining animals either showed a complete block of import (14%) or the import was not affected (9%). In contrast, in hypodermal cells, the import of mKate2::DAF-22 was not affected by *prx-5(RNAi)* (Figure 3.3C). However, qualitative analysis of the images suggested that the number of membrane-labeled peroxisomes was higher under *prx-5(RNAi)* conditions compared to *tag-208(RNAi)*. Since the expression of the reporter in hypodermal cells was weak, it was not possible to analyze this effect quantitatively. To summarize, the partial knock-down of *prx-5* leads to a reduction in peroxisomal matrix protein import in the intestine.

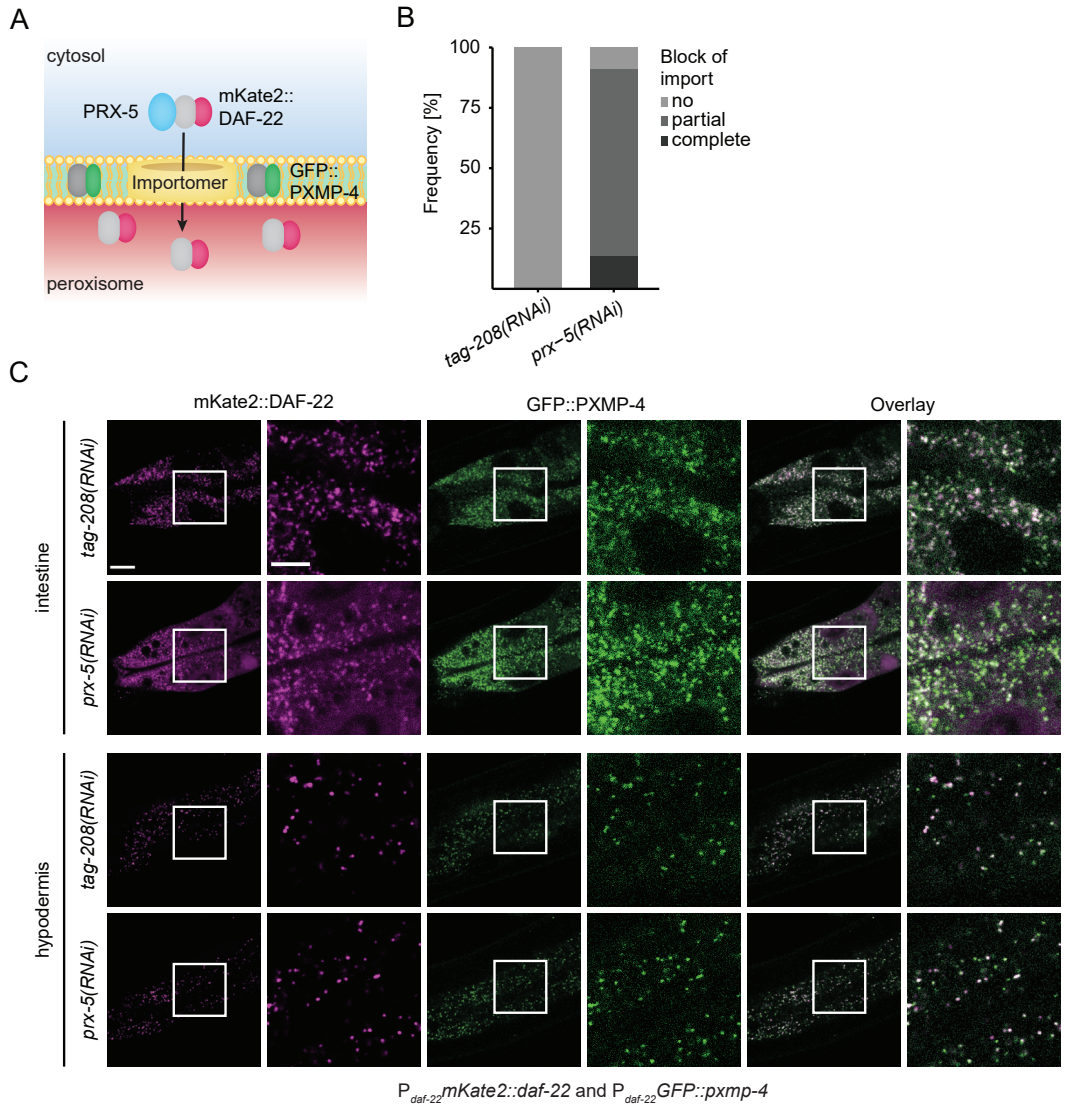

Figure 3.3: Knock-down of *prx-5* leads to a reduction of peroxisomal matrix protein import in the intestine. (A) Schematic representation of the $P_{daf\text{-}22}$*mKate2::daf-22* and $P_{daf\text{-}22}$*GFP::pxmp-4* reporters. (B) L4 larvae carrying the $P_{daf\text{-}22}$*mKate2::daf-22* and $P_{daf\text{-}22}$*GFP::pxmp-4* reporters were subjected to *tag-208(RNAi)* or *prx-5(RNAi)* and adults of the next generation were analyzed by confocal microscopy. The *prx-5(RNAi)* was diluted 1:2 with *tag-208(RNAi)* to reduce the slow growth phenotype. Semi-quantitative analysis of the mKate2::DAF-22 import upon *prx-5(RNAi)* in intestinal cells. (n=22 (n=number of animals analyzed in 3 independent experiments)). (C) Representative images of the experiment. The scale bar represents 10 μm and 5 μm in the enlarged images. For the intestinal cells, representative images of a partial block of mKate2::DAF-22 import upon *prx-5(RNAi)* is shown.

3.1.4 Reduced peroxisomal biogenesis induces an increase in the peroxisomal number in the hypodermis

To quantify the the effect of *prx-5(RNAi)* on the peroxisomal number in hypodermal cells, I used the $P_{vha\text{-}7}$*GFP::PTS1* and $P_{vha\text{-}7}$*mKate2::pxmp-4* (*bcIs140*) multi-copy reporter strain (see chapter 3.1.1). Additionally to *prx-5(RNAi)*, the effect of the knock-down of *prx-19* on peroxisomal number was analyzed. *prx-19* encodes a homolog of the human receptor for peroxisomal membrane protein insertion *PEX19* [Petriv et al., 2002]. L4 larvae carrying the $P_{vha\text{-}7}$*GFP::PTS1* and $P_{vha\text{-}7}$*mKate2::pxmp-4* (*bcIs140*) reporters were subjected to the different RNAi and adults of the next generation were analyzed by fluorescence microscopy. The fluorescence intensity, size and number of peroxisomes in the images was quantified in the GFP and mKate2 channel using a Fiji-implemented macro. The negative control *tag-208(RNAi)* showed the same number of GFP::PTS1 or mKate2::PXMP-4 labeled peroxisomes as the negative control mock (RNAi bacteria carrying the empty vector L4440) (Figure 3.4B). Knock-down of *prx-5* and *prx-19* did not lead to a significant change in the number of GFP::PTS1 labeled peroxisomes compared to *tag-208(RNAi)* (Figure 3.4A,C). In contrast, the number of peroxisomes labeled by mKate2::PXMP-4 increased about 1.5-fold compared to the control. Thus, about one third of the peroxisomes detected in the mKate2 channel did not import GFP::PTS1.

Activation of the mammalian PPARα leads to increased peroxisome proliferation [Reddy and Chu, 1996]. In *C. elegans*, the nuclear hormone receptor NHR-49 is a functional homolog of PPARα [Gilst et al., 2005]. Therefore, we asked if NHR-49 is required for the increase in peroxisomal abundance upon knock-down of *prx-5*. A double RNAi experiment showed that *prx-5(RNAi)* led to an increase in mKate2::PXMP-4 labeled peroxisomes, whereas the additional knock-down of *nhr-49* suppressed the response and the peroxisomal number was similar to the control *tag-208(RNAi)* (Figure 3.4D). Furthermore, I observed that a knock-down of *nhr-49* in the control (*nhr-49(RNAi)* + *tag-208(RNAi)*) led to a decrease in the number of peroxisomes labeled with mKate2::PXMP-4. This suggests that the peroxisomal number is dependent on NHR-49.

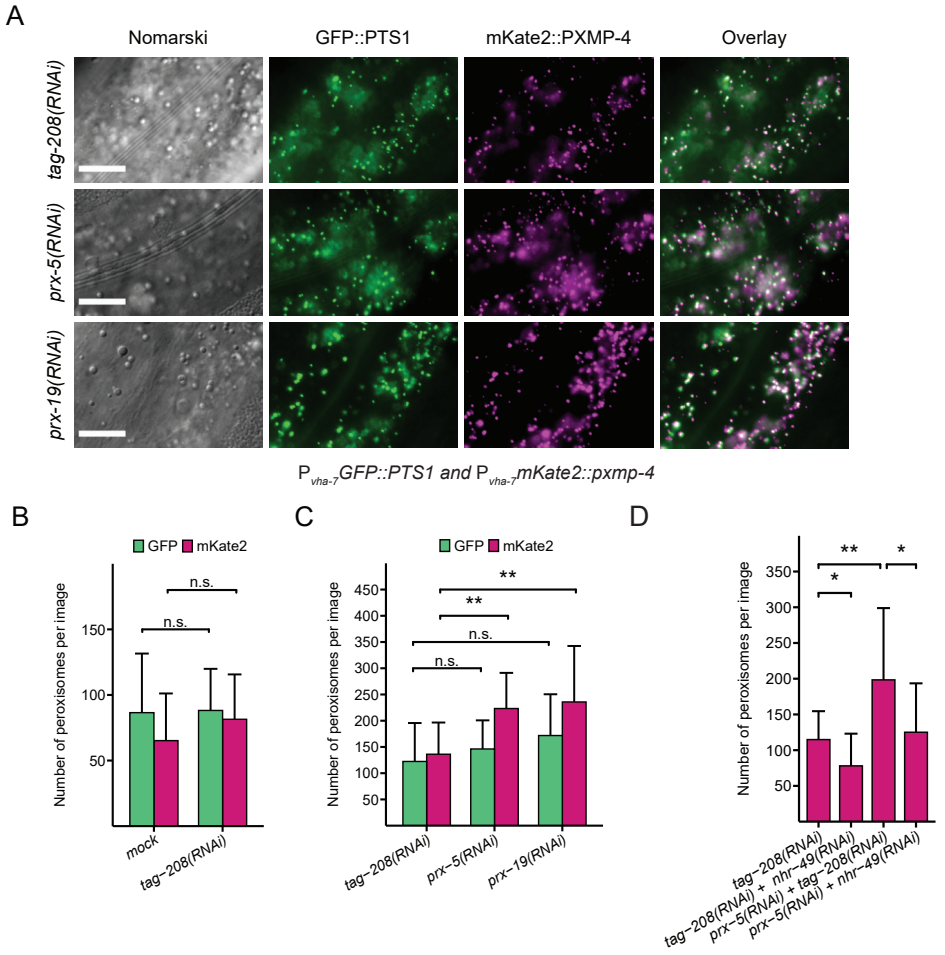

Figure 3.4: Perturbation of peroxisomal biogenesis leads to an increase in peroxisomal abundance, which is dependent on the transcription factor NHR-49. (A) L4 larvae carrying the $P_{vha\text{-}7}$*GFP::PTS1* and $P_{vha\text{-}7}$*mKate2::pxmp-4* (*bcIs140*) reporters were subjected to different RNAi. The RNAi clones were diluted 1:2 with *tag-208(RNAi)* to reduce the slow growth phenotype. Adults of the next generation were analyzed by DIC and fluorescent microscopy. The scale bar represents 10 μm. (B) The number of peroxisomes per image of the two controls mock and *tag-208(RNAi)* was quantified in the GFP or mKate2 channel (n=11-16 (n=total number of animals analyzed from 3 independent experiments); mean and SD are shown; n.s.=not significant by a two sample t-test). (C) The number of peroxisomes per image was quantified in the GFP or mKate2 channel (n=13-20 (n=total number of animals analyzed from 3 independent experiments); mean and SD are shown; n.s.=not significant and ** $p<0.01$ by a Kruskal-Wallis test with Dunn's post hoc test). (D) Dependence of the peroxisomal abundance on NHR-49. The RNAi clones were diluted 1:2 with the RNAi clone indicated in the x-axis label. (n=18 (n=total number of animals analyzed from 3 independent experiments); mean and SD are shown; n.s.=not significant, * $p<0.05$ and ** $p<0.01$ by Welch's ANOVA with Games-Howell post hoc test.)

Next, I analyzed the effect of knock-down of *prx-5* and *prx-19* on the fluorescence intensity and peroxisome size. Knock-down of both peroxins led to a slight increase in the fluorescence intensity of the GFP::PTS1 labeled peroxisomes (Figure 3.5A). This suggests that some peroxisomes might have an increased import to compensate for the non-functional peroxisomes. The median of the measured mKate2 fluorescence intensities was similar in all three RNAi conditions. However, upon *prx-19(RNAi)*, the proportion of peroxisomes with weak mKate2 signal was higher than in the control *tag-208(RNAi)*. Knock-down of both peroxins did not change the distribution of the size of the peroxisomes measured in both channels (Figure 3.5B). Taken together, a perturbation of peroxisomal biogenesis leads to an increase in peroxisomal abundance. However, not all peroxisomes are import competent. Furthermore, upon reduction of the receptor PRX-19, a fraction of peroxisomes inserts less peroxisomal membrane proteins.

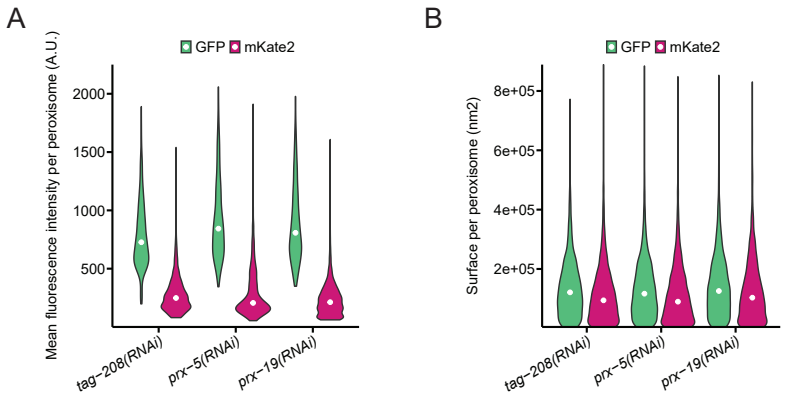

Figure 3.5: Perturbation of peroxisomal biogenesis affects the import of GFP::PTS1 and the insertion of mKate2::PXMP-4. The images of the experiment shown in Figure 3.4 were analyzed for an effect on peroxisomal fluorescence intensity and size. (A) The violin plot shows the distribution of the fluorescence intensity of the peroxisomes quantified in the GFP or mKate2 channel. The white dot represents the median. (n=1713-4465 (n=total number of peroxisomes analyzed from 3 independent experiments)). (B) The violin plot shows the distribution of the size of the peroxisomes quantified in the GFP or mKate2 channel. The white dot represents the median. (n=1713-4465 (n=total number of peroxisomes analyzed from 3 independent experiments)).

3.1.5 The *prx-5(tm4948)* loss of function mutation causes a block in peroxisomal matrix protein import and affects peroxisomal morphology

To test the effect of the loss of the import receptor PRX-5 on peroxisomal biogenesis, I crossed the *prx-5(tm4948)* loss of function allele into the $P_{vha\text{-}7}$*GFP::PTS1* and

$P_{vha\text{-}7}$*mKate2::pxmp-4* (*bcIs140*) reporter strain. The *prx-5(tm4948)* allele is a 437 bp deletion that affects the first two exons of *prx-5*. Upon loss of PRX-5, the import of GFP::PTS1 was impaired and the animals showed a cytosolic GFP signal (Figure 3.6). The animals carrying the *prx-5(tm4948)* mutation showed two different phenotypes in the mKate2 channel. Either the peroxisomes were very large and showed high mKate2 intensity or their size was similar to wild-type but some of the peroxisomes were elongated. Taken together, a loss of matrix protein import induces changes in peroxisomal morphology. In contrast, a mild reduction of peroxisomal matrix protein import by RNAi leads to an NHR-49-dependent increase in peroxisomal abundance.

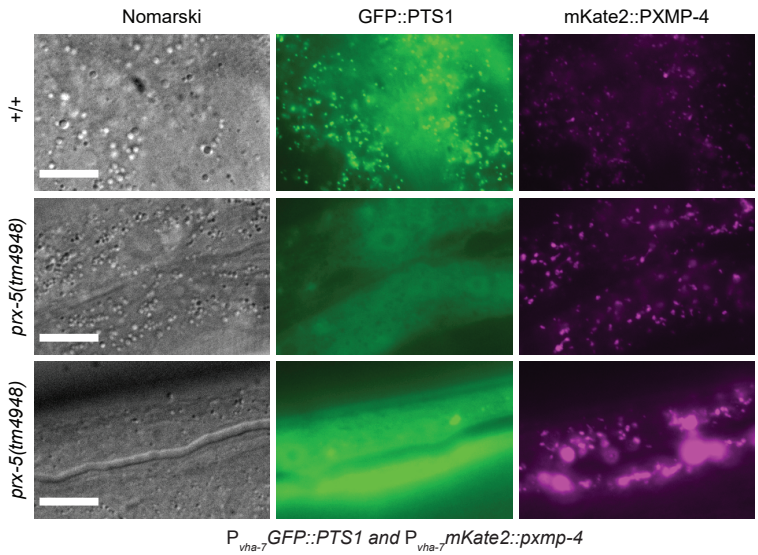

Figure 3.6: The *prx-5(tm4948)* loss of function mutation affects peroxisomal morphology. The $P_{vha\text{-}7}$*GFP::PTS1* and $P_{vha\text{-}7}$*mKate2::pxmp-4* (*bcIs140*) reporter carrying the *prx-5(tm4948)* mutation was analyzed by DIC and fluorescence microscopy. Representative images of two different phenotypes are shown. The scale bar represents 10 μm. (n=2 (n=number of independent experiments)).

3.2 Characterization of the peroxisomal Lon protease in *C. elegans*

3.2.1 The peroxisomal Lon protease homolog LONP-2 is targeted to peroxisomes

The *C. elegans* protein LONP-2 shows 35.3% identity and 65.9% similarity to the human peroxisomal Lon protease (LALIGN; [Huang and Miller, 1991]). LONP-2 has an N-terminal Lon substrate binding domain, an AAA+ ATPase domain and a C-terminal

proteolytic domain (InterPro) (Figure 3.7A). Furthermore, it has a C-terminal putative peroxisomal targeting sequence AKL. To confirm that LONP-2 localizes to peroxisomes in *C. elegans*, I generated a reporter strain co-expressing LONP-2 tagged with GFP at the N-terminus and a peroxisomal membrane marker mKate2::PXMP-4 in hypodermal cells. Analysis of the reporter strain by fluorescent microscopy showed that the GFP and mKate2 signals co-localized (Figure 3.7B). This indicates that LONP-2 is targeted to peroxisomes in *C. elegans*.

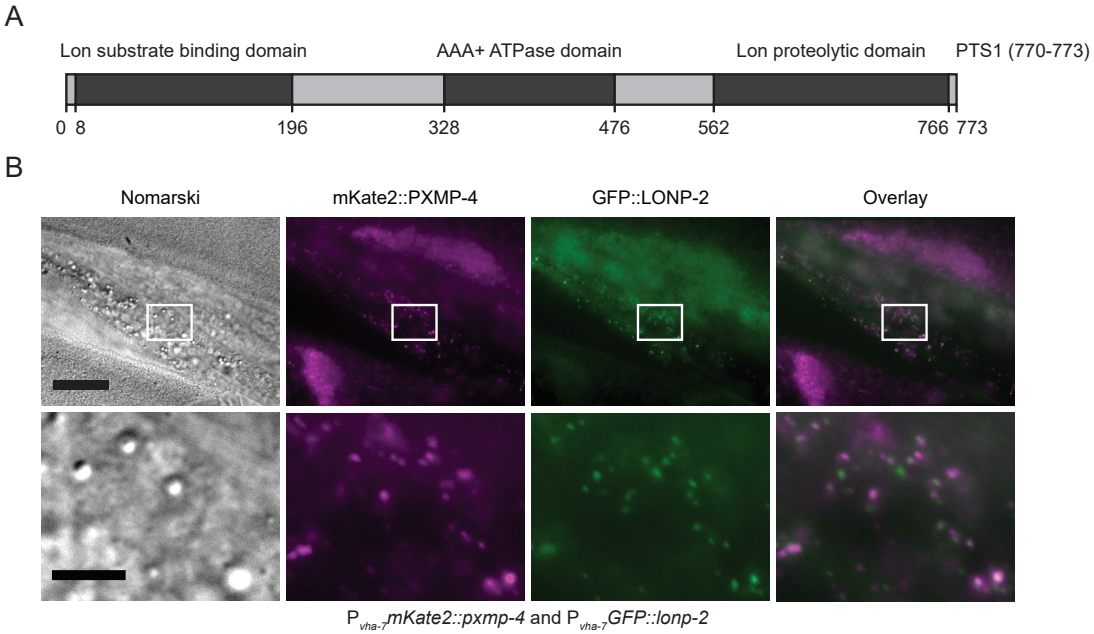

Figure 3.7: Sub-cellular localization of the *C. elegans* peroxisomal Lon protease LONP-2. (A) Predicted functional domains of LONP-2 (InterPro). The numbers represent the amino acids. (B) Analysis of the $P_{vha\text{-}7}$*mKate2::pxmp-4* and $P_{vha\text{-}7}$*GFP::lonp-2* (*bcEx1305;bcEx1316*) reporter by DIC and fluorescent microscopy. The scale bar represents 20 μm (top panels) or 5 μm in the enlarged images (bottom panels).

3.2.2 The degradation of an unfolded protein is dependent on the peroxisomal Lon protease

The peroxisomal Lon protease degrades non-functional proteins in yeast and fungi [Bartoszewska et al., 2012, Aksam et al., 2007]. Furthermore, it shows chaperone activity *in vitro* [Bartoszewska et al., 2012]. The function of the peroxisomal Lon protease in *C. elegans* has not been described so far. To express an unfolded protein in peroxisomes, I used a mutant form of the *E. coli* dihydrofolate reductase ($DHFR^{mut}$), which is without binding

of a stabilizing ligand constitutively degraded by the 26S proteasome. Upon addition of the ligand Trimethoprim (TMP), $DHFR^{mut}$ is stabilized [Cho et al., 2013]. By fusion of $DHFR^{mut}$ to YFP, the stability of the protein can be monitored by fluorescence microscopy and Western blotting. To target YFP::$DHFR^{mut}$ to peroxisomes, a C-terminal peroxisomal targeting sequence (PTS1) was added (Figure 3.8A). The YFP::$DHFR^{mut}$::PTS1 was expressed under the control of the promotor of the peroxisomal thiolase *daf-22*. To confirm the peroxisomal localization, I injected a reporter to label the hypodermal peroxisomes ($P_{vha\text{-}7}$*mCherry::PTS1*) into the $P_{daf\text{-}22}$*YFP::dhfr^{mut}::PTS1* (*bcSi112*) strain. Upon treatment of the resulting reporter strain with TMP (1 mM in DMSO) for 24 h, the construct was stabilized and the YFP signal intensity strongly increased compared to the DMSO control (Figure 3.8B). The co-localization of the YFP signal with the mCherry signal confirms that YFP::$DHFR^{mut}$::PTS1 is targeted to peroxisomes.

To test if the degradation of $DHFR^{mut}$ is dependent on the peroxisomal Lon protease, the $P_{daf\text{-}22}$*YFP::dhfr^{mut}::PTS1* (*bcSi112*) reporter strain was treated with *lonp-2(RNAi)* or the negative control mock for one generation. The L4 larvae were then transferred onto TMP or DMSO control plates. After 24 h of incubation, whole worm lysates were analyzed by Western blotting. The analysis showed that the knock-down of *lonp-2* was efficient (Figure 3.9A). Upon *lonp-2(RNAi)*, the LONP-2 band completely disappeared. Hardly any YFP signal was visible in the samples of animals that were grown on mock and DMSO plates (Figure 3.9A). In contrast, treatment by mock and TMP led to a stabilization of $DHFR^{mut}$ and thus to an increase in the YFP signal. Interestingly, also the knock-down of *lonp-2* led to a strong increase in the YFP signal in animals grown on DMSO plates. This indicates that LONP-2 is required for the degradation of destabilized $DHFR^{mut}$ in peroxisomes. Although $DHFR^{mut}$ is stabilized by TMP treatment, a further increase in YFP signal upon *lonp-2(RNAi)* could be observed. It is possible that the stabilization by TMP is not complete and that there is still a fraction of unfolded $DHFR^{mut}$ that is imported into peroxisomes and is degraded by LONP-2. Another possibility is that LONP-2 is involved in the degradation of proteins that are mislocalized to peroxisomes.

To get an insight about the sub-cellular localization of the accumulated YFP, the treated animals were analyzed by fluorescent microscopy. Images of the anterior part

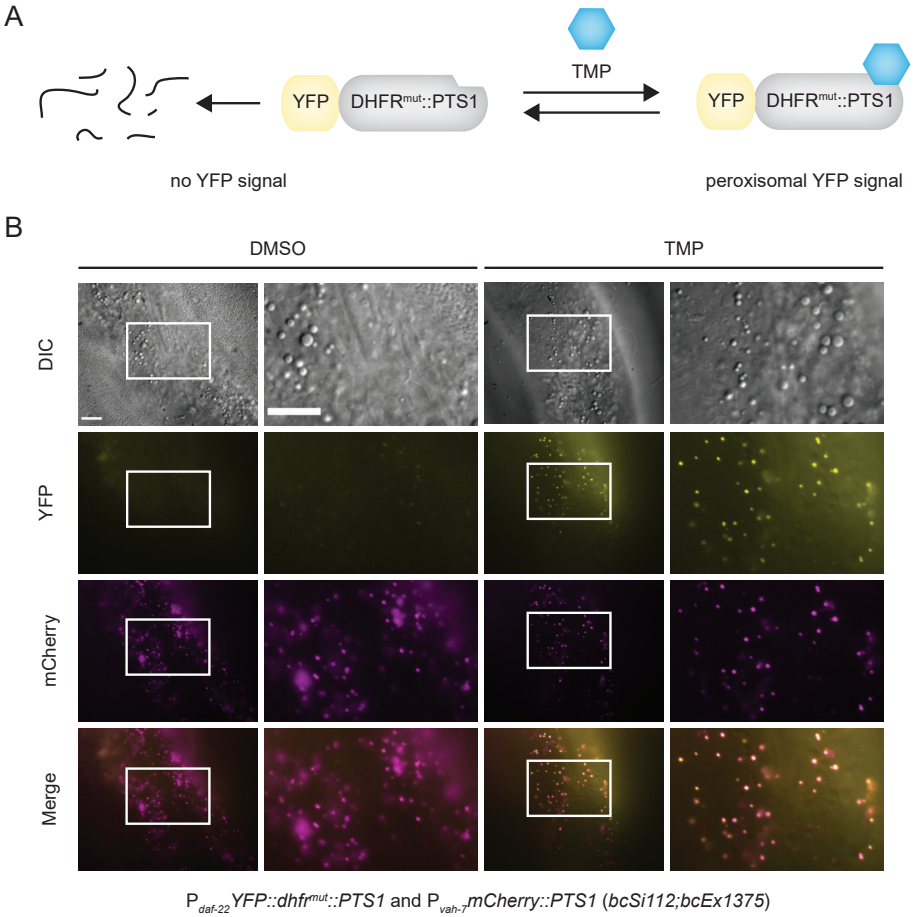

Figure 3.8: Reporter to express an unfolded protein in peroxisomes. (A) Schematic of the stabilization of DHFR^{mut} by Trimethoprim (TMP). DHFR^{mut} is fused to a peroxisomal targeting sequence (PTS1). In the absence of the stabilizing ligand, the construct is degraded by the proteasome. Upon addition of TMP, the construct is stabilized and localizes to peroxisomes. (B) YFP::DHFR^{mut}::PTS1 localizes to peroxisomes. Three independent lines carrying the reporter P$_{daf\text{-}22}$*YFP::dhfr^{mut}::PTS1* and P$_{vha\text{-}7}$*mCherry::PTS1* (*bcSi112;bcEx1375*) were treated for 24 h by TMP or DMSO control and were analyzed by DIC and fluorescent microscopy. Representative images of one line are shown. The scale bar represents 10 μm.

of the intestine of 15 animals per condition were taken. Moreover, the peroxisomes in the hypodermis of the same region of the animal were imaged, since they are more suitable for quantitative analysis. The intestinal peroxisomes showed an overall increase in YFP signal upon *lonp-2(RNAi)* or TMP treatment, similar to the result of the Western analysis (Figure 3.9B). Upon knock-down of *lonp-2*, some peroxisomes showed a very strong YFP signal. The qualitative observation was confirmed by the quantitative analysis of the hypodermal peroxisomes. The total number of peroxisomes and the fluorescence intensity per peroxisome was quantified by an Fiji-implemented macro. The overall signal intensity per

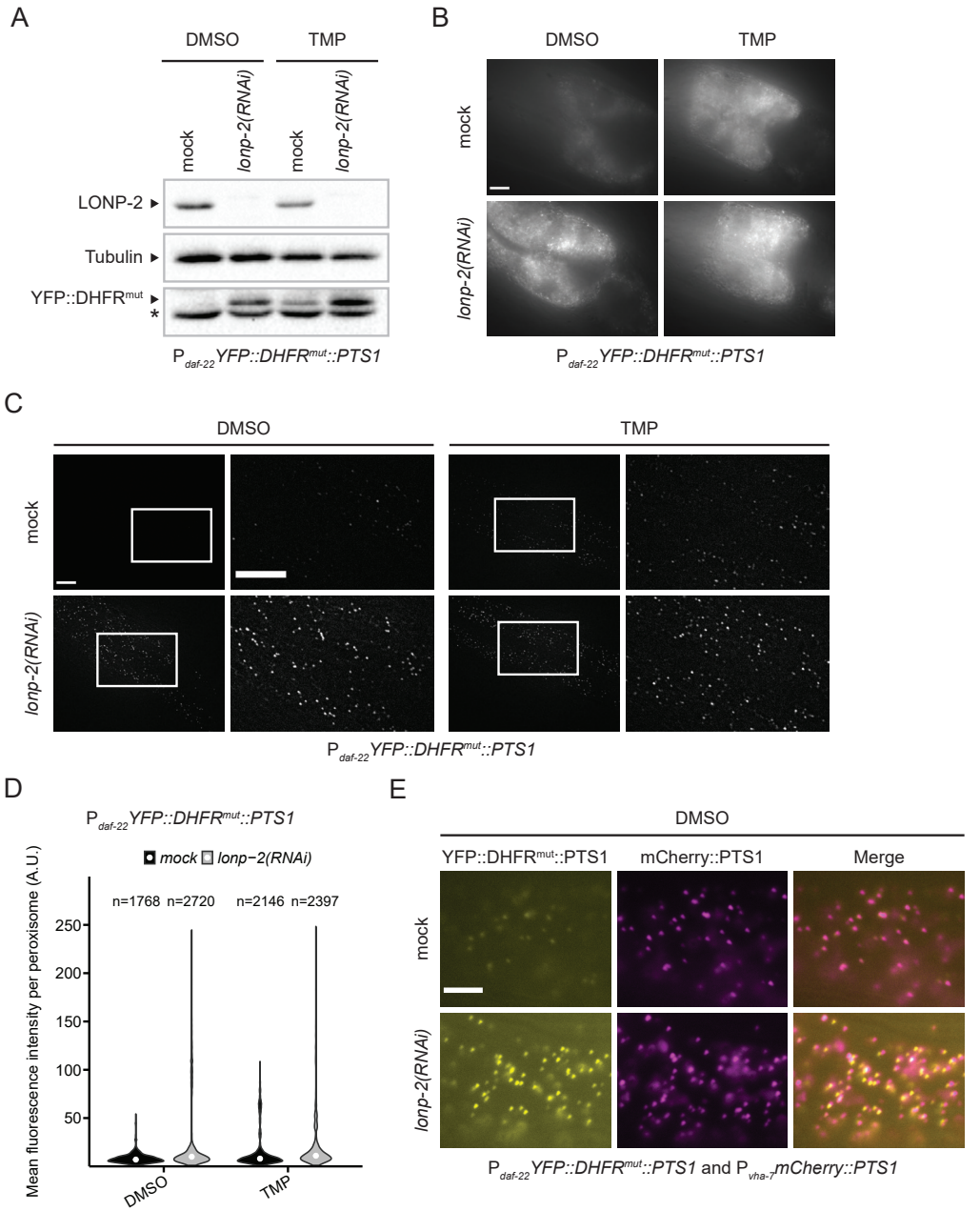

Figure 3.9: Dependence of the degradation of DHFR^{mut} on LONP-2. The P$_{daf\text{-}22}$*YFP::dhfr^{mut}::PTS1* (*bcSi112*) reporter was treated with mock (empty vector control) or *lonp-2(RNAi)* for one generation and then L4 larvae were transferred onto TMP or DMSO control plates. After 24 h of incubation, the adults were analyzed by fluorescent microscopy and Western blotting. (A) Western blotting analysis of the RNAi experiment. A representative blot of three independent experiments is shown. The non-specific band by the GFP antibody is marked by an asterisks. (B) Analysis of the YFP signal in intestinal cells. The scale bar represents 10 μm. Representative images of three independent experiments are shown. (C) Analysis of the YFP signal in hypodermal cells. Fiji background subtraction with a rolling ball radius of five pixels was applied. The scale bar represents 10 μm. Representative images of three independent experiments are shown. (D) The violin plot shows the distribution of the fluorescence intensity of the peroxisomes in hypodermal cells. The white dot represents the median. n=total number of peroxisomes analyzed from 3 independent experiments. *(Continued on the next page.)*

Figure 3.9: *Continued*: (E) Fluorescent microscopy analysis of the $P_{daf\text{-}22}$*YFP::dhfr*^{mut}*::PTS1* and $P_{vha\text{-}7}$*mCherry::PTS1* (*bcSi112;bcEx1375*) reporter treated with mock control or *lonp-2(RNAi)*. The scale bar represents 5 μm. Representative images of one experiment are shown.

peroxisome slightly increased and, additionally, a small fraction of peroxisomes showed a very strong YFP signal upon the knock-down of *lonp-2* (Figure 3.9C, D). Additionally, the number of YFP-positive peroxisomes increased upon *lonp-2(RNAi)* or TMP treatment. Qualitative analysis of the $P_{daf\text{-}22}$*YFP::dhfr*^{mut}*::PTS1* and $P_{vha\text{-}7}$*mCherry::PTS1* (*bcSi112;bcEx1375*) reporter revealed that not all mCherry-positive peroxisomes also contained YFP in mock treated animals, whereas the co-localization was almost complete in *lonp-2(RNAi)* treated animals (Figure 3.9E). Since this experiment was only done once, this observation is only a preliminary result but it suggests that the increase in YFP signal observed in whole worm lysates is caused by an accumulation of YFP in the peroxisome.

3.2.3 The expression of an unfolded protein does not affect endogenous LONP-2 levels

To test if LONP-2 is up-regulated to degrade unfolded proteins, I analyzed endogenous LONP-2 levels upon expression of DHFR^{mut} in peroxisomes. The L4 larvae of the $P_{daf\text{-}22}$*YFP::dhfr*^{mut}*::PTS1* (*bcSi112*) reporter strain were transferred onto TMP or DMSO control plates. The reporter strain was analyzed after 6 h and 24 h of TMP treatment by fluorescent microscopy and Western blotting. The transfer onto TMP should stabilize DHFR^{mut}. Thus, the load of unfolded proteins is reduced in these peroxisomes, which might lead to a reduction of the LONP-2 levels. After 24 h growth on TMP plates, the worms were transferred to DMSO plates. The effect of the washout of TMP was analyzed at 3 h and 6 h post-transfer. Upon washout of TMP, the levels of unfolded proteins in peroxisomes increase, which in turn might lead to an increase in LONP-2 levels. Fluorescent microscopy showed that the number of peroxisomes containing YFP increased upon TMP treatment (Figure 3.10A). When DHFR^{mut} was destabilized during the washout, the number of YFP-positive peroxisomes again decreased. This was also reflected by an increasing and subsequent decreasing band intensity of YFP in the Western blotting (Figure 3.10B). The effect of the stabilization and unfolding of DHFR^{mut} on endogenous LONP-2

levels was also analyzed by Western blotting. The LONP-2 levels upon TMP treatment or washout did not change compared to the DMSO controls (Figure 3.10B). This experiment indicates that the endogenous level of the peroxisomal Lon protease does not adjust to the amount of unfolded protein present in the organelle under our experimental conditions.

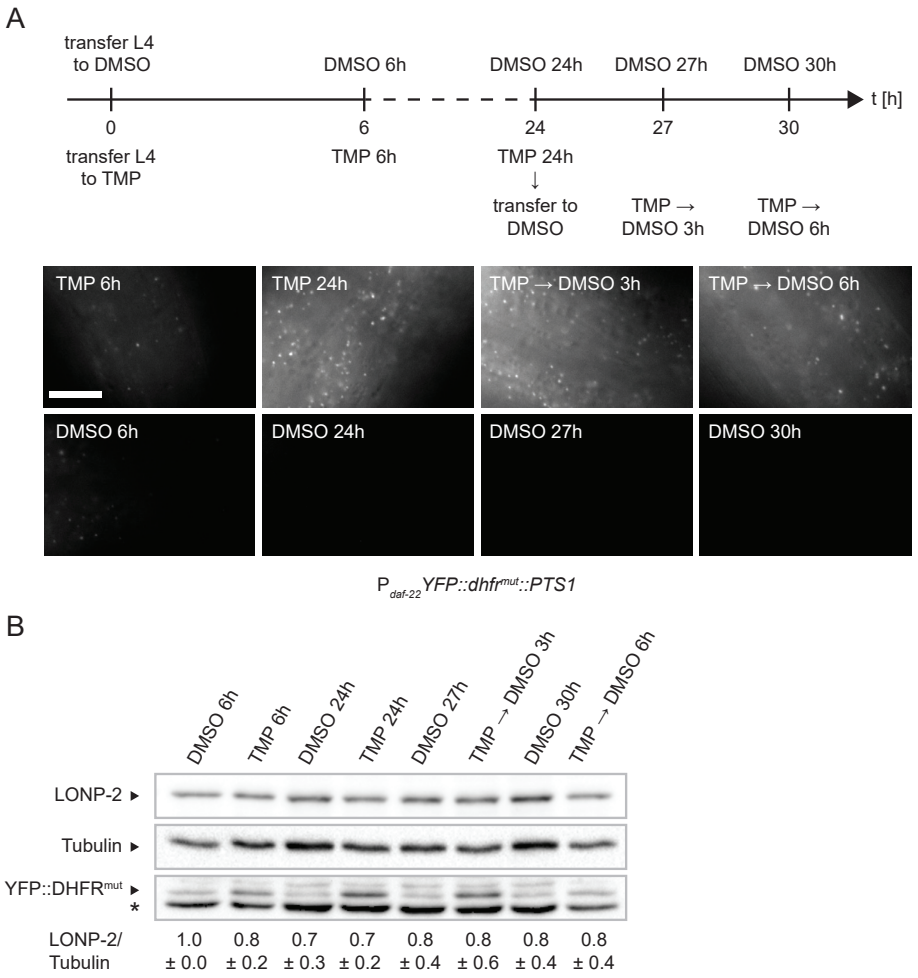

Figure 3.10: Expression of DHFR^{mut} targeted to peroxisomes. (A) Time course of the stabilization of DHFR^{mut} by TMP. L4 larvae of the reporter P$_{daf\text{-}22}$*YFP::dhfr^{mut}::PTS1* (*bcSi112*) were treated for 24 h with TMP and then transferred to DMSO plates for wash out. Additionally, control worms remained continuously on DMSO plates. Analysis of the YFP signal in hypodermal cells by fluorescent microscopy. Representative images of three independent experiments are shown. The scale bar represents 10 μm. (B) Analysis of the time course experiment by Western blotting. The LONP-2 band intensities were normalized to the respective Tubulin loading controls and quantified relative to the DMSO 6 h control. The non-specific band by the GFP antibody is marked by an asterisks. (Mean and SD are shown. n=3 (n=number of independent experiments)).

3.3 The peroxisomal retrograde signaling pathway

3.3.1 Perturbation of peroxisomal biogenesis induces the peroxisomal retrograde signaling

The aim of the study is to analyze the peroxisomal stress response. We hypothesized that peroxisomal stress might induce a retrograde signaling similar to stress responses that have been described for other organelles. It has been shown that stress in other organelles leads to the transcriptional up-regulation of protease and chaperone genes (reviewed in [Sasaki and Yoshida, 2015]). To test if the peroxisomal Lon protease is also part of such a retrograde signaling for peroxisomes in *C. elegans*, I used different transcriptional reporter strains expressing a construct of 1 kb of the putative promoter of the peroxisomal Lon protease *lonp-2* fused to GFP ($P_{lonp\text{-}2}GFP$) (Figure 3.11A). Two strains contained multi-copy insertion alleles (*bcIs126* and *bcIs128*) and one strain had a single-copy insertion allele (*bcSi75*) of the $P_{lonp\text{-}2}GFP$ construct. To induce peroxisomal stress, I impaired the peroxisomal biogenesis by individual knock-down of the 11 *C. elegans* homologs of the human peroxins. L4 larvae of the $P_{lonp\text{-}2}GFP$ (*bcIs128*) multi-copy reporter strain were subjected to the different peroxin knock-downs and the GFP expression was analyzed by fluorescent microscopy in adult animals of the next generation. The GFP intensity was quantified and normalized to the negative control *tag-208(RNAi)*. Knock-down of *tag-208* did not induce the reporter compared to the empty vector control mock (Figure 3.11A,B). Knock-down of *prx-5*, *prx-11*, *prx-13*, *prx-14* and *prx-19* led to a more than 2-fold induction of the $P_{lonp\text{-}2}GFP$ (*bcIs128*) reporter compared to *tag-208(RNAi)* (Figure 3.11). In contrast, *prx-2(RNAi)* did not induce the GFP expression of the reporter. The knock-down of the remaining five peroxins led to a weak induction of the reporter. In general, the reporter showed a high variation between the different experiments. The peroxins that induce the reporter when knocked-down function in the peroxisomal biogenesis as receptors (PRX-5 and PRX-19), are part of the docking complex (PRX-13 and PRX-14) or are required for peroxisomal division (PRX-11) (Figure 3.11C). Taken together, perturbation of specific steps of peroxisomal biogenesis induces a retrograde signaling form the

peroxisome to the nucleus (hereafter referred to as peroxisomal retrograde signaling or 'PRS') to up-regulate the peroxisomal Lon protease.

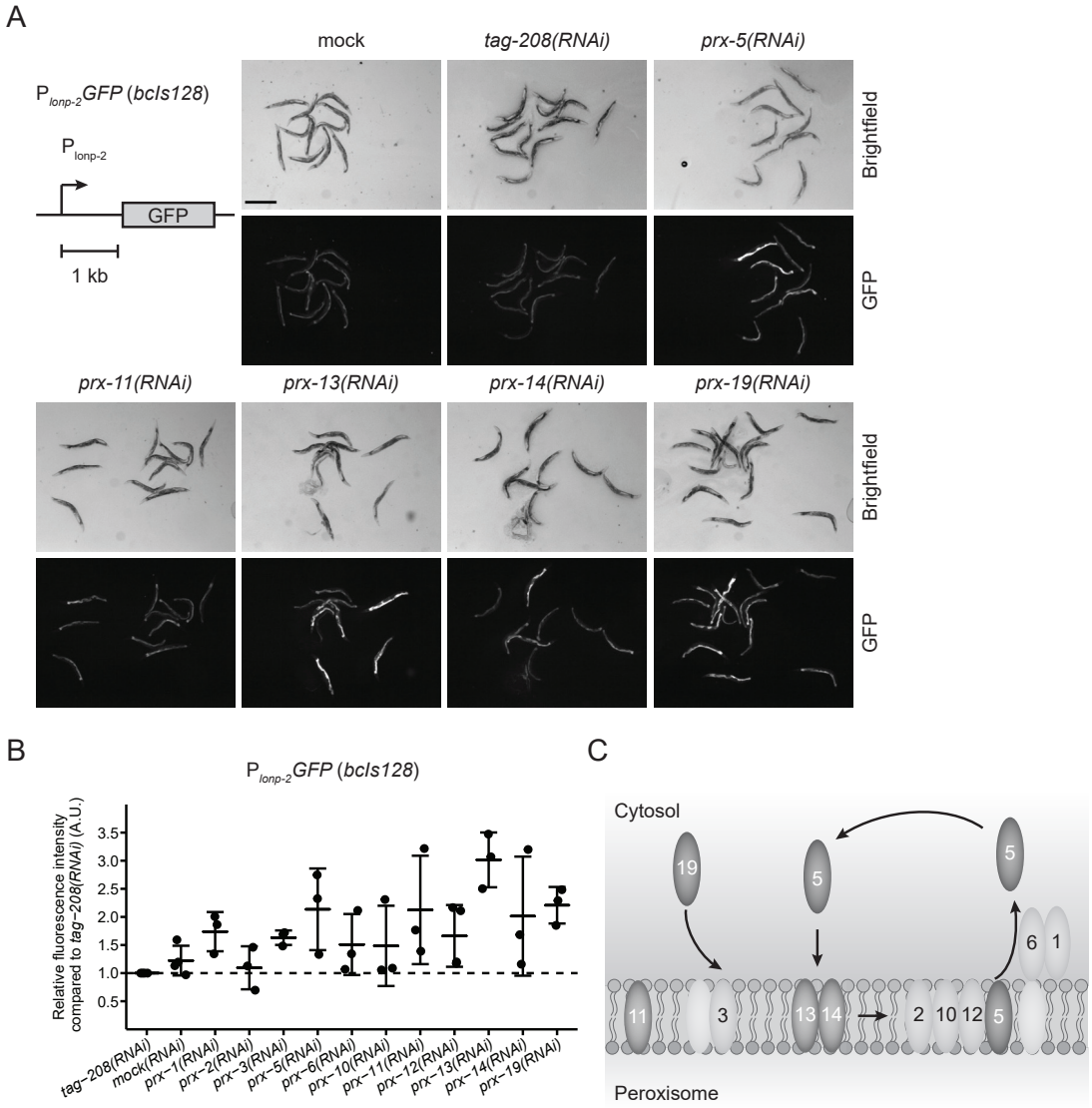

Figure 3.11: Inactivation of some peroxins leads to the transcriptional activation of the peroxisomal Lon protease *lonp-2*. (A) Schematic of the P$_{lonp\text{-}2}$*GFP* (*bcIs128*) reporter containing 1 kb of the putative promoter of *lonp-2* fused to GFP. L4 larvae carrying the reporter were subjected to the knock-down of different peroxins. Adults of the next generation were analyzed by brightfield and fluorescence microscopy. Representative images of RNAi conditions that induce the reporter more than 2-fold are shown. The scale bar represents 0.5 mm. (B) The fluorescence intensity was quantified relative to the negative control *tag-208(RNAi)* (Mean and SD are shown; n=3 (n=number of biological replicates)). (C) *C. elegans* homologs of human peroxins. The numbers represent the number of the respective peroxin (PRX). Proteins shown in dark grey induce a more than 2-fold transcriptional up-regulation of the P$_{lonp\text{-}2}$*GFP* (*bcIs128*) reporter when knocked-down.

3.3.2 The peroxisomal Lon protease is transcriptionally up-regulated by a perturbation of peroxisomal biogenesis

To confirm that the peroxisomal Lon protease is up-regulated upon the perturbation of peroxisomal biogenesis, I tested the induction of the other two $P_{lonp\text{-}2}GFP$ reporters by the knock-down of *prx-5(RNAi)* and *prx-19(RNAi)*. *prx-5* and *prx-19* encode homologs of the human receptors for peroxisomal matrix protein import *PEX5* and peroxisomal membrane protein insertion *PEX19*, respectively (Figure 3.11C). Since the receptors are the most up-stream components of the import/insertion pathway of peroxisomal proteins, we decided to focus our analysis on these two peroxins. Knock-down of *prx-5* and *prx-19* induced the $P_{lonp\text{-}2}GFP$ (*bcIs126*) multi-copy reporter about 2.4 and 2.7-fold, respectively (Figure 3.12A). In contrast, the induction of the $P_{lonp\text{-}2}GFP$ (*bcSi75*) single-copy reporter by knock-down of *prx-5* and *prx-19* was only 1.4-fold (Figure 3.12B). To confirm the observation by RNAi, I crossed the *prx-5(tm4948)* loss of function allele into the $P_{lonp\text{-}2}GFP$ (*bcIs126*) multi-copy reporter. The *prx-5(tm4948)* homozygous mutation induced the GFP expression of the reporter about 1.8-fold compared to wild-type (Figure 3.12C). To summarize, inactivation of the receptors required for peroxisomal biogenesis induces the PRS. Since the $P_{lonp\text{-}2}GFP$ (*bcIs126*) multi-copy reporter showed a consistent and strong induction, I used this reporter for further analysis of the PRS pathway.

Perturbation of the peroxisomal biogenesis induces the transcriptional up-regulation of the peroxisomal Lon protease. Next, we asked if LONP-2 is also up-regulated on the protein level. Therefore, I subjected wild-type L4 larvae to *prx-5(RNAi)* and *prx-19(RNAi)* and analyzed adults of the next generation by Western blotting. Quantification of the LONP-2 band intensities relative to the loading control Tubulin showed that the endogenous LONP-2 levels were decreased by 30% upon *prx-5(RNAi)* compared to the control *tag208(RNAi)* (Figure 3.13A). In contrast, *prx-19(RNAi)* induced a 1.6-fold increase in endogenous LONP-2 compared to the control. Additionally, I analyzed the LONP-2 levels in the *prx-5(tm4948)* mutant compared to the wild-type N2, which confirmed the observation by *prx-5(RNAi)* (Figure 3.13B). These results indicate that impaired peroxisomal matrix protein import leads to a post-transcriptional and/or translational regulation

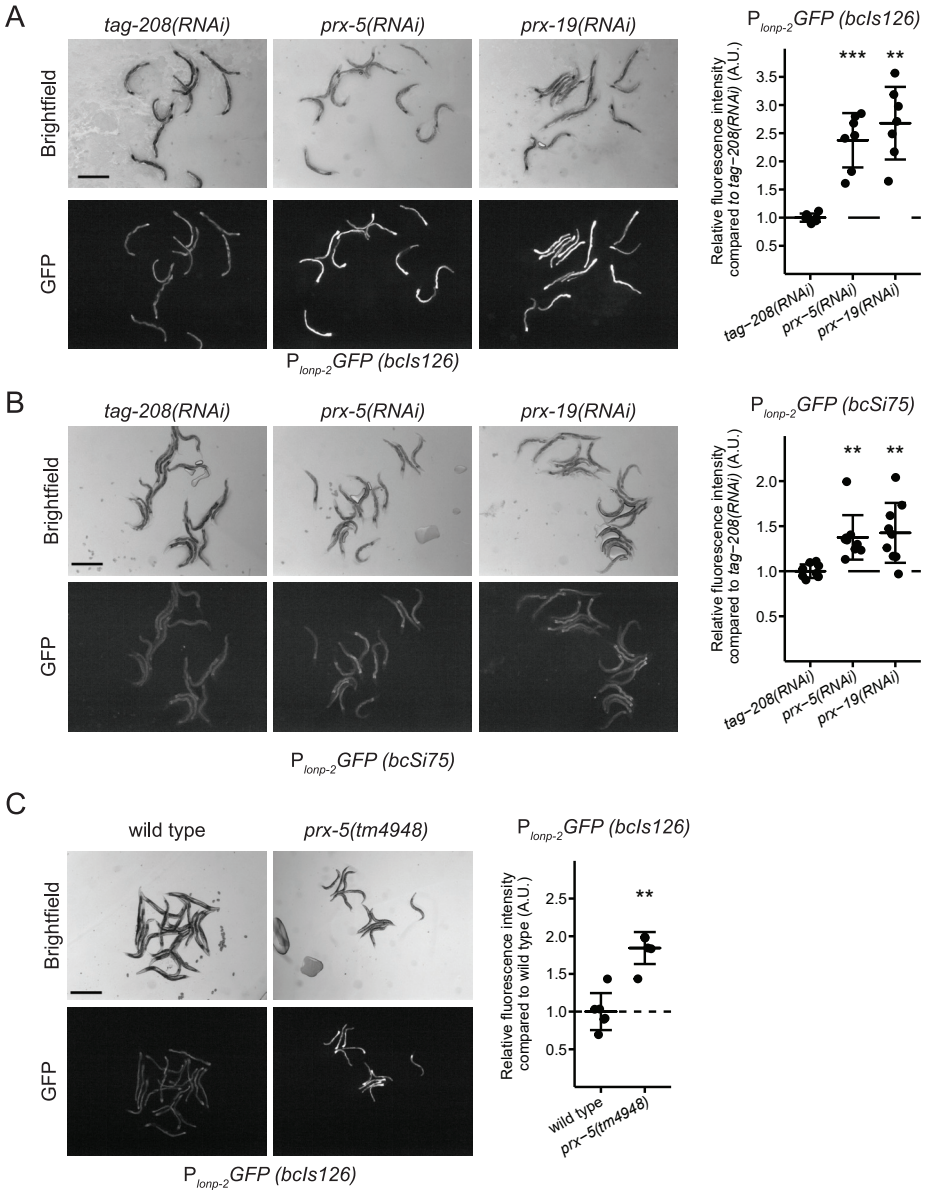

Figure 3.12: Knock-down of the receptors required for peroxisomal biogenesis leads to the transcriptional activation of the peroxisomal Lon protease. (A and B) Representative images and quantification of the P$_{lonp\text{-}2}$*GFP* reporters upon knock-down of *prx-5* or *prx-19*. The RNAi clones were diluted 1:2 with *tag-208(RNAi)* to reduce the slow growth phenotype. The scale bar represents 0.5 mm. (A) Analysis of the P$_{lonp\text{-}2}$*GFP* (*bcIs126*) reporter. (Mean and SD are shown: n=7 (n=number of biological replicates); ** p<0.01 and *** p<0.001 in a Welch's ANOVA with Games-Howell post hoc test to *tag-208(RNAi)*). (B) Analysis of the P$_{lonp\text{-}2}$*GFP* (*bcSi75*) reporter. (Mean and SD are shown: n=9 (n=number of biological replicates); ** p<0.01 in a Kruskal-Wallis test with Dunn's post hoc test to *tag-208(RNAi)*). (C) Representative images and quantification of the P$_{lonp\text{-}2}$*GFP* (*bcIs126*) reporter either wild-type (+/+) or carrying a *prx-5(tm4948)* mutation. The scale bar represents 0.5 mm. (Mean and SD are shown: n=6 (n=number of biological replicates); ** p< 0.01 in a Mann-Whitney-Wilcoxon-U test).

of *lonp-2* in addition to its transcriptional regulation. In contrast, perturbation of the peroxisomal membrane protein insertion leads to a transcriptional up-regulation of *lonp-2* as well as in an increase in the LONP-2 protein level.

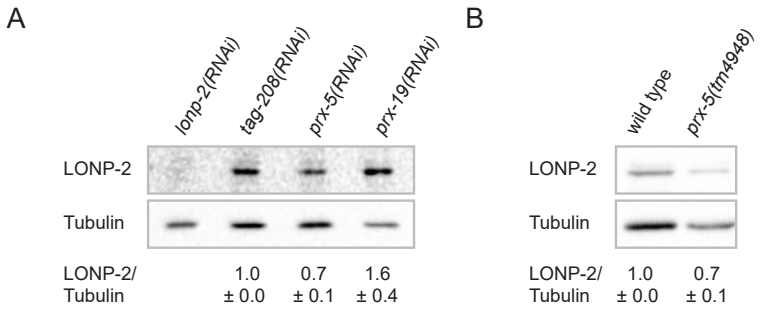

Figure 3.13: Perturbation of peroxisomal biogenesis affects endogenous LONP-2 protein levels. (A) Wild-type L4 larvae were subjected to different RNAi. The RNAi clones were diluted 1:2 with *tag-208(RNAi)* to reduce the slow growth phenotype. Adults of the next generation were lysed and analyzed by Western blotting. The LONP-2 band intensities were normalized to the respective Tubulin loading controls and quantified relative to the negative control *tag-208(RNAi)*. (Mean and SD are shown. n=4 (n=number of independent experiments)). (B) Staged populations of either wild-type (+/+) or *prx-5(tm4948)* mutant day 1 adults were analyzed by Western blotting. The LONP-2 band intensities were normalized to the respective Tubulin loading controls and quantified relative to the wild-type. (Mean and SD are shown. n=3 (n=number of biological replicates)).

3.3.3 The peroxisomal catalase is transcriptionally up-regulated by a perturbation of peroxisomal biogenesis

We hypothesized that the peroxisomal catalase CTL-2 might also be part of the PRS, as it is required to degrade toxic hydrogen peroxide produced in peroxisomes. To test this hypothesis, I generated a $P_{ctl\text{-}2}$*GFP* (*bcSi76*) single-copy reporter (Figure 3.14A). L4 larvae of the reporter strain were subjected to the knock-down of the two peroxisomal biogenesis receptors and the GFP fluorescence was analyzed in adult animals of the next generation. The negative control *tag-208(RNAi)* did not induce the reporter compared to the empty vector control mock (Figure 3.14A, B). Upon knock-down of *prx-5* and *prx-19*, the reporter was induced 1.7 and 1.8-fold compared to *tag-208(RNAi)*, respectively (Figure 3.14A, B).

To confirm the observations by RNAi, I generated a $P_{ctl\text{-}2}$*GFP* (*bcSi76*) reporter carrying the *prx-5(tm4948)* homozygous mutation. The reporter was induced 4.7-fold com-

pared to wild-type (Figure 3.14C). These results show that the peroxisomal catalase is also an effector gene of the PRS pathway.

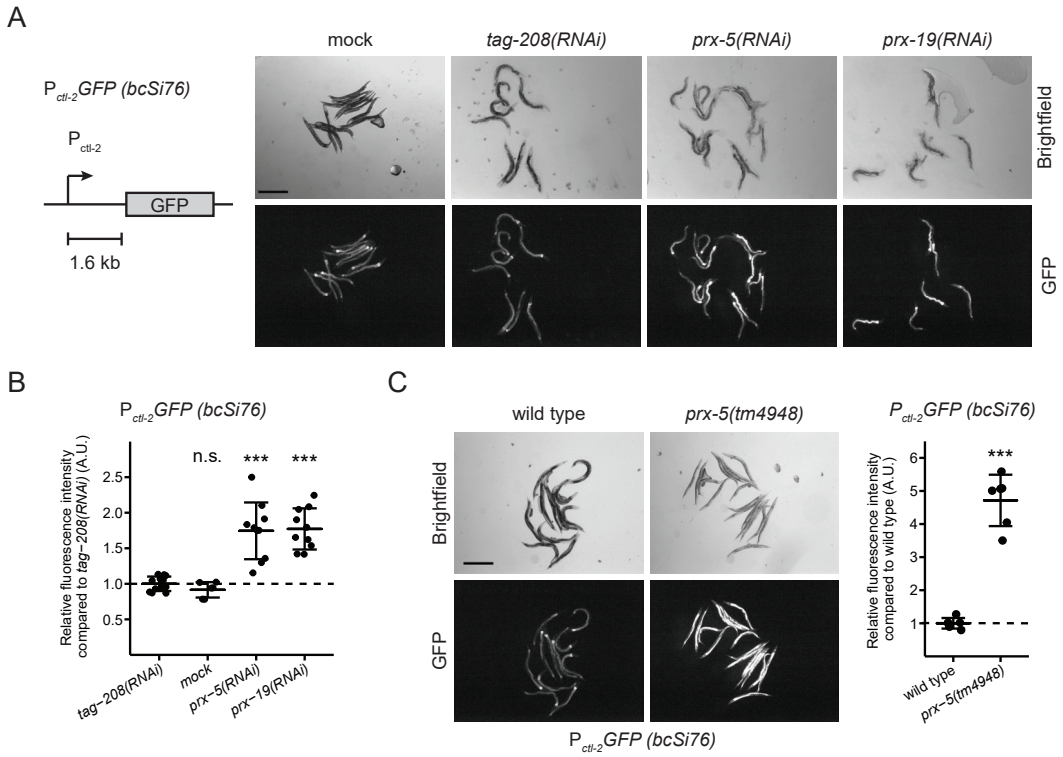

Figure 3.14: Perturbation of peroxisomal biogenesis leads to the transcriptional up-regulation of the peroxisomal catalase. (A) Schematic of the P$_{ctl\text{-}2}$*GFP* (*bcSi76*) reporter containing 1.6 kb of the putative promoter of *ctl-2* fused to GFP. L4 larvae carrying the P$_{ctl\text{-}2}$*GFP* (*bcSi76*) reporter were subjected to different RNAi. The RNAi clones were diluted 1:2 with *tag-208(RNAi)* to reduce the slow growth phenotype. Adults of the next generation were analyzed by brightfield and fluorescence microscopy. Representative images are shown and the scale bar represents 0.5 mm. (B) The fluorescence intensity was quantified relative to the negative control *tag-208(RNAi)*. (Mean and SD are shown: n=10-12 (n=number of biological replicates); n.s.=not significant, *** $p<0.001$ in a Welch's ANOVA with Games-Howell post hoc test to *tag-208(RNAi)*). (C) Representative images and quantification of the P$_{ctl\text{-}2}$*GFP* (*bcSi76*) reporter either wild-type (+/+) or carrying a *prx-5(tm4948)*) mutation. The scale bar represents 0.5 mm. (Mean and SD are shown: n=6 (n=number of biological replicates); *** $p< 0.001$ in a Welch two-sample t-test).

3.3.4 The peroxisomal retrograde signaling is dependent on the nuclear hormone receptor NHR-49

To identify transcription factors involved in the PRS pathway, I conducted a candidate screen. As candidates, we chose transcription factors that were predicted to bind to the 1 kb region of the putative *lonp-2* promoter, which was present in the P$_{lonp\text{-}2}$*GFP* re-

porter strains. Furthermore, we included transcription factors that have previously been shown to be required for the regulation of peroxisomal genes. The GFP expression of the P*lonp-2*GFP (*bcIs126*) reporter strain was induced by *prx-19(RNAi)* and I tested for the suppression of the GFP expression upon additional knock-down of the transcription factors. Only the knock-down of *nhr-49* suppressed the *prx-19(RNAi)*-induced PRS (Figure 3.15).

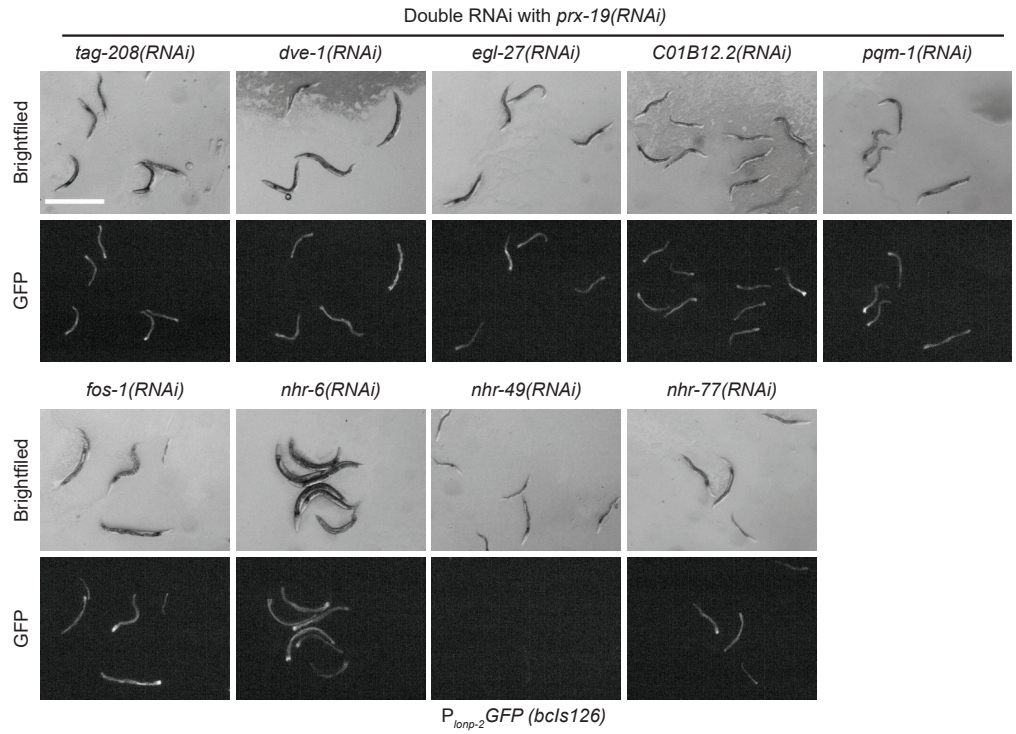

Figure 3.15: Candidate screen for suppressors of the PRS. L4 larvae carrying the P*lonp-2*GFP (*bcIs126*) reporter were subjected to double RNAi. They were treated with *prx-19(RNAi)* and RNAi clones against candidate transcription factors. Adults of the next generation were analyzed by brightfield and fluorescence microscopy and screened for suppression of the GFP expression. Representative images are shown and the scale bar represents 0.5 mm. (n=3 (n=number of independent experiments)).

To confirm the result, the double RNAi experiment was repeated with the P*lonp-2*GFP (*bcIs126*) and the P*ctl-2*GFP (*bcSi76*) reporter strains. Knock-down of *nhr-49* suppressed the GFP expression of the P*lonp-2*GFP (*bcIs126*) reporter strain induced by *prx-5(RNAi)* and *prx-19(RNAi)* (Figure 3.16A). The GFP level decreased to 0.7-fold (*prx-5(RNAi)* + *nhr-49(RNAi)*) and 0.3-fold (*prx-19(RNAi)* + *nhr-49(RNAi)*) compared to the control *tag-208(RNAi)*. Under *nhr-49(RNAi)* conditions, GFP expression of the P*ctl-2*GFP

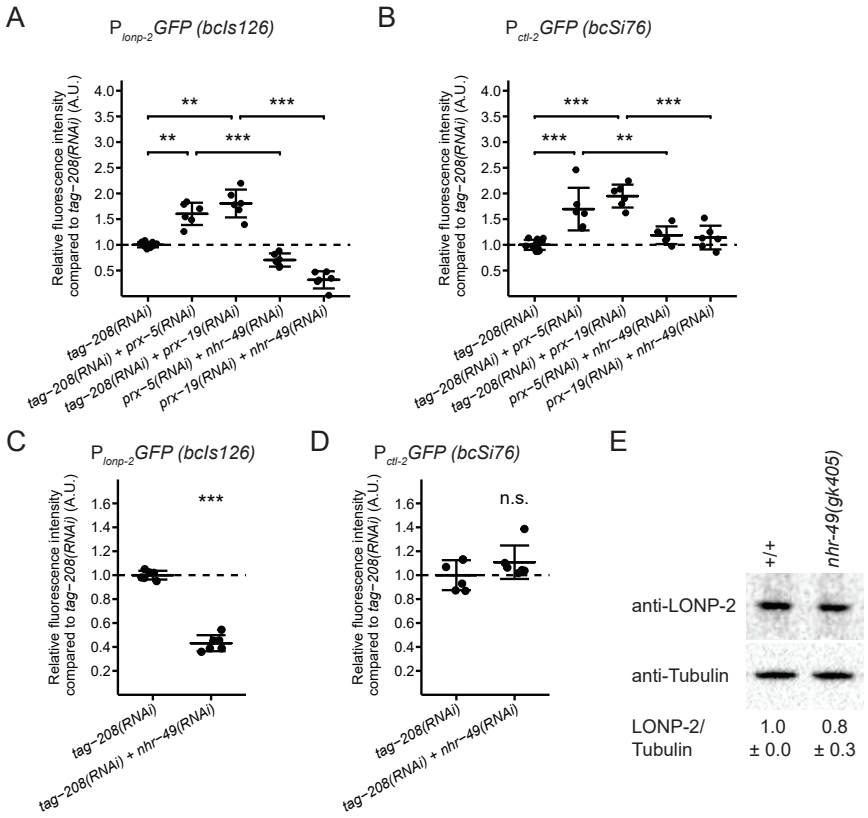

Figure 3.16: The PRS pathway is dependent on NHR-49. (A and B) Quantification of the suppression of the PRS by NHR-49. L4 larvae carrying the P$_{lonp\text{-}2}$*GFP* (*bcIs126*) (A) or P$_{ctl\text{-}2}$*GFP* (*bcSi76*) (B) reporter were subjected to double RNAi and adults of the next generation were analyzed and fluorescence microscopy. The RNAi clones were diluted 1:2. Quantification of the fluorescence intensity relative to *tag-208(RNAi)*. (Mean and SD are shown: n=6-12 (n=number of biological replicates); ** $p<0.01$ and *** $p<0.001$ in a Welch's ANOVA with Games-Howell post hoc test). (C and D) Dependence of the basal expression of *lonp-2* and *ctl-2* on NHR-49. The RNAi clones were diluted 1:2. (Mean and SD are shown: n=6 (n=number of biological replicates); *** $p<0.001$ by a two sample t-test (C). n.s.=not significant by a Mann-Whitney-Wilcoxon-U-Test (D)). (E) Dependence of endogenous LONP-2 levels on NHR-49. Staged populations of either wild-type (+/+) or *nhr-49(gk405)* mutant day 1 adults were analyzed by Western blotting. The LONP-2 band intensities were normalized to the respective Tubulin loading controls and quantified relative to the wild-type (Mean and SD are shown: n=7 (n=number of biological replicates))

(*bcSi76*) reporter strain was no longer up-regulated by *prx-5(RNAi)* and *prx-19(RNAi)* (Figure 3.16B). Furthermore, a knock-down of *nhr-49* in the control (*tag-208(RNAi)* + *nhr-49(RNAi)*) led to a decrease in GFP expression of the $P_{lonp\text{-}2}GFP$ (*bcIs126*) reporter strain indicating that basal *lonp-2* expression is dependent on NHR-49 (Figure 3.16C), whereas the basal expression of *ctl-2* was not dependent on NHR-49 (Figure 3.16D). In contrast to the transcriptional regulation of *lonp-2* by *nhr-49*, the endogenous LONP-2 level was only slightly decreased in the *nhr-49(gk405)* mutant compared to the wild-type (Figure 3.16E). Taken together, I identified the nuclear hormone receptor NHR-49 as a transcription factor required for the PRS pathway.

3.3.5 The peroxisomal retrograde signaling is dependent on the NHR-49 co-factor MDT-15

It has been shown that NHR-49 can regulate different pathways depending on its interacting co-factor [Pathare et al., 2012]. I hypothesized that also the regulation of PRS by NHR-49 requires a co-factor. Therefore, I knocked-down all six NHR-49 co-factors that have previously been identified [Pathare et al., 2012]. Furthermore, I tested other factors that have been shown to interact with NHR-49 [Xu et al., 2011, Liang et al., 2010, Cuppen et al., 2003]. Only the knock-down of *mdt-15*, which is an ortholog of the mammalian mediator subunit MED15, led to a suppression of the GFP expression of the $P_{lonp\text{-}2}GFP$ (*bcIs126*) reporter induced by *prx-19(RNAi)* (Figure 3.17).

Repetition of the experiment showed that *mdt-15(RNAi)* suppressed the GFP expression of the $P_{lonp\text{-}2}GFP$ (*bcIs126*) and $P_{ctl\text{-}2}GFP$ (*bcSi76*) reporter strains induced by either *prx-5(RNAi)* or *prx-19(RNAi)* (Figure 3.18A, B). Upon *mdt-15(RNAi)*, the induction of the $P_{lonp\text{-}2}GFP$ (*bcIs126*) reporter strain by *prx-5(RNAi)* and *prx-19(RNAi)* was reduced to 0.6-fold and 0.8-fold compared to *tag-208(RNAi)*, respectively (Figure 3.18A). Under these double RNAi conditions, the GFP expression of the $P_{ctl\text{-}2}GFP$ (*bcSi76*) reporter was similar to the *tag-208(RNAi)* levels (Figure 3.18B). The knock-down of *mdt-15* in the control (*tag-208(RNAi)* + *mdt-15(RNAi)*) showed that the basal expression of *lonp-2* and *ctl-2* is dependent on MDT-15 (Figure 3.18C, D). To summarize, the PRS pathway is dependent on the NHR-49 co-factor MDT-15.

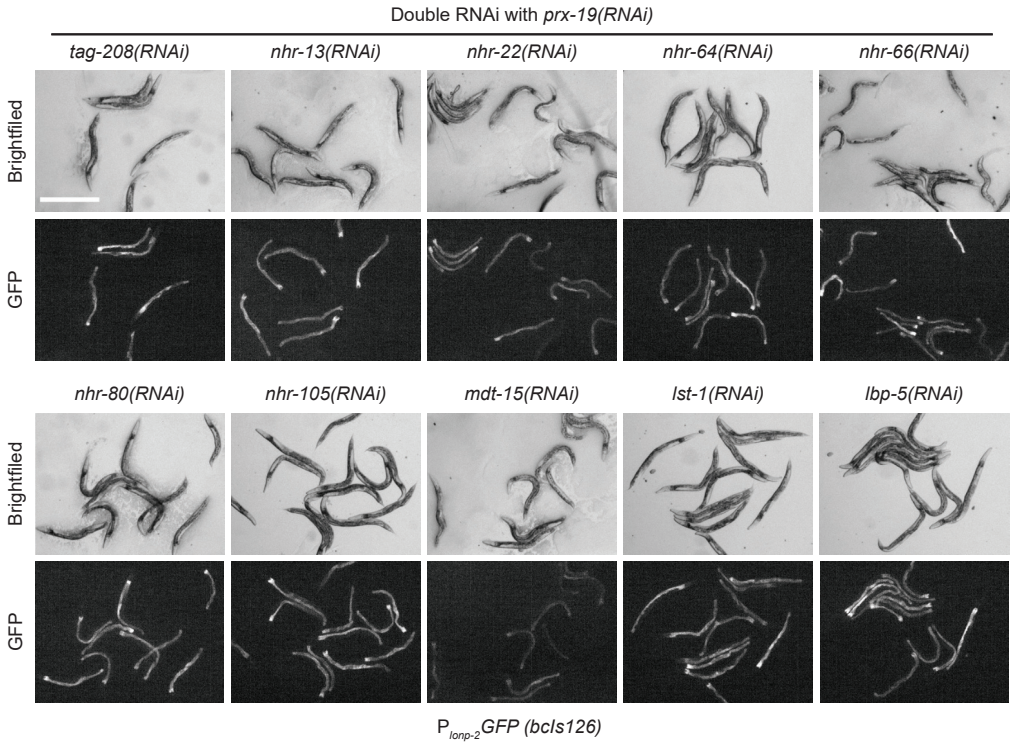

Figure 3.17: Dependence of the PRS on NHR-49 co-factors. L4 larvae carrying the $P_{lonp\text{-}2}GFP$ (*bcIs126*) reporter were subjected to double RNAi. They were treated with *prx-19(RNAi)* and RNAi clones against NHR-49 co-factors. Adults of the next generation were analyzed by bright-field and fluorescence microscopy and screened for suppression of the GFP expression. Representative images are shown and the scale bar represents 0.5 mm. (n=6 (n=number of biological replicates)).

3.3.6 The peroxisomal retrograde signaling is induced by a block of peroxisomal beta-oxidation

The knock-down of *prx-5* might affect the import of peroxisomal beta-oxidation enzymes. By this, the peroxisomal beta-oxidation might be reduced, which could lead to an accumulation of fatty acids that would not be degraded in the peroxisomes. Accumulated lipids or fatty acids could act as signaling molecules in the PRS pathway. To test this hypothesis, we decided to block peroxisomal beta-oxidation, which leads to an accumulation of fatty acids. Peroxisomal beta-oxidation not only degrades fatty acids but also reduces the chain length of ascarosides, which are nematode specific pheromones. Enzymes required for ascaroside biosynthesis can function in the beta-oxidation of ascarosides as well as of triacylglyerols [Zhang et al., 2010, von Reuss et al., 2012, Artyukhin et al., 2018]. I knocked-down all genes encoding enzymes for peroxisomal beta-oxidation [Gilst

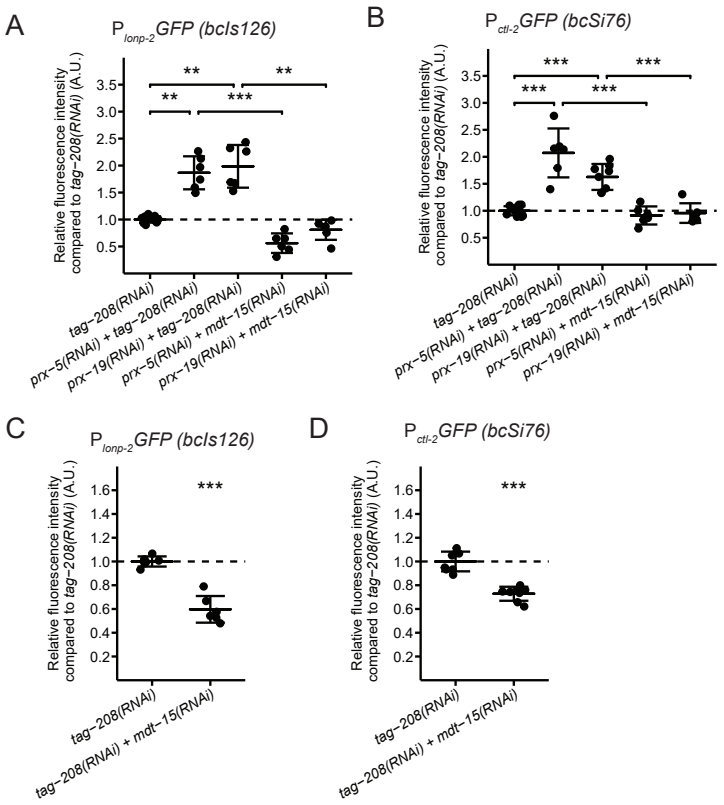

Figure 3.18: The PRS pathway is dependent on the NHR-49 co-factor MDT-15. (A and B) L4 larvae carrying the P$_{lonp\text{-}2}$*GFP* (*bcIs126*) (A) or P$_{ctl\text{-}2}$*GFP* (*bcSi76*) (B) reporter were subjected to double RNAi. Adults of the next generation were analyzed by fluorescence microscopy and the fluorescence intensity was quantificed relative to *tag-208(RNAi)*. The RNAi clones were diluted 1:2. (Mean and SD are shown: n=6-14 (n=number of biological replicates); ** $p<0.01$ and *** $p<0.001$ in a (Welch's) ANOVA with Games-Howell or TukeyHSD post hoc test). (C and D) Dependence of the basal expression of *lonp-2* and *ctl-2* on MDT-15. The RNAi clones were diluted 1:2. (Mean and SD are shown: n=6-8 (n=number of biological replicates); *** $p<0.001$ by a two sample t-test).

et al., 2005, von Reuss et al., 2012] and analyzed the GFP expression of the P$_{lonp\text{-}2}$*GFP* (*bcIs126*) and P$_{ctl\text{-}2}$*GFP* (*bcSi76*) reporters. First, the fatty acids or ascarosides are imported into peroxisomes. Three ABC subfamily D proteins have been proposed to be involved in the transport of fatty acids into peroxisomes [van Roermund et al., 2011, van Roermund et al., 2014]. In *C. elegans*, homologs of these ABCD proteins are encoded by five *pmp* genes. Only PMP-1, PMP-2 and PMP-4 have been shown to localize to peroxisomes [Lee et al., 2014]. Since the RNAi clones for *pmp-1* and *pmp-2* were not present in our RNAi libraries, I only tested the induction of GFP expression of the P$_{lonp\text{-}2}$*GFP* (*bcIs126*) and P$_{ctl\text{-}2}$*GFP* (*bcSi76*) transcriptional reporters upon knock-down of *pmp-4*.

Only the P$_{ctl\text{-}2}$*GFP* (*bcSi76*) reporter was induced upon *pmp-4(RNAi)* (Figure 3.19). This suggests that an accumulation of fatty acids in the cytosol only partially induces the PRS. However, it is possible that the transporters act redundantly.

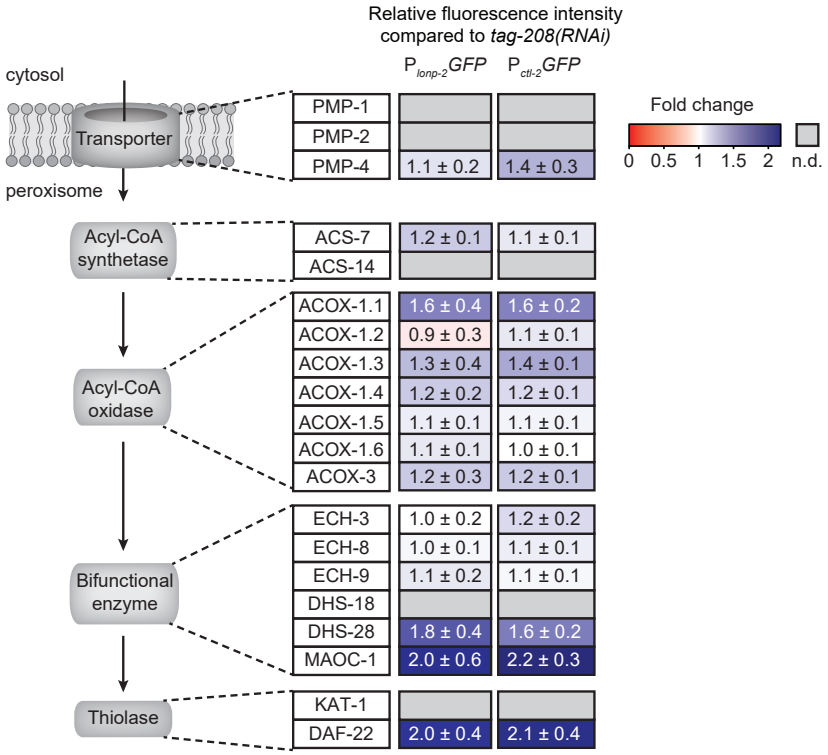

Figure 3.19: The PRS is induced by a block of peroxisomal beta-oxidation. L4 larvae carrying the P$_{lonp\text{-}2}$*GFP* (*bcIs126*) or P$_{ctl\text{-}2}$*GFP* (*bcSi76*) reporter were subjected to RNAi against peroxisomal beta-oxidation enzymes. Adults of the next generation were analyzed by fluorescence microscopy. The fluorescence intensity was quantified relative to the negative control *tag-208(RNAi)*. (Mean and SD are shown: n=6-36 (n=number of biological replicates); n.d.=not determined).

Knock-down of several enzymes that function in peroxisomal beta-oxidation (*acox*, *dhs-28*, *maoc-1* and *daf-22*) induced the PRS about 2-fold (Figure 3.19, 3.20A, B). More specifically, I knocked-down the six genes encoding acyl-CoA oxidases in *C. elegans* (*acox-1.1* to *acox-1.6*), which catalyze the first step of the peroxisomal beta-oxidation. Only the knock-down of the genes encoding the acyl-CoA oxidases ACOX-1.1 and ACOX-1.3 led to an increase in GFP expression in both reporter strains. The bifunctional enzyme is acting down-stream of the acyl-CoA oxidase. Knock-down of *dhs-28* and *maoc-1* induced the GFP expression of both reporters, whereas knock-down of *ech-3*, *ech-6* and *ech-9* did not change the GFP expression. The last step of peroxisomal beta-oxidation is catalyzed by thiolases. The effect of the knock-down of the potential homolog

of the human ACAA1 *kat-1* was not tested . However, knock-down of the homolog of the human SCPx *daf-22* induced both reporters. Additionally, the P$_{lonp\text{-}2}$*GFP* (*bcIs126*) and P$_{ctl\text{-}2}$*GFP* (*bcSi76*) reporters carrying a *daf-22(m130)* mutation showed an increased GFP expression compared to wild-type (Figure 3.20C,D). ACS-7 and ACOX-3 are required to further modify ascaroside pheromones [Zhou et al., 2018]. Knock-down of *acs-7* and *acox-3* did not result in an increase in GFP expression of both reporters (Figure 3.20A,B).

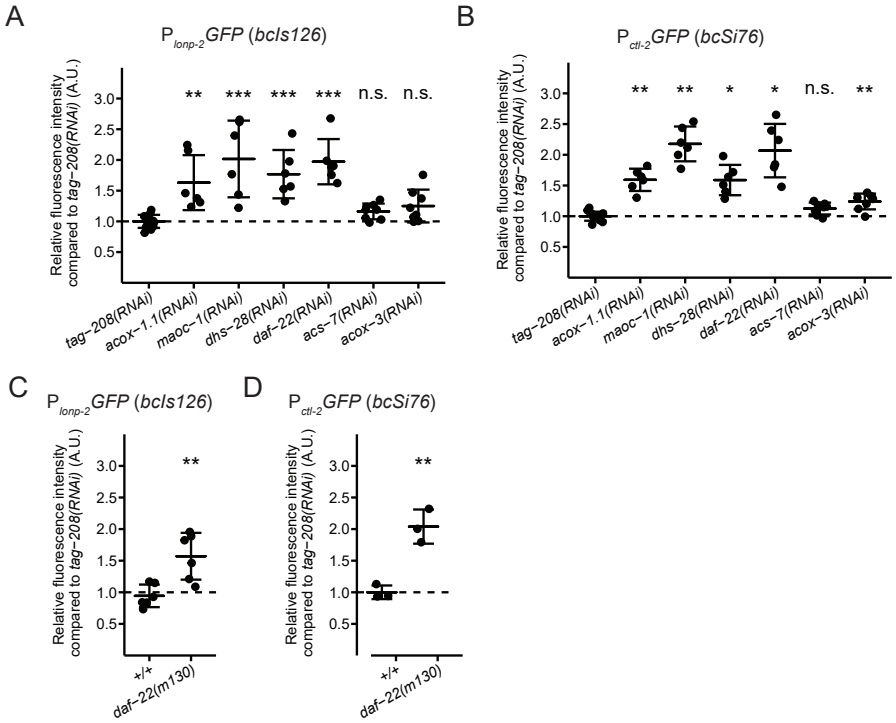

Figure 3.20: The PRS is induced by a block of peroxisomal beta-oxidation. (A and B) L4 larvae carrying the P$_{lonp\text{-}2}$*GFP* (*bcIs126*) (A) or P$_{ctl\text{-}2}$*GFP* (*bcSi76*) (B) reporter were subjected to RNAi against peroxisomal beta-oxidation enzymes. Adults of the next generation were analyzed by brightfield and fluorescence microscopy. The fluorescence intensity was quantified relative to the negative control *tag-208(RNAi)*. (Mean and SD are shown: n=6-14 (n=number of biological replicates); n.s.=not significant, * $p<0.05$, ** $p<0.01$ and *** $p<0.001$ in a Welch's ANOVA with Games-Howell post hoc test to *tag-208(RNAi)*). (C and D) Quantification of the fluorescence intensity of the P$_{lonp\text{-}2}$*GFP* (*bcIs126*) (C) or P$_{ctl\text{-}2}$*GFP* (*bcSi76*) (D) reporter either wild-type (+/+) or carrying a *daf-22(m130)* mutation. (Mean and SD are shown: n=3-4 (n=number of biological replicates); ** $p< 0.01$ in a two-sample t-test).

Next, we asked if the induction of the PRS by the knock-down of beta-oxidation genes is dependent on NHR-49. To this end, I induced the GFP expression in the P$_{lonp\text{-}2}$*GFP* (*bcIs126*) and P$_{ctl\text{-}2}$*GFP* (*bcSi76*) reporters by the knock-down of *maoc-1* (Figure 3.21).

Additional knock-down of *nhr-49* suppressed the response. This shows that the PRS pathway induced by a defect in peroxisomal beta-oxidation is dependent on the transcription factor NHR-49.

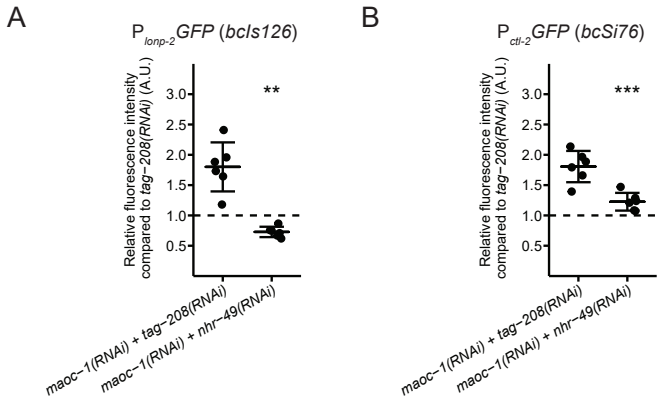

Figure 3.21: Dependence of induction of PRS by the block of peroxisomal beta-oxidation on NHR-49. L4 larvae carrying the $P_{lonp\text{-}2}GFP$ (*bcIs126*) (A) or $P_{ctl\text{-}2}GFP$ (*bcSi76*) (B) reporter were subjected to double RNAi. The RNAi clones were diluted 1:2. The fluoresence intensity of adults of the next generation was quantified relative to *tag-208(RNAi)*. (Mean and SD are shown: n=6 (n=number of biological replicates); ** $p<0.01$ and *** $p<0.001$ in a (Welch's) two-sample t-test).

To show that perturbation of peroxisomal matrix protein import by *prx-5(RNAi)* indirectly leads to an accumulation of fatty acids, wild-type L4 larvae were stained with the fat-soluble dye Oil Red O. Animals with higher fat content incorporate more of the dye and, therefore, show a stronger staining. Surprisingly, animals treated with *tag-208(RNAi)* showed a slight increase in signal intensity compared to the empty vector control mock. The fat content of animals treated with *prx-5(RNAi)* had a comparable signal intensity compared to mock (Figure 3.22). Thus, perturbation of peroxisomal matrix protein import does not lead to a detectable accumulation of fatty acids.

3.3.7 Block of mitochondrial beta-oxidation does not induce the peroxisomal retrograde signaling

Very long-chain and long-chain fatty acids are first shortened by peroxisomal beta-oxidation and then further degraded in mitochondria. Therefore, we asked if a block of mitochondrial beta-oxidation also induces the PRS. To this end, I knocked-down two genes encoding enzymes of the mitochondrial beta-oxidation pathway and analyzed the

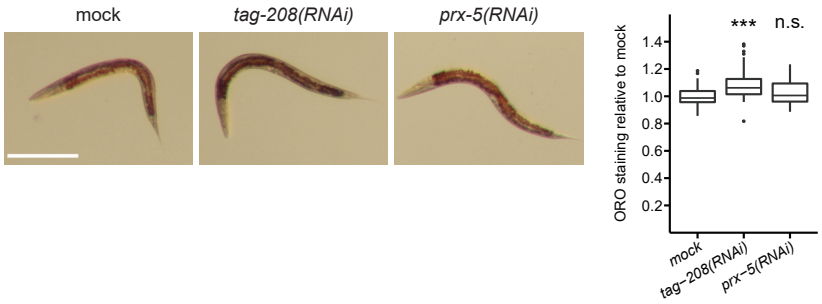

Figure 3.22: Wild-type L4 larvae were treated with different RNAi and the animals of the next generation were stained with Oil Red O. *prx-5(RNAi)* was diluted 1:2 with mock to reduce the slow-growth phenotype. Representative images are shown. The scale bar represents 200 μm. Quantification of the signal intensity of the staining. (n=39-50 (n=number of animals analyzed from 3 independent experiments); n.s.=not significant and *** $p<0.001$ by a Kruskal Wallis test with Dunn's post hoc test).

expression of the $P_{lonp\text{-}2}$*GFP* (*bcIs126*) and $P_{ctl\text{-}2}$*GFP* (*bcSi76*) reporters. Knock-down of *ech-6* and *acdh-13* did not affect the expression of the PRS reporters (Figure 3.23A, B). In contrast, *ech-6(RNAi)* and *acdh-13(RNAi)* caused a strong up-regulation of the mitochondrial unfolded protein response transcriptional reporter $P_{hsp\text{-}6}$*GFP* (*zcIs13*) (Figure 3.23C). Conversely, knock-down of *maoc-1*, which caused an up-regulation of the PRS reporters, did not affect the $P_{hsp\text{-}6}$*GFP* (*zcIs13*) reporter (Figure 3.23). To summarize, these results indicate that the PRS is specifically activated by a perturbation of peroxisomal beta-oxidation. Interestingly, *prx-5(RNAi)* weakly induced the UPR^{mt} transcriptional reporter (Figure 3.23C). This hints at the existence of a cross talk between the mitochondrial and the peroxisomal stress responses, which will be further discussed below (see chapter 3.4).

3.3.8 The PRS is not induced by a redox imbalance between peroxisomes and the cytosol

We observed that a perturbation of peroxisomal beta-oxidation induces the PRS. Therefore, one can speculate that fatty acids act as signaling molecules in the PRS. However, it is also conceivable that reactive oxygen species (ROS) act as signaling molecules in the PRS, since many metabolic pathways taking place in peroxisomes generate ROS like hydrogen peroxide (see chapter 1.4). Hydrogen peroxide derived from peroxisomes

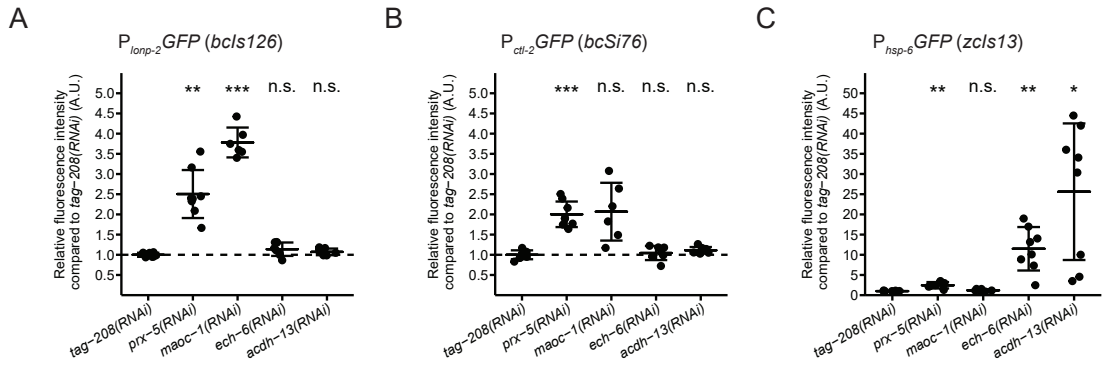

Figure 3.23: The PRS is specifically induced by a perturbation of peroxisomal beta-oxidation. L4 larvae carrying the P$_{lonp\text{-}2}$*GFP* (*bcIs126*) (A), P$_{ctl\text{-}2}$*GFP* (*bcSi76*) (B) or P$_{hsp\text{-}6}$*GFP* (*zcIs13*) (C) reporter were subjected to different RNAi conditions. The *prx-5(RNAi)* clone was diluted 1:2 with *tag-208(RNAi)* to reduce the slow growth phenotype. The fluorescence intensity of the reporters in adults of the next generation was quantified relative to the negative control *tag-208(RNAi)*. (Mean and SD are shown: n=6-8 (n=number of biological replicates); n.s.=not significant, * $p<0.05$, ** $p<0.01$ and *** $p<0.001$ in a Welch's ANOVA with Games-Howell post hoc test to *tag-208(RNAi)*).

can modulate various biological processes and the peroxisomal catalase is an important enzyme to maintain balanced hydrogen peroxide levels in the cell [Brown et al., 1999, Koepke et al., 2008, Ivashchenko et al., 2011]. We hypothesized that the knock-down of *prx-5* might result in a decreased import of the peroxisomal catalase CTL-2 and thus in a disruption of the redox balance between peroxisomes and the cytosol. Besides the peroxisomal catalase CTL-2, *C. elegans* has also a cytosolic catalase CTL-1. A third catalase CTL-3 also exists in a small subset of cells, but its sub-cellular localization has not been analyzed [Petriv and Rachubinski, 2004]. The knock-down of *ctl-1* and *ctl-2* would lead to a disruption of the ROS metabolism in the cytosol and the peroxisome, respectively. The resulting imbalance of the redox state between the two compartments might induce the PRS.

To test this hypothesis, I analyzed the GFP expression of the P$_{lonp\text{-}2}$*GFP* (*bcIs126*) and P$_{ctl\text{-}2}$*GFP* (*bcSi76*) reporters upon knock-down of *ctl-1* and *ctl-2*. Neither RNAi condition induced the transcriptional reporters compared to the control *tag-208(RNAi)* (Figure 3.24A, B). Consistent with the result of *ctl-2(RNAi)*, the *ctl-2(ua90)* mutation also did not cause an up-regulation of the P$_{lonp\text{-}2}$*GFP* (*bcIs126*) and P$_{ctl\text{-}2}$*GFP* (*bcSi76*) reporters compared to wild-type (Figure 3.24C, D). The *ctl-2(ua90)* mutation is a deletion

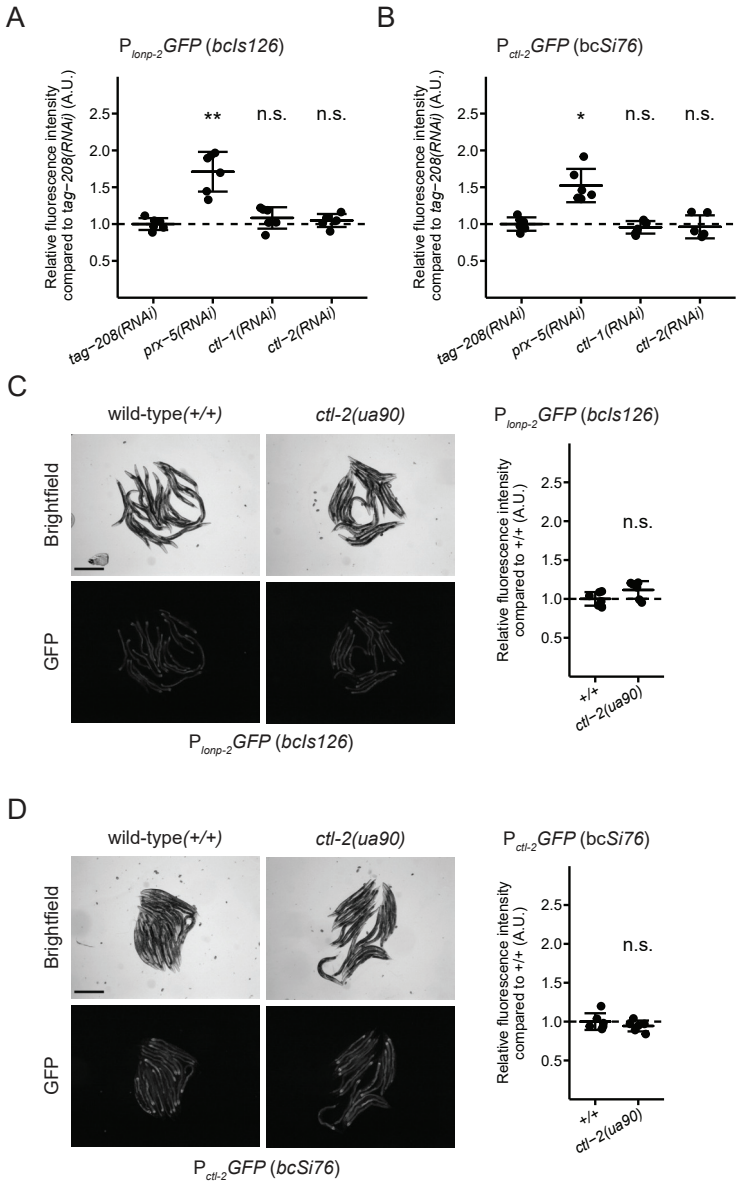

Figure 3.24: The PRS is not induced by a redox imbalance between peroxisomes and the cytosol. (A and B) L4 larvae carrying the P$_{lonp\text{-}2}$*GFP* (*bcIs126*) (A) or P$_{ctl\text{-}2}$*GFP* (*bcSi76*) (B) reporters were subjected to different RNAi and adults of the next generation were analyzed by brightfield and fluorescence microscopy. The expression of the reporters was quantified relative to *tag-208(RNAi)*. (n=6 (n=number of biological replicates); mean and SD are shown; n.s.=not significant, ** $p<0.01$ by a Welch's ANOVA with Games-Howell post hoc test and * $p<0.05$ by a Kruskal-Wallis test with Dunn's multiple comparisons test to *tag-208(RNAi)*). (C and D) Brightfield and fluorescence microscopy analysis of the fluorescence intensity of the P$_{lonp\text{-}2}$*GFP* (*bcIs126*) (C) or P$_{ctl\text{-}2}$*GFP* (*bcSi76*) (D) reporters carrying the *ctl-2(ua90)* mutation and the respective wild-type (+/+) strain. (n=6 (n=number of biological replicates); mean and SD are shown; ns=not significant by a two sample t-test).

in the upstream and 5' region of the *ctl-2* gene and results in lack of detectable CTL-2 activity [Petriv and Rachubinski, 2004]. Taken together, this experiment indicates that a perturbation of the redox balance between peroxisomes and the cytosol does not induce the PRS.

3.3.9 Genes involved in the defense response and lipid metabolic processes are up-regulated in the PRS

We identified the peroxisomal Lon protease and peroxisomal catalase as effector genes of the PRS. Next, we aimed to identify further effector genes by analyzing the *C. elegans* transcriptome upon induction of the PRS. To this end, we knocked-down *prx-5* in wild-type animals and adults of the next generation were analyzed by RNA-seq by Eurofins Genomics Germany GmbH. *tag-208(RNAi)* served as a negative control. Out of 15,796 identified genes, 1,372 genes were significantly up-regulated and 662 genes were significantly down-regulated in *prx-5(RNAi)* samples compared to control samples (FDR$<$0.05) (Figure 3.25A). I analyzed the dataset using gene set enrichment analysis (GSEA). The advantage of this analysis is that no arbitrary cut-off is applied and the direction of change is taken into account. GSEA of Kyoto Encyclopedia of Genes and Genomes (KEGG) pathways using WebGestalt [Liao et al., 2019] revealed a strong enrichment of the pathways "peroxisome" (cel04146) and "lysosome" (cel0414) (Figure 3.25B, Appendix Table A.1). Furthermore, several metabolic pathways like for example "fatty acid elongation" (cel00062) or "metabolism of xenobiotics by cytochrome P450" (cel00980) were enriched. In contrast, genes that are assigned to for example the pathways "ribosome" (cel03010), "spliceosome" (cel03040) and "proteasome" (cel03050) were underrepresented under *prx-5(RNAi)* conditions.

To reduce the number of significantly changed genes, we chose a cut-off of a $\log_2$(fold change) value $\geq$1 (increased) or $\leq$-1 (decreased) and asked which KEGG pathways or Gene Ontology (GO) terms were enriched among these genes with a stronger differential expression. This cut-off resulted in a list of 1,157 genes that were significantly up-regulated and 267 genes that were significantly down-regulated. KEGG pathway enrichment was analyzed using DAVID [Huang et al., 2009a, Huang et al., 2009b]. Similar to

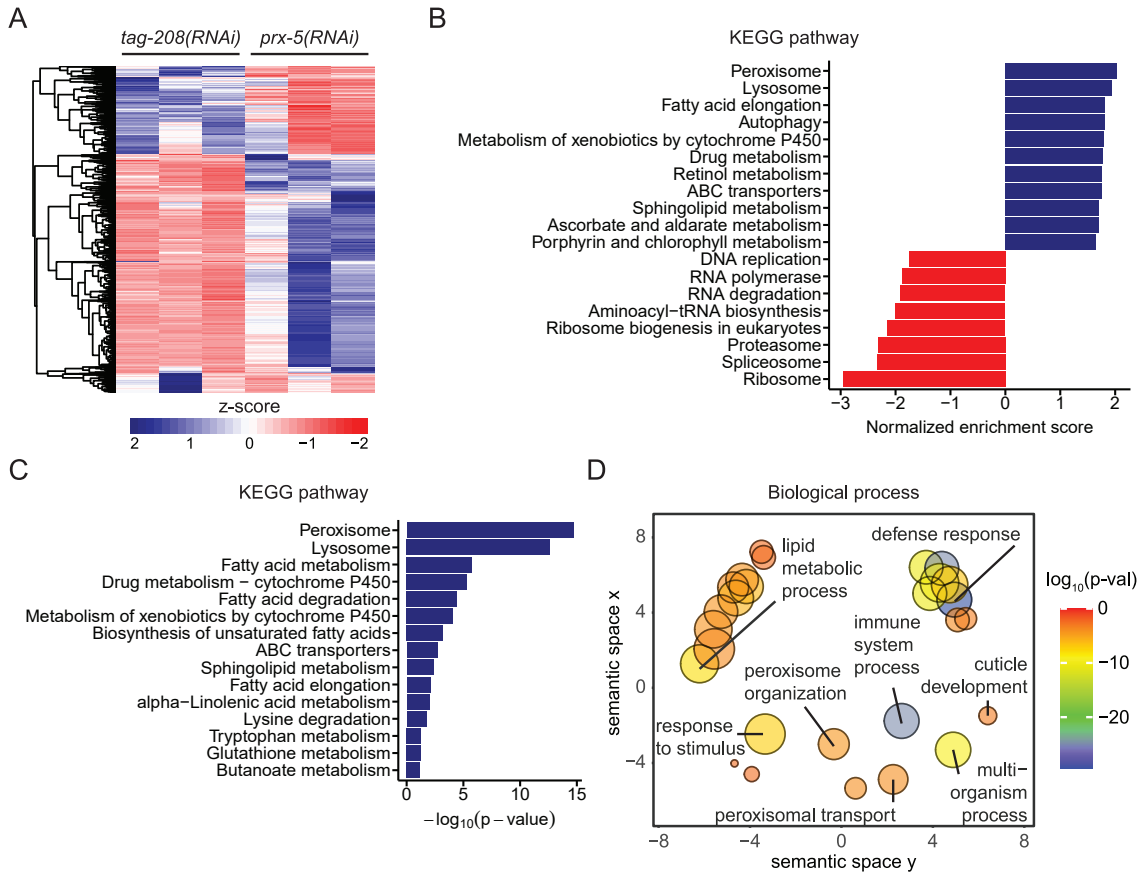

Figure 3.25: RNA-seq analysis of genes differentially expressed upon knock-down of *prx-5*. (A) Wild-type L4 larvae were subjected to *prx-5(RNAi)* and *tag-208(RNAi)* and adults of the next generation were analyzed by RNA-seq. The *prx-5(RNAi)* clone was diluted 1:2 with *tag-208(RNAi)* to reduce the slow growth phenotype. The heat map shows the z-score of genes significantly changed (FDR$<$0.05) of *tag-208(RNAi)* control samples and *prx-5(RNAi)* samples. (n=3 (n=number of biological replicates)). (B) Gene set enrichment analysis of KEGG pathways in *prx-5(RNAi)* samples compared to *tag-208(RNAi)* control samples. (C) KEGG pathway enrichment analysis of genes significantly changed upon *prx-5(RNAi)*. Genes with a $\log_2$(fold change) value $\geq$1 (increased) or $\leq$-1 (decreased) and an FDR$<$0.05 were considered as significantly changed. (D) GO enrichment analysis of genes significantly changed upon *prx-5(RNAi)* summarized using REVIGO. Genes with a $\log_2$(fold change) value $\geq$1 (increased) or $\leq$-1 (decreased) and an FDR$<$0.05 were considered as significantly changed. GO terms are represented by circles and are plotted according to semantic similarities to other GO terms (adjoining circles are most closely related). The color indicates the $\log_{10}$(p-value).

the GSEA, the pathways ”peroxisome” (cel04146; p=1.96e-15) and ”lysosome” (cel0414; p=2.19e-13) were enriched (Figure 3.25C, Appendix Table A.2). In contrast, the enriched metabolic pathways only partially overlapped between the two analyses. While the pathways ”fatty acid elongation” (cel00062) and ”metabolism of xenobiotics by cytochrome P450” (cel00980) were enriched in both datasets, the pathways for amino acid metabolism (”lysine degradation” (cel00310; p=1.75e-02) and ”tryptophan metabolism” (cel00380; p=5.27e-02)) were only enriched in the dataset with high differential expression. GO enrichment analysis of the domain ”biological process” of this dataset using GOrilla [Eden et al., 2009] and REVIGO [Supek et al., 2011] revealed two large clusters of enriched GO terms (Figure 3.25D, Appendix Table A.3). Representative terms of these clusters are ”defense response” (GO:0006952; p=1.06e-35) and ”lipid metabolic process” (GO:0006629; p=3.72e-10). Notably, about 95% of the genes assigned to these two biological processes were up-regulated upon knock-down of *prx-5*. Taken together, the GSEA, KEGG pathway enrichment analysis and GO enrichment analysis showed matching results. For instance, lipid metabolic processes were enriched in all three analyses. Furthermore, the degradation of fatty acids takes place in peroxisomes, which were also enriched in the GSEA and KEGG pathway enrichment analysis.

To test if specific peroxisomal pathways were enriched, I mapped the significantly changed genes to KEGG pathways using KEGG Mapper [Kanehisa and Sato, 2020]. Analysis of the mapping result of the KEGG pathway ”peroxisome” (cel04146) showed that all genes mapped to this pathway were significantly up-regulated. Specifically, genes coding for components of the alpha- and beta-oxidation pathways as well as the ether-phospholipid biosynthesis and were significantly up-regulated (Figure 3.26). In contrast, only specific genes required for amino acid metabolism and the antioxidant system were up-regulated. Moreover, almost all genes coding for peroxins were up-regulated. Specifically, only *prx-11* and *prx-19* were not significantly changed and *prx-14* and *prx-10* were not determined in the RNA-seq analysis. Surprisingly, *prx-5* was also up-regulated although it was knocked-down by RNAi. However, this up-regulation could be part of the response. For instance, it has been shown for mitochondria, that the induction of UPR^{mt} by knock-down of the gene encoding the protease SPG-7 by RNAi leads to the transcrip-

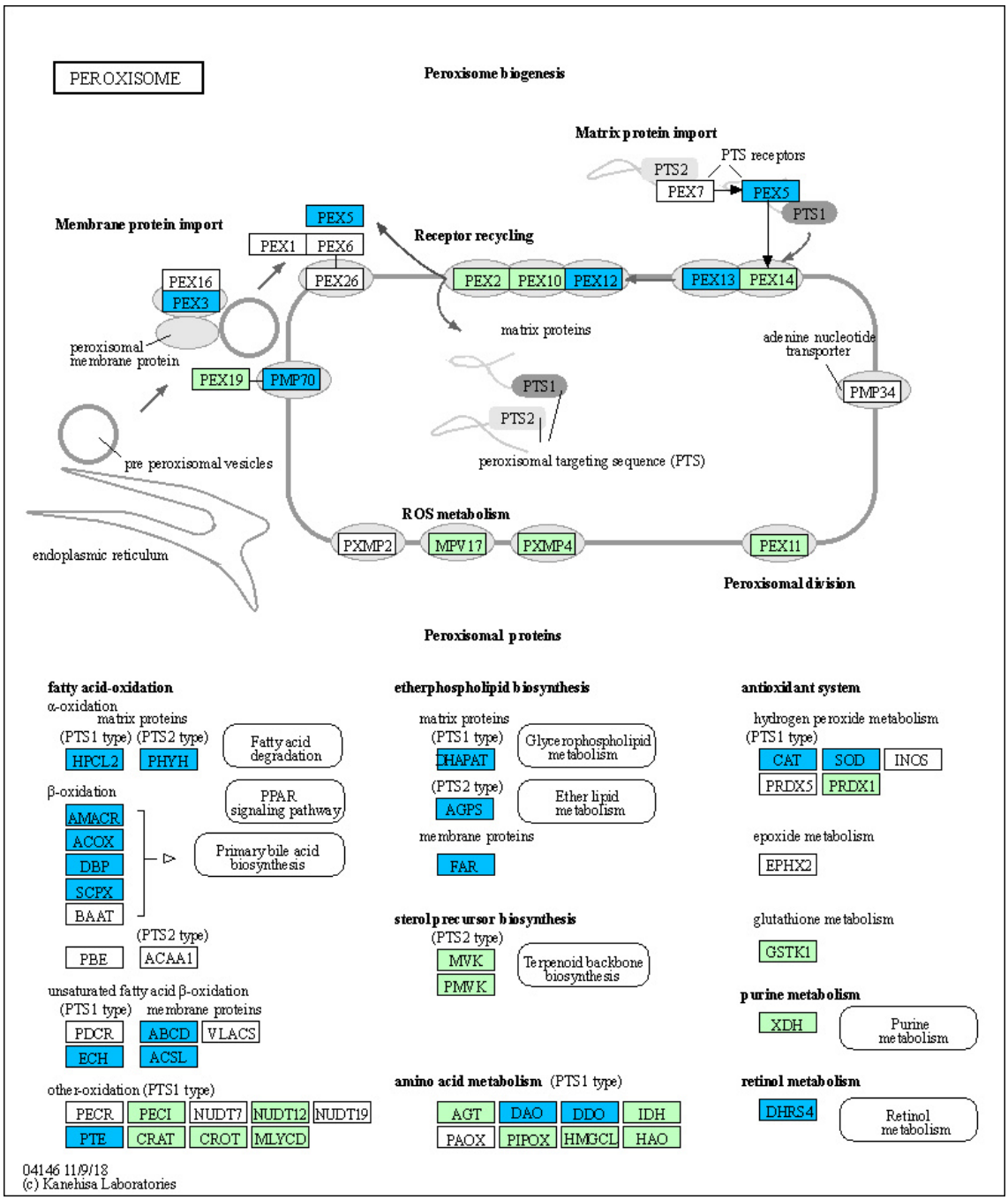

Figure 3.26: KEGG Mapper result of genes significantly changed upon *prx-5(RNAi)*. The KEGG pathway map "peroxisome" (cel04146) is shown. Components of the pathway that have a homolog in *C. elegans* are colored. Components of which at least one gene is significantly changed (FDR$<$0.05 and $\log_2$(fold change) $\geq$1) are shown in blue and components that are not significantly changed are shown in green.

tional up-regulation of *spg-7* [Nargund et al., 2012].

In general, the assignment of genes to KEGG pathways or GO terms is mostly done automatically and can therefore be incomplete. For example, the KEGG pathway map "peroxisome" (cel04146) shows that there is no homolog of the human PEX1 and PEX6 in *C. elegans*. However, homologs of genes encoding these two peroxins have been described in the literature [Ghenea et al., 2001, Petriv et al., 2002]. Therefore, we manually generated a list of 62 peroxisomal proteins using WormBase (release WS272) [Lee et al., 2017], PeroxisomeDB [Schluter et al., 2010] and literature research (Appendix Table A.4). Genes coding for 57 of the 62 peroxisomal proteins were identified in the RNA-seq analysis. 60% (34/57) of the identified genes were significantly up-regulated, whereas none (0/57) of them was down-regulated. Interestingly, among the not significantly changed genes (23/57) were genes coding for proteins required for peroxisomal biogenesis by fission (*fis-1*, *fis-2*, *drp-1* and *prx-11*).

3.3.10 Proteins involved in the immune response and lipid metabolic processes are up-regulated in the PRS

In light of the different regulation of the peroxisomal Lon protease at the transcriptional and protein level, we aimed to analyze the *C. elegans* proteome upon induction of the PRS. To this end, wild-type animals were subjected to *prx-5(RNAi)*, *prx-19(RNAi)* and *tag-208(RNAi)* as negative control. The protein lysates of the next generation were analyzed by LC-MS by our collaborators Ignasi Forne and Axel Imhoff (BMC Munich). However, the RNAi efficiency differed between the samples. The protein level of PRX-19 was not significantly reduced by *prx-19(RNAi)*. In contrast, the level of PRX-5 was significant reduced by 60% in the *prx-5(RNAi)* sample as compared to the control *tag-208(RNAi)* (Appendix Table B.1). Therefore, only the proteome of the *prx-5(RNAi)* samples was further analyzed. Under these RNAi conditions, 6,353 proteins were identified, of which 120 proteins were significantly up-regulated and 57 proteins were significantly down-regulated, based on a p-value of < 0.05 and an expression change ratio of *prx-5(RNAi)* treated samples relative to the *tag-208(RNAi)* treated control samples with a $\log_2$(fold change) value $\geq$1 (increased) or $\leq$-1 (decreased) (Figure 3.27A). Thus, a partial knock-down of the

import receptor *prx-5* is sufficient to induce changes in the *C. elegans* proteome.

First, I analyzed the protein-protein interaction network of the proteins significantly changed upon *prx-5(RNAi)* using the database STRING [Szklarczyk et al., 2019]. The analysis showed four different clusters (Figure 3.27B). The first cluster included peroxisomal proteins. Except for PRX-5, all proteins in this cluster were up-regulated and all of them have been shown to be involved in peroxisomal fatty acid metabolism [Fredens et al., 2011]. The second cluster comprised proteins that were up-regulated upon *prx-5(RNAi)* and that have been shown to be involved in the *C. elegans* innate immune response [Hahm et al., 2011, Liu et al., 2016, Yunger et al., 2017, Lee et al., 2013, Wong et al., 2007]. The third cluster consisted of T28H10.3 and T22C1.3, two uncharacterized proteins that were up-regulated upon *prx-5(RNAi)* and the other cluster with only two nodes consisted of IFY-1 and F32D1.7, which were both down-regulated upon knock-down of *prx-5*.

The GO enrichment analysis of the significantly changed proteins revealed a similar result. The dataset was analyzed for GO enrichment using the GOrilla [Eden et al., 2009] and REVIGO [Supek et al., 2011] (Appendix Table B.2). Two highly significant representative GO terms of the domain "biological process" were "lipid metabolic process" (GO:006629, p=1.29e-05) and "immune response" (GO:006955; p=2.11e-05) (Figure 3.27C). Examples for representative GO terms of the domain "molecular function" were "acyl-CoA oxidase activity" (GO:0003997, p=3.45e-04) and "aspartic-type endopeptidase activity" (GO:0004190, p=2.96e-05). Taken together, the enriched GO terms of the two GO domains match each other as acyl-CoA oxidase activity is required for lipid metabolic processes and the immune response involves the activity of endopeptidases. The GO enrichment and STRING analysis both provide evidence that peroxisomal lipid metabolism and the immune response are the main biological processes, which are affected upon knock-down of *prx-5*.

A more detailed analysis of the representative GO terms revealed that 90% of the proteins assigned to the enriched GO terms were up-regulated upon knock-down of *prx-5*. In the GO domain biological process, most of the proteins belonged to the GO term "lipid metabolic process" (19 proteins) followed by the GO terms "immune system process" and "immune response", which were comprised of the same eleven proteins (Figure 3.27C).

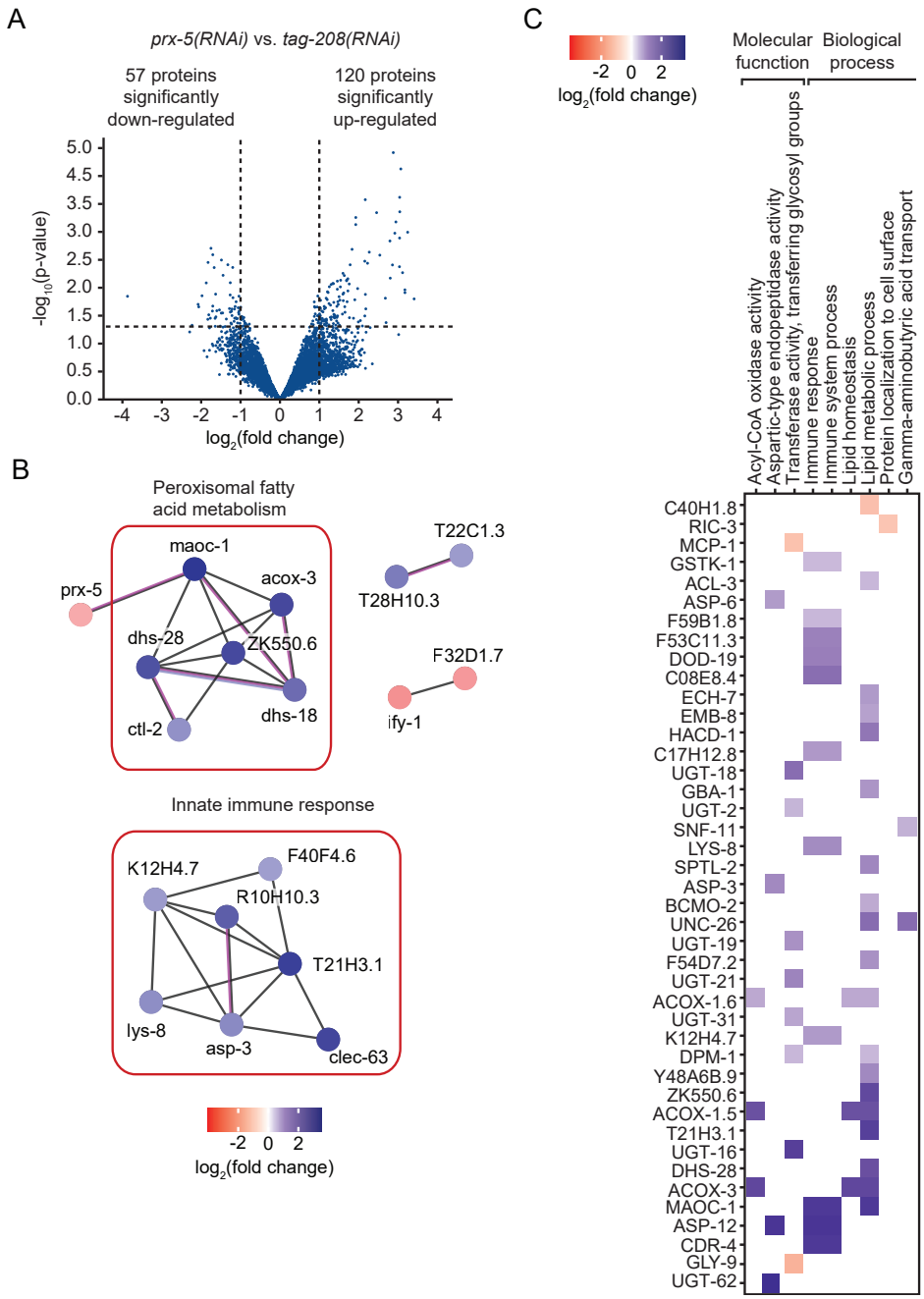

Figure 3.27: Analysis of changes of the proteome upon knock-down of *prx-5*. (A) The volcano plot represents the $\log_2$(fold change) and -$\log_{10}$(p-value) of proteins identified in the LC-MS analysis of *prx-5(RNAi)* samples compared to *tag-208(RNAi)* samples. The *prx-5(RNAi)* clone was diluted 1:2 with *tag-208(RNAi)* to reduce the slow growth phenotype. Proteins with a $\log_2$(fold change) value $\geq$1 (increased) or $\leq$-1 (decreased) and $p<0.05$ by a limma moderated t-test were considered as significantly changed. (B) Interaction analysis of proteins significantly changed upon *prx-5(RNAi)* using STRING. The color of the nodes indicates the $\log_2$(fold change). Black lines show co-expression, blue lines represent protein homology and purple lines represent experimentally determined interactions. (C) GO enrichment analysis of proteins significantly changed upon *prx-5(RNAi)* summarized using REVIGO. The color indicates the $\log_2$(fold change).

In the GO domain molecular function, the majority of proteins was assigned to the GO term “transferase activity, transferring glycosyl groups”. 7 of the 11 proteins assigned to this GO were UDP-glucuronosyl transferases (UGT). Interestingly, several of the genes encoding these proteins have been shown to be up-regulated in response to mitochondrial stress (i.e. upon knock-down of the mitochondrial protease *spg-7*) [Nargund et al., 2012]. Therefore, UDP-glucuronosyl transferases may be part of a general stress response pathway that is activated upon peroxisomal as well as mitochondrial stress.

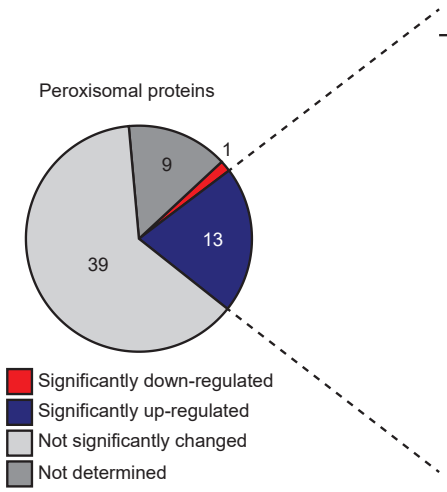

Name	Enzyme function	Metabolic function
CTL-2	Catalase	Degradation of H_2O_2
PMP-4	ABC class D transporter	Fatty acid transport
ACS-7	Acyl-CoA synthetase	Beta-oxidation
ACOX-3	Acyl-CoA oxidase	Beta-oxidation
ACOX-1.6	Acyl-CoA oxidase	Beta-oxidation
ACOX-1.5	Acyl-CoA oxidase	Beta-oxidation
MAOC-1	Dehydogenase	Beta-oxidation
DHS-28	Dehydogenase	Beta-oxidation
DHS-18	Dehydogenase	Beta-oxidation
F53C11.3	2,3-dienoyl-CoA reductase	Beta-oxidation
ZK550.6	Phytanoyl-CoA 2-hydoxylase	Alpha-oxidation
GSTK-1	Gluthatione S transferase kappa	Lipid metabolism
C24A3.4	Alpha-methylacy-CoA racemase	Bile acid biosynthesis

Figure 3.28: Peroxisomal proteins that were significantly changed upon *prx-5(RNAi)*. Proteins with a $\log_2$(fold change) value $\geq$1 (increased) or $\leq$-1 (decreased) and p$<$0.05 by a limma moderated t-test compared to *tag-208(RNAi)* were considered as significantly changed. The enzyme function and metabolic pathway is based on experimental data in *C. elegans* or on homology to the mammalian enzyme. (not determined: the enzyme was not detected by LC-MS).

The GO enrichment analysis of the domain cellular component revealed two enriched GO terms: “microbody” (GO:0042579, p=5.35e-04) and “peroxisome” (GO:0005777, p=1.90e-05). In the proteomic analysis, 53 of the 62 peroxisomal proteins (Appendix Table A.4) were identified. PRX-5 was the only significantly down-regulated peroxisomal protein and $\sim$25% (13/53) of the identified peroxisomal proteins were significantly up-regulated upon *prx-5(RNAi)* (Figure 3.28). Only one of these up-regulated proteins was a peroxisomal membrane protein (PMP-4) and the remaining were peroxisomal matrix proteins. Among them was also the peroxisomal catalase (3.1-fold, p=0.012), which is consistent with the transcriptional up-regulation of the $P_{ctl\text{-}2}GFP$ (*bcSi76*) reporter (see chapter 3.3.1). In contrast, the protein levels of the peroxisomal Lon protease were

not significantly changed (1.1-fold, p=0.874). In the Western blotting analysis of *prx-5(RNAi)* samples, the endogenous LONP-2 levels were even decreased (see chapter 3.3.1). Both observations support the hypothesis that *lonp-2* is additionally regulated at the post-transcriptional and/or translational level. Interestingly, all significantly up-regulated peroxisomal proteins are involved in lipid metabolism (Figure 3.28). Therefore, we hypothesize that reduced peroxisomal matrix protein import leads to a compensatory increase in peroxisomal beta-oxidation proteins.

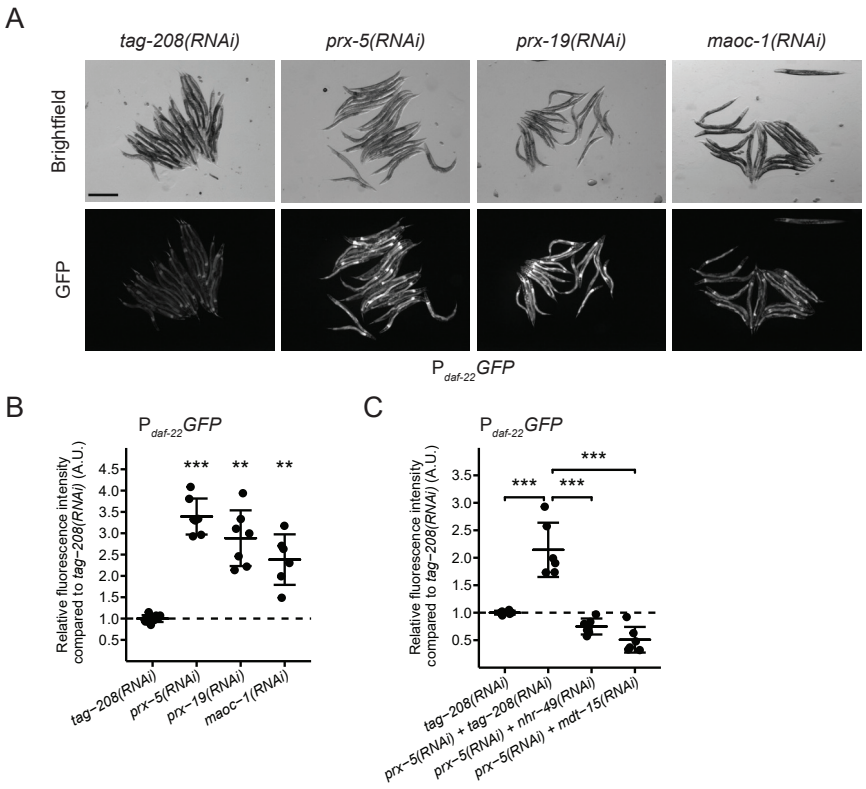

Figure 3.29: The thiolase *daf-22* is up-regulated upon perturbation of peroxisomal biogenesis. (A) L4 larvae carrying the P$_{daf\text{-}22}$*GFP* (*bcSi110*) reporter were subjected to different RNAi and the expression of the reporter was analyzed by brightfield and fluorescent microscopy. The *prx-5(RNAi)* and *prx-19(RNAi)* clones were diluted 1:2 with *tag-208(RNAi)* to reduce the slow growth phenotype. Representative images are shown. The scale bar represents 1 mm. (B) The fluorescence intensity of the P$_{daf\text{-}22}$*GFP* (*bcSi110*) reporter was quantified relative to the negative control *tag-208(RNAi)*. (Mean and SD are shown: n=6-13 (n=number of biological replicates); ** $p<0.01$ and *** $p<0.001$ by a Welch's ANOVA with Games-Howell post hoc test to *tag-208(RNAi)*). (C) Dependence of the induction on NHR-49. The RNAi clones were diluted 1:2. Quantification of the reporter relative to the control *tag-208(RNAi)*. (Mean and SD are shown: n=6 (n=number of biological replicates); *** $p<0.001$ by a One-way ANOVA with Tukey HSD post hoc test.)

The protein level of the thiolase DAF-22 was up-regulated, albeit not significantly (4.9-fold, p=0.051) in the proteomic analysis of the *prx-5(RNAi)* samples. To test if *daf-*

22 is up-regulated at a transcriptional level, I generated a $P_{daf\text{-}22}GFP$ (*bcSi110*) reporter. Upon perturbation of peroxisomal biogenesis by knock-down of *prx-5* and *prx-19*, the reporter was induced about 3-fold compared to the control *tag-208(RNAi)* (Figure 3.29A, B). Moreover, a block of peroxisomal beta-oxidation by *maoc-1(RNAi)* also induced the reporter (Figure 3.29A, B). Furthermore, the induction was dependent on NHR-49 and its co-factor MDT-15 (Figure 3.29C). Taken together, *daf-22* is also a target gene of the PRS. Moreover, this experiment suggests that the PRS induced by *prx-19(RNAi)* also leads to an up-regulation of peroxisomal beta-oxidation.

To summarize the results of this chapter, I have shown that perturbation of peroxisomal biogenesis by knock-down of peroxins induces the PRS, which leads to the transcriptional up-regulation of the peroxisomal Lon protease and peroxisomal catalase. Furthermore, I have shown that the signaling pathway is dependent on the nuclear hormone receptor NHR-49 and its co-factor MDT-15. Perturbation of peroxisomal biogenesis might lead to impaired peroxisomal lipid metabolism. Indeed, I observed that knock-down of peroxisomal beta-oxidation enzymes also induced the PRS. Finally, transcriptomic and proteomic analysis revealed that the activation of the PRS induces the up-regulation of lipid metabolism enzymes and the innate immune response.

3.4 The mitochondrial chaperone *hsp-6* is induced by a perturbation of peroxisomal biogenesis

The knock-down of peroxisomal beta-oxidation genes specifically induced the PRS and not the mitochondrial unfolded protein response (see chapter 3.3.6). In contrast, perturbation of peroxisomal matrix protein import by *prx-5(RNAi)* induced both organellar stress responses. Therefore, we asked if a perturbation of peroxisomal biogenesis is generally inducing UPR^{mt}. To this end, I subsequently knocked-down all peroxins and tested for the induction of the UPR^{mt} transcriptional reporter $P_{hsp\text{-}6}GFP$ (*zcIs13*). Knock-down of *prx-10* induced the reporter by about 20-fold compared to the control *tag-208(RNAi)* (Figure 3.30A, B). Sequencing of the RNAi clone revealed that it also targets *wars-2*, which encodes the homolog of a mitochondrial tryptophanyl tRNA synthetase. Knock-down of

prx-12 and *prx-19* induced the GFP expression of the reporter about 3-fold compared to the control *tag-208(RNAi)*. In these experiments, the induction of the P*hsp-6*GFP (*zcIs13*) reporter by *prx-5(RNAi)* was very weak. Taken together, the block of peroxisomal membrane protein insertion and perturbation of PRX-5 recycling induces the UPR^{mt} transcriptional reporter P*hsp-6*GFP (*zcIs13*) (Figure 3.30C).

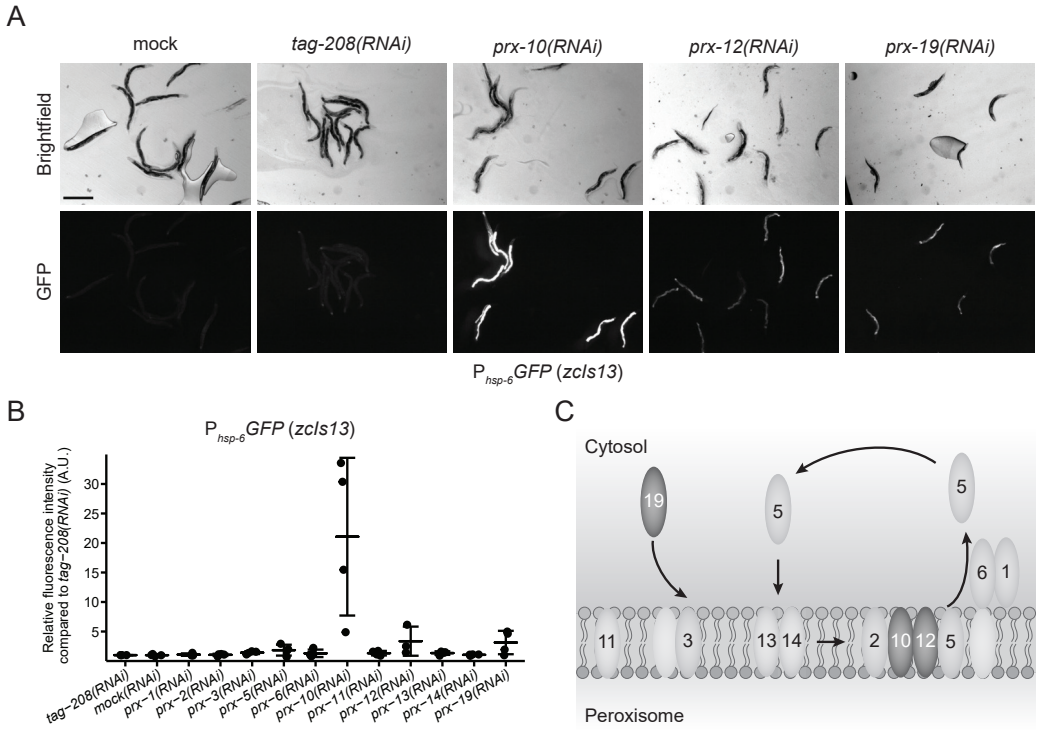

Figure 3.30: The UPR^{mt} transcriptional reporter P*hsp-6*GFP (*zcIs13*) is induced upon perturbation of peroxisomal biogenesis. (A) L4 larvae carrying the P*hsp-6*GFP (*zcIs13*) reporter were subjected to different peroxin RNAi and the expression of the reporter was analyzed by brightfield and fluorescent microscopy. Representative images of RNAi conditions that induce the reporter more than 2-fold are shown. The scale bar represents 0.5 mm. (B) The fluorescence intensity of the P*hsp-6*GFP (*zcIs13*) reporter was quantified relative to the negative control *tag-208(RNAi)* (n=4 (n=number of biological replicates)). (C) *C. elegans* homologs of human peroxins. The numbers represent the number of the respective peroxin (PRX). Proteins shown in dark grey induce a more than 2-fold transcriptional up-regulation of the P*hsp-6*GFP (*zcIs13*) reporter.

Since the results for the induction of UPR^{mt} by the perturbation of peroxisomal biogenesis were not consistent, the experiment was repeated. The positive control *spg-7(RNAi)* induced the reporter P*hsp-6*GFP (*zcIs13*) about 15-fold compared to the negative control *tag-208(RNAi)* (Figure 3.31A). *spg-7* encodes the *C. elegans* homolog of the mitochondrial peptidase AFG3L2. The induction of the reporter by knock-down of the peroxins *prx-5* and *prx-12* was only 2.3-fold and 5.4-fold, respectively. *prx-19(RNAi)* in-

duced the reporter by 3.7-fold, albeit not significantly. To test if the induction is specific to *hsp-6*, the experiment was repeated using the UPR^{mt} transcriptional reporter P$_{hsp-60}$*GFP* (*zcIs9*). In this case, the positive control *spg-7(RNAi)* up-regulated the reporter 1.8-fold and *prx-12(RNAi)* led to a 1.4-fold induction. However, in both conditions the induction was not significant (Figure 3.31B). Since in this experiment the knock-down by RNAi was not efficient enough, it is not possible to conclude if the induction of UPR^{mt} is specific to *hsp-6*.

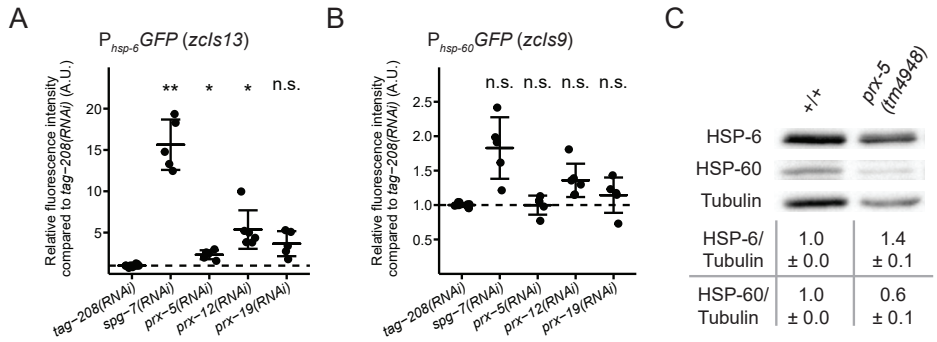

Figure 3.31: HSP-6 is up-regulated upon perturbation of peroxisomal biogenesis. (A and B) L4 larvae carrying the UPR^{mt} reporter were subjected to different RNAi and the expression of the reporter was analyzed by fluorescent microscopy. The fluorescence intensity of the P$_{hsp-6}$*GFP* (*zcIs13*) reporter (A) and P$_{hsp-60}$*GFP* (*zcIs9*) reporter (B) was quantified relative to the negative control *tag-208(RNAi)*. *spg-7(RNAi)* was diluted 1:5 with *tag-208(RNAi)* to reduce slow growth. (Mean and SD are shown: n=5-11 (n=number of biological replicates); n.s.=not significant, * $p<0.05$ and ** $p<0.01$ by a Welch's ANOVA with Games-Howell post hoc test to *tag-208(RNAi)*). (C) The same Western blot membrane as in chapter 2.6 was decorated with anti-HSP-6 and anti-HSP-60 antibodies. The band intensities were normalized to the respective Tubulin loading controls and quantified relative to the wild-type. (Mean and SD are shown: n=3 (n=number of biological replicates)).

To avoid the issue of RNAi efficiency, I tested if the loss of function mutation *prx-5(tm4948)* leads to an increase in the mitochondrial chaperones HSP-6 and HSP-60. Western blotting analysis of *prx-5(tm4948)* animals revealed that the HSP-6 levels increased 1.4-fold compared to wild-type animals (Figure 3.31C). In contrast, the HSP-60 levels decreased by 40%. Taken together, this experiment suggest that the perturbation of peroxisomal biogenesis causes an up-regulation of the mitochondrial chaperonne *hsp-6* but not *hsp-60*. It therefore remains to determined whether the perturbation of peroxisomal biogenesis triggers UPR^{mt} or causes only the specific up-regulation of *hsp-6*.

4

Discussion

4.1 Analysis of peroxisomes in *C. elegans* by fluorescent microscopy

To analyze the tissue-specific localization of peroxisomes in *C. elegans*, peroxisomes were visualized by fluorescent microscopy. A fusion protein of the peroxisomal thiolase DAF-22 with mKate2 was expressed under the control of the endogenous *daf-22* promoter ($P_{daf\text{-}22}$*mKate2::daf-22*). Like previously reported, mKate2::DAF-22 labeled peroxisomes were observed in the intestine and the hypodermis [Yokota et al., 2002, Petriv et al., 2002, Butcher et al., 2009]. Since these two tissues are the primary sites of fat storage in *C. elegans* [Wang et al., 2011] and peroxisomes are required for the beta-oxidation of stored fat [Srinivasan et al., 2008b], it seems logical that peroxisomes are present in these tissues. Butcher *et al.* additionally described the expression of a GFP::DAF-22 reporter in body wall muscle cells [Butcher et al., 2009]. In my experiment, it was difficult to determine if mKate2::DAF-22 labeled peroxisomes were present in body wall muscle cells because of the strong expression of the reporter in the surrounding tissues. However, I observed that head muscle cells only contain very few peroxisomes that only import low amounts of the mKate2::DAF-22 fusion protein. Similar to the body wall muscle cells, it was not possible to exactly determine if neurons contain peroxisomes. To overcome this issue, reporters under the control of tissue-specific promoters could be used. Moreover, reporters that label specific cells could be co-expressed to facilitate the identification of the right cell. Additionally, using confocal instead of wide-field fluorescent microscopy would improve the resolution and imaging contrast, thus reducing the problem of out-of-focus light.

4.2 Characterization of the peroxisomal Lon protease in *C. elegans*

The peroxisomal Lon protease has not been characterized in *C. elegans* so far. I showed that LONP-2 localizes to peroxisomes and that it is required for the degradation of an unfolded protein that is targeted to peroxisomes ($DHFR^{mut}$::PTS1). The unfolded protein $DHFR^{mut}$::PTS1 can be stabilized by the addition of the small molecule ligand TMP. The experiment showed that in the absence of TMP, $DHFR^{mut}$::PTS1 is very efficiently

degraded by LONP-2, whereas upon addition of TMP, only a small faction is degraded. This fraction might be not fully stabilized DHFR^{mut}::PTS1 or LONP-2 is also required for the degradation of proteins that are mislocalized peroxisomes. To test if LONP-2 is required for the degradation of mislocalized proteins, a stable and correctly folded wild-type form of DHFR could be targeted to peroxisomes. If LONP-2 is also required for the degradation of the wild-type DHFR, it would accumulate under *lonp-2(RNAi)* conditions.

The experiment also suggested that the unfolded protein carrying a peroxisomal targeting sequence is protected from the degradation in the cytosol and is imported into peroxisomes in *C. elegans*. These results are similar to a study of the peroxisomal Lon protease in the yeast *Hansenula polymorpha* [Aksam et al., 2007]. The authors suggest that DHFR^{mut}::PTS1 is protected from the degradation by the ubiquitin/proteasome system in the cytosol but is then degraded in peroxisomes by the peroxisomal Lon protease. However, Aksam *et al.* and I used Western analysis of whole cell/worm extracts as a read out. Therefore, we cannot exclude that the accumulation of DHFR^{mut} upon knock-out/down of *lonp-2* might also occur in the cytosol. However, I observed in a preliminary fluorescence microscopy experiment an increase in YFP-tagged DHFR^{mut} in peroxisomes upon knock-down of *lonp-2*. Additionally, a cell fractionation assay could be done to exclude this possibility.

Aksam *et al.* suggest that the degradation of peroxisomes by autophagy is another important mechanism to prevent the accumulation of non-functional peroxisomal proteins or peroxisomes in yeast cells [Aksam et al., 2007]. However, they did not test if the expression of DHFR^{mut}::PTS1 leads to the induction of autophagy or pexophagy. One way to study pexophagy is the RedGreen-assay, which is a fluorescence-based technique used to visualize the targeting of substrates to the autolysosome. The reporter construct contains of a tandem GFP-mCherry that is targeted to peroxisomes. When the organelle is targeted for degradation in the autolysosome, the GFP signal is quenched due to the low pH environment and only the mCherry signal will be observed [Deosaran et al., 2013]. A similar reporter targeted to lysosomes has been used in *C. elegans* to study autophagy [Chang et al., 2017]. The reporter P$_{daf\text{-}22}$*YFP::dhfr^{mut}::PTS1* and P$_{vha\text{-}7}$*mCherry::PTS1* (*bcSi112;bcEx1375*) used to analyze the localization of DHFR^{mut}::PTS1 should display

similar properties. I observed that without the stabilizing ligand some mCherry-labeled peroxisomes colocalize with a weak YFP signal and others are YFP negative. Either the YFP::DHFR^{mut} in these peroxisomes was completely degraded by LONP-2 or these peroxisomes undergo pexophagy and therefore the YFP signal is quenched in the autolysosome. Using a lysosome marker could reveal if these peroxisomes are indeed localized to lysosomes for degradation. In future, also a mCherry::GFP::PTS1 tandem reporter could be used as a tool to analyze pexophagy. In this case, DHFR^{mut}::PTS1 should not be fused to YFP, because the GFP and YFP signals cannot be distinguished by wide-field fluorescent microscopy.

We hypothesized that the increased level of an unfolded protein targeted to peroxisomes could lead to an up-regulation of the peroxisomal Lon protease. However, the expression of DHFR^{mut}::PTS1 did not lead to a change in LONP-2 levels in a time course experiment. Assuming that the time point when the LONP-2 levels changed was not missed due to the experimental design, the data suggests that the levels of LONP-2 in peroxisomes are sufficient to cope with the overexpression of an unfolded protein targeted to peroxisomes.

4.3 The peroxisomal retrograde signaling pathway

4.3.1 Proposed model for the PRS

In this thesis, I have identified for the first time the existence of retrograde signaling pathway from peroxisomes to the nucleus (PRS) that is induced by the perturbation of peroxisomal biogenesis by knock-down of peroxins (Figure 4.1). This signaling pathway is dependent on the nuclear hormone receptor NHR-49 and its co-factor MDT-15. We speculated that perturbation of peroxisomal biogenesis might lead to impaired peroxisomal lipid metabolism. Consistent with this hypothesis, I showed that knock-down of peroxisomal beta-oxidation enzymes also induced the PRS. We propose that the resulting change in lipid composition might activate NHR-49 and its co-factor MDT-15 thereby leading to the transcriptional up-regulation of the peroxisomal Lon protease. Moreover, lipid metabolism enzymes and the innate immune response are up-regulated upon induc-

tion of the PRS. We propose that this up-regulation represents a compensatory mechanism, which is induced to restore the peroxisomal function in response to a perturbation of peroxisomal biogenesis. The results that led to this proposed model are discussed in the following sections in more detail.

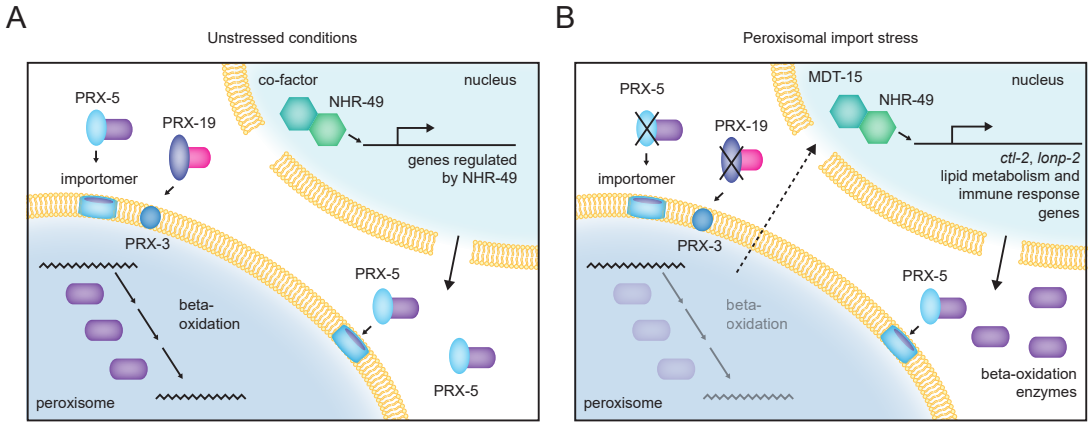

Figure 4.1: The peroxisomal retrograde signaling pathway. (A) Under physiological conditions, some genes encoding peroxisomal proteins are under the control of the nuclear hormone receptor NHR-49 and its co-factors. These proteins are imported into the peroxisomal matrix by the import receptor PRX-5. (B) Peroxisomal stress due to perturbation of peroxisomal biogenesis leads to an impaired peroxisomal beta-oxidation. We hypothesize that the resulting change in lipid composition activates NHR-49. It interacts with its co-factor MDT-15 and activates the expression of genes coding for lipid metabolism enzymes and immune response proteins. We suggest that an increase in the levels of these enzymes increases their probability to be recognized by the remaining PRX-5 receptors for import into peroxisomes.

4.3.2 The PRS is induced by a perturbation of peroxisomal biogenesis

To induce peroxisomal stress, all *C. elegans* homologs of human peroxins were subsequently knocked-down. Notably, the knock-down of the peroxins induced the transcriptional up-regulation of the peroxisomal Lon protease to different extent. Specifically, perturbation of the first steps of the peroxisomal matrix protein import pathway induces the transcriptional response. For example, reduced levels of the import receptor PRX-5 and the components of its docking complex PRX-13 and PRX-14 strongly induced the response. In contrast, perturbation of the following step, the receptor recycling, only led to a weak induction. Similarly, reduced levels of the membrane protein receptor PRX-19 induces the response stronger than the knock-down of its docking partner PRX-3. Therefore, we focused in the study on the two import receptors PRX-5 and PRX-19.

4.3.3 Perturbation of peroxisomal biogenesis induces an up-regulation of the peroxisomal Lon protease and the peroxisomal catalase

Peroxisomal import stress in *C. elegans* caused by the knock-down of the receptors *prx-5* or *prx-19* induced the up-regulation of the transcriptional reporters of the peroxisomal Lon protease *lonp-2*. Interestingly, the LONP-2 protein levels only increased upon *prx-19(RNAi)*, whereas upon knock-down or knock-out of *prx-5* the levels even decreased. It is conceivable that upon reduction of peroxisomal membrane protein insertion by *prx-19(RNAi)*, LONP-2 can still be imported into the peroxisomal matrix. In contrast, upon loss of the matrix protein import receptor PRX-5, the peroxisomal Lon protease might accumulate in the cytosol, which could be harmful for the cell. Therefore, a post-transcriptional and/or post-translational regulation of LONP-2 might exist. This observation is similar to the regulation of the mitochondrial Lon protease LONP1 during the mitochondrial unfolded protein response. LONP1 is up-regulated at the transcriptional level but this does not result in an increased protein level, which is consistent with several post-transcriptional responses occurring during UPR^{mt} (e.g. protein degradation, attenuation of protein synthesis or mitophagy) [Fiorese et al., 2016].

In contrast to LONP-2, knock-down of *prx-5* led to the transcriptional up-regulation of the peroxisomal catalase *ctl-2*, which resulted in increased CTL-2 protein levels. This indicates that the cell does not need to counteract a cytosolic accumulation of the peroxisomal catalase. Conversely, it even has been shown in PEX5-/- mouse embryonic fibroblasts that a cytosolic localization of catalase can protect the cytosol against oxidative stress [Walton et al., 2017].

4.3.4 The PRS is regulated by the transcription factor NHR-49 and its co-factor MDT-15

We define the up-regulation of effector genes upon peroxisomal biogenesis stress as peroxisomal retrograde signaling. The retrograde signal from the peroxisome to the nucleus is dependent on the nuclear hormone receptor NHR-49 and its co-factor MDT-15. It is possible, that other transcription factors are also involved in the response but that the

knock-down in the double RNAi experiment was not efficient enough to show a suppression. Strains that carry mutations in the respective genes could be used to verify the observations by RNAi. Moreover, only selected candidates were tested. Thus, a genome-wide suppressor screen could reveal more candidates required for the induction of the PRS.

The experiment showed that in the absence of peroxisomal stress, the basal expression of *lonp-2* is dependent on NHR-49, whereas the basal expression of *ctl-2* is not. This observation is also reflected at the protein level as shown by a published *nhr-49(RNAi)* proteome [Fredens et al., 2011]. Comparison of the *prx-5(RNAi)* proteomic data with the *nhr-49(RNAi)* proteome revealed that only about a quarter of the proteins changed upon *prx-5(RNAi)* are regulated by NHR-49 under physiological conditions (i.e. in the absence of peroxisomal import stress). This suggests that NHR-49 can activate the expression of genes upon peroxisomal import stress, although these genes are not under its control under physiological conditions.

The basal expression of the $P_{lonp\text{-}2}GFP$ (*bcIs126*), $P_{ctl\text{-}2}GFP$ (*bcSi76*) and $P_{daf\text{-}22}GFP$ (*bcSi110*) reporter is dependent on MDT-15. It might appear that GFP levels are generally reduced under *mdt-15(RNAi)* conditions. However, it has been shown that the basal expression of the transcriptional UPR^{mt} reporter $P_{hsp\text{-}6}GFP$ *(zcIs13)* is not affected by *mdt-15(RNAi)* [Hou et al., 2014].

4.3.5 Reduced peroxisomal biogenesis leads to an import defect in intestinal cells and induces an increase in the peroxisomal number in hypodermal cells

Knock-down of *prx-5* by RNAi impairs peroxisomal matrix protein import [Petriv et al., 2002]. In contrast to the study by Petriv *et al.*, we use milder RNAi conditions leading to a partial knock-down of *prx-5* ($\sim$60% reduction of PRX-5 protein). Therefore, I analyzed the effect of the partial reduction of PRX-5 on peroxisomal matrix protein import. Fluorescence microscopy analysis of the import of the peroxisomal thiolase DAF-22 fused to mKate2 revealed that our *prx-5(RNAi)* condition leads to a partial block of peroxisomal matrix protein import in the intestine. In contrast, the import was not affected in hypodermal cells. However, *prx-5(RNAi)* or *prx-19(RNAi)* treatment led to an increase in

peroxisomes labeled with the peroxisomal membrane marker mKate2::PXMP-4, whereas the number of peroxisomes importing GFP::PTS1 was similar to control RNAi conditions. This indicates that a subset of the hypodermal peroxisomes might not be import competent. A concurrent increase in the fluorescence intensity of some peroxisomes labeled by GFP::PTS1 indicates that the import of some peroxisomes might be actually increased to compensate for the non-functional peroxisomes. It is conceivable that the peroxisomes that do not show a GFP::PTS1 signal might undergo pexophagy. Red fluorescent proteins are more stable in lysosomes than GFP. This could explain an increase in mKate2-labeled peroxisomal membranes while the number of GFP::PTS1-labeled peroxisomes remains constant. Using a mCherry::GFP::PTS1 tandem reporter could reveal if the increase in mKate2-labeled peroxisomes is indeed due to increased pexophagy. The proteomic analysis of *prx-5(RNAi)* treated animals showed that there was no significant increase in peroxisomal membrane proteins compared to the control. This supports the idea that the number of peroxisomes does not increase due to a *de novo* formation but that they arise by division. However, the homologs of proteins involved in peroxisomal fission like DRP-1, MFF-2, FIS-2 and PRX-11 were not significantly up-regulated upon *prx-5(RNAi)*.

Interestingly, knock-down of *prx-5* as well as the loss of function by a mutation in *prx-5* induce the peroxisomal retrograde signaling. The RNAi treatment only leads to impaired peroxisomal matrix protein import in the intestine whereas the import in hypodermal cells is not affected. In contrast, in the *prx-5* mutant, the peroxisomal import is almost completely blocked in hypodermal cells. Due to the high cytosolic signal of GFP::PTS1 in the mutant, it cannot be excluded that some of the peroxisomes are still import competent but their signal is not visible by fluorescent microscopy. Also the effect on the mKate2::PXMP-4 labeled peroxisomes is different in the two cases. The number of peroxisomes increases upon RNAi treatment, whereas fewer and enlarged peroxisomes are visible in the mutant. Although the effects on import and morphology are very different, both conditions induce the PRS. This indicates that already a minor defect in peroxisomal biogenesis is sufficient to induce the PRS, but that a strong peroxisomal import defect also induces the same pathway. Analyzing the proteome of the *prx-5(tm4948)* loss

of function mutant would give insights if the response is similar in both cases or if there are differences in the PRS depending on the severity of the peroxisomal import defect.

PRX-19 is a homolog of the mammalian import receptor for peroxisomal membrane proteins PEX19. Peroxisomal membrane proteins can be imported in a PEX19 dependent or independent manner. To study the function of PRX-19 for peroxisomal membrane protein insertion in *C. elegans*, we generated a fusion construct of the homolog of the mammalian peroxisomal membrane protein PXMP4 to target mKate2 to the peroxisomal membrane in hypodermal cells. PXMP4 has been shown to be imported in a PEX19 dependent manner [Pinto et al., 2006]. If this is conserved for the *C. elegans* protein PXMP-4, a knock-down of *prx-19* would lead to a disrupted insertion of PXMP-4 into the peroxisomal membrane and the signal intensity of the peroxisomes labeled by mKate2 would be decreased or even absent. Indeed, a fraction of peroxisomes showed a very weak mKate2 signal upon *prx-19(RNAi)*. This indicates that PXMP-4 is imported in a PRX-19 dependent manner similar to its mammalian homolog.

4.3.6 Lipids are potential signaling molecules in the PRS

We hypothesized that a block in peroxisomal biogenesis would also lead to a perturbation of peroxisomal beta-oxidation. In *C. elegans*, peroxisomal beta-oxidation has a dual role. The shortening of very long chain fatty acids has either metabolic functions or it contributes to the biosynthesis of ascaroside pheromones. Specifically the knock-down of *acox-1.1*, *dhs-28*, *maoc-1* and *daf-22* induced the PRS. These enzymes have been studied in the context of ascaroside biosynthesis and lack of these genes leads to a change in the ascaroside and fatty acid composition of *C. elegans* [Butcher et al., 2009, von Reuss et al., 2012, Artyukhin et al., 2018, Zhang et al., 2018]. In contrast, knock-down of genes that are only predicted by sequence homology to code for peroxisomal beta-oxidation enzymes [Gilst et al., 2005] (e.g. *ech-6*, *ech-8* and *ech-9*) did not induce the PRS. Analysis of the lipid content of *prx-5(RNAi)* treated animals using the fat-soluble dye Oil Red O did not show an accumulation of lipids compared to control animals. This indicates that lipids do not accumulate upon knock-down of *prx-5*. However, the approach is not sensitive enough to sense minor changes in the lipid content. Thus, we hypothesize that

the lipids not generally accumulate but the fatty acid or ascaroside composition might be changed. To test this hypothesis, the metabolome of *prx-5(RNAi)* treated animals could be analyzed by mass spectrometry.

The lipids might act as signaling molecules in the PRS. It has been shown that lipid binding proteins can provide a link between lipids and nuclear hormone receptors like NHR-49 [Xu et al., 2011, Folick et al., 2015]. Identifying the lipid binding protein involved in the PRS would support the hypothesis that lipids are the signaling molecules. Moreover, based on the results of the metabolic analysis, different lipids or ascarosides could be fed to the PRS reporter strains to test if they can induce the signaling.

Many metabolic pathways taking place in peroxisomes generate hydrogen peroxide and other reactive oxygen species (ROS). Hydrogen peroxide derived from peroxisomes can act as cellular signaling molecule regulating various biological processes [Brown et al., 1999, Koepke et al., 2008, Ivashchenko et al., 2011]. Thus, one could speculate that ROS and not fatty acids are the signaling molecules in the PRS. It is conceivable that the knock-down of *prx-5* might result in a decreased import of the peroxisomal catalase CTL-2 and thus in a disruption of the redox balance between peroxisomes and the cytosol. However, a disrupted redox balance between the peroxisome and the cytosol caused by the knock-down of genes coding for the cytosolic catalase CTL-1 or the peroxisomal catalase CTL-2 did not induce the PRS. However, it would be necessary to confirm that the knock-down of the catalases leads to a disrupted redox balance using redox sensors targeted to the peroxisome and the cytosol. Another possibility to induce a redox imbalance would be to target the photosensitizer KillerRed to peroxisomes, where it would produce ROS upon green light illumination [Ivashchenko et al., 2011].

Miranda-Vizuete and Veal provide in their review a list of 14 ROS metabolizing enzymes in *C. elegans* [Miranda-Vizuete and Veal, 2017]. We identified 12 proteins of this list in our *prx-5(RNAi)* proteome and three of them (CTL-1, CTL-2 and SOD-3) were significantly up-regulated upon *prx-5(RNAi)*. Interestingly, CTL-1 localizes to the cytosol, CTL-2 localizes to peroxisomes and SOD-3 localizes to mitochondria [Taub et al., 1999, Hunter et al., 1997]. This suggests that upon perturbation of peroxisomal matrix protein import, ROS are produced in several compartments of the cell and, therefore, ROS

scavenging enzymes localizing to these compartments are up-regulated. Zhou *et al.* observe reduced ROS levels in *C. elegans* animals treated with *prx-5(RNAi)* [Zhou et al., 2012], which could be explained by the up-regulation of ROS scavenging enzymes. It would be interesting, if we can reproduce under our RNAi conditions the observation that *prx-5(RNAi)* leads to a decreased ROS level.

4.3.7 RNA-seq and proteomic analysis of the PRS show similar results

We identified the peroxisomal Lon protease and peroxisomal catalase as effector genes of the PRS. To identify further effectors, we analyzed the effect of the knock-down of *prx-5* on the *C. elegans* transcriptome by RNA-seq and on the proteome by mass spectrometry. GO enrichment analysis of both datasets showed similar results. For instance, the GO terms "lipid metabolic process" (GO:0006629) and "immune response" (GO:006955) were enriched in both analyses and will be discussed in more detail below (see chapters 4.3.8 and 4.3.9). However, it is not possible to compare the two datasets directly because the samples for the two experiments were prepared separately and the RNAi protocol was slightly different. To be able to compare multi-omics data, it should ideally be generated from the same set of samples (i.e. under the same conditions). Besides the experimental design, there are also biological reasons why the two datasets can differ. Changes at the mRNA level are not always reflected by changes at the protein level because of post-transcriptional and/or translation regulation. Furthermore, the transcriptional response may precede the change in protein levels. Therefore, conducting a time course experiment can reveal these differences between the transcriptome and the proteome.

To identify if specifically peroxisomal proteins were changed, we generated a list of peroxisomal proteins in *C. elegans*. The list includes 62 proteins that have a clear PTS1 sequence or a PEX19 targeting prediction in *C. elegans* and/or the mammalian homolog localizes to peroxisomes. This number of proteins is consistent with a proteomic study of human liver peroxisomes [Gronemeyer et al., 2013]. We observed that under our *prx-5(RNAi)* conditions about 60% of peroxisomal genes but only 25% of peroxisomal proteins were up-regulated. It is conceivable that activation of the PRS induces a general increase in peroxisomal biogenesis but due to the lack of the import receptor PRX-5, the

levels of some proteins are regulated post-trancriptionally and/or post-translationally. Surprisingly, upon *prx-5(RNAi)*, the *prx-5* transcripts were also increased 4.3-fold, whereas the change in PRX-5 protein level is 0.4-fold. One explanation might be that we analyzed the transcriptome and the proteome at the same time point. It is conceivable that the gene was knocked-down at an earlier time point leading to reduced protein levels. In turn the PRS was activated, which leads to a general transcriptional up-regulation of peroxisomal genes, including *prx-5*. Supporting this notion, it has been shown for mitochondria that the induction of UPR^{mt} by knock-down of the gene encoding the protease SPG-7 by RNAi leads to the transcriptional up-regulation of *spg-7* [Nargund et al., 2012]. Since the protein levels of PRX-5 are nevertheless decreased and we see a reduction of peroxisomal matrix protein import by fluorescence microscopy, our RNAi conditions are still suitable to study the PRS induced by reduced peroxisomal matrix protein import.

4.3.8 The PRS induces a compensatory up-regulation of the peroxisomal lipid metabolism

25% of the peroxisomal proteins were significantly changed in the *prx-5(RNAi)* proteome and all of them play a role in peroxisomal lipid metabolism. Futhermore, genes encoding proteins involved in lipid metabolism were significantly enriched in the RNA-seq dataset. We hypothesize that the defect in peroxisomal matrix protein import by *prx-5(RNAi)* leads to perturbation of peroxisomal lipid metabolism, which in turn activates a compensatory up-regulation of the respective enzymes. Since the amount of PRX-5 molecules is only decreased by 60% in our RNAi conditions, an increase in the level of peroxisomal lipid metabolism enzymes could increase their chance to be recognized by the few PRX-5 receptors and thus being imported into the remaining functional peroxisomes. In support this notion, I did not observe an accumulation of lipids stained by the fat-soluble dye Oil Red O upon the induction of the PRS, indicating that the function of peroxisomes in beta-oxidation is maintained. Why no other peroxisomal metabolic pathways are up-regulated requires further investigation. Interestingly, KEGG pathway enrichment analysis of the RNA-seq data showed an enrichment on genes assigned to several amino acid metabolism pathways. However, the levels of the respective proteins were not significantly changed.

4.3.9 The PRS induces the innate immune response

GO enrichment analysis of the *prx-5(RNAi)* transcriptome and proteome showed that not only the peroxisomal fatty acid metabolism but also the innate immune response was up-regulated. Interestingly, MAOC-1 was the only protein assigned to GO terms of both processes. MAOC-1 is required for peroxisomal beta-oxidation and for the resistance to the pathogen *Pseudomonas aeruginosa* [Shapira et al., 2006]. However, one of the caveats of GO terms is that the automated assignments can be incomplete and, therefore, manual assignments are still necessary. Literature research revealed that MAOC-1 is not the only protein significantly up-regulated upon *prx-5(RNAi)* that has a dual role in peroxisomal beta-oxidation and innate immune response. Among the beta-oxidation enzymes that were identified in the proteomic analysis, the genes coding for ACS-7, ACOX-1.5, CTL-2, DHS-18, DHS-28, MAOC-1 and DAF-22 have been shown to be up-regulated upon infection with different bacteria [Troemel et al., 2006, Wong et al., 2007]. Moreover, ZK550.6, which encodes a homolog of a peroxisomal alpha-oxidation enzyme, is also up-regulated [Troemel et al., 2006]. A link between lipid metabolism and the immune response has previously been described in *C. elegans* [Nandakumar and Tan, 2008]. We hypothesize that the cell tries to compensate for the peroxisomal defect upon *prx-5(RNAi)* by an up-regulation of both pathways. It would be interesting to test, if the up-regulation of the immune response effectors by the PRS is sufficient to maintain the immune response in the animal. In this case, the animals would be not more susceptible to an infection by a pathogen compared to untreated animals. However, it has been shown in the fruit fly *Drosophila melanogaster* that in infected animals a knock-down of Pex5 leads to a reduced survival compared to animals without RNAi treatment. This indicates that the immune response is impaired due to peroxisomal dysfunction [Di Cara et al., 2017]. A killing assay in *C. elegans* could reveal if the PRS is sufficient to restore the immune function of peroxisomes or if the damage is too strong and the animals also show a reduced survival.

Similar to the PRS, the mitochondrial unfolded protein response in *C. elegans* also up-regulates immune response and detoxification genes. Moreover, the UPR^{mt} is induced

by the exposure of *C. elegans* to various pathogens. It has been proposed that UPR^{mt} is induced to reduce mitochondrial damage caused by pathogen exposure [Pellegrino et al., 2014, Liu et al., 2014]. The UPR^{mt} transcription factor ATFS-1 has been shown to be required for the regulation of immune response genes upon mitochondrial dysfunction [Pellegrino et al., 2014]. Remarkably, also the PRS transcription factor MDT-15 is required for the activation of a detoxification response in *C. elegans* animals with dysfunctional mitochondria [Mao et al., 2019]. Moreover, NHR-49 and MDT-15 play a role in the regulation of immune response genes [Pukkila-Worley et al., 2014, Dasgupta et al., 2019]. *C. elegans* lacking ATFS-1, NHR-49 or MDT-15 show a reduced survival when challenged by a pathogen [Pellegrino et al., 2014, Sim and Hibberd, 2016, Mao et al., 2019]. Given the parallels between the UPR^{mt} and the PRS, one can speculate that the PRS similarly functions in the restoration of peroxisomal function upon pathogen infection. To test this hypothesis, the transcriptional PRS reporter strains could be exposed to a pathogen and then be analyzed to test if the peroxisomal retrograde signaling is induced.

Interestingly, the immune response genes up-regulated by UPR^{mt} and PRS overlap but are yet distinct. This indicates that some of the genes are more involved in a general stress response, like for example the UDP-glucuronosyl transferases, whereas other genes are more organelle stress specific.

4.4 The mitochondrial chaperone *hsp-6* is induced by a perturbation of peroxisomal biogenesis

The disruption of peroxisomal biogenesis by *prx-5(RNAi)* not only induced the peroxisomal retrograde signaling, but also the mitochondrial unfolded protein response reporter P$_{hsp\text{-}6}$*GFP* (*zcIs13*). Subsequent knock-down of all peroxins showed that the knock-down of *prx-12* also induces the response and upon *prx-19(RNAi)*, the reporter was also slightly up-regulated, albeit not significantly. Peroxisomes and mitochondria exhibit a functional interplay in several metabolic pathways like the degradation of fatty acids or redox metabolism (reviewed in [Lismont et al., 2015, Wanders et al., 2016]). Defects in peroxisomal lipid or ROS metabolism have an impact on the mitochondrial redox bal-

ance. For example, the inhibition of a peroxisomal very long chain fatty acid transporter ABCD1 impairs mitochondrial oxidative phosphorylation triggering mitochondrial ROS production [López-Erauskin et al., 2013]. Moreover, the inhibition of peroxisomal catalase activity leads to an increase in mitochondrial ROS levels [Walton, 2012]. Also impaired peroxisomal biogenesis by a loss of peroxins compromises mitochondrial function. For instance, it has been shown in mammals that a loss of PEX5 among others depletes mitochondrial DNA and impairs mitochondrial oxidative phosphorylation [Peeters et al., 2015]. Depletion of mitochondrial DNA in mammals causes the induction of UPR^{mt} [Martinus et al., 1996]. Thus, depleted mitochondrial DNA could be a reason for the induction of UPR^{mt} reporter P$_{hsp\text{-}6}$*GFP* (*zcIs13*) carrying the *prx-5(tm4948)* mutation. In contrast to *hsp-6*, another UPR^{mt} target gene *hsp-60* was not up-regulated upon the knock-down of the peroxins and the endogenous HSP-60 levels were even decreased in the *prx-5(tm4948)* mutant. It has previously been described that some UPR^{mt} inducers only up-regulate the expression of the P$_{hsp\text{-}6}$*GFP* (*zcIs13*) reporter but not the P$_{hsp\text{-}60}$*GFP* (*zcIs9*) reporter [Bennett et al., 2014]. This could be due to the different functions of HSP-6 and HSP-60 in mitochondria or due to different sensitivities of the reporters. Analysis of the *hsp-6* or *hsp-60* mRNA levels would be necessary to rule out the latter possibility.

4.5 Conclusion and future perspective

In this study, I have demonstrated that perturbation of peroxisomal biogenesis leads to the induction of a peroxisomal retrograde signaling to restore peroxisomal function. To my knowledge, it is the first description of a peroxisomal stress signaling pathway. Organellar stress response pathways generally consist of four parts. First, there can be several genetic defects or external cues that induce the organellar stress and, hence, the signaling. Second, the stress is recognized and the information is transmitted to the nucleus by signaling molecules. Third, the transcriptional response is activated through transcription factors. Finally, the protein levels of effector proteins is adjusted according to the needs of the organelle. I was able to shed light on three of the four parts of the peroxisomal stress response. In this thesis, I describe two different peroxisomal stresses that

induce the response: the perturbation of peroxisomal biogenesis and the perturbation of peroxisomal beta oxidation. It is conceivable that the perturbation of beta-oxidation is a downstream effect of a perturbed biogenesis. Moreover, I identified the nuclear hormone receptor NHR-49 and its co-factor MDT-15 to be required for the transcriptional response. Finally, using a global transcriptomic and proteomic approach, we identified two groups of effector proteins. The innate immune response and peroxisomal lipid metabolism are up-regulated upon peroxisomal stress. Taken together, the main question that remains to be answered is how the signal is transmitted from the peroxisome to the nucleus. Genetic screens could provide candidates in this regard. We suggest that lipids might act as signaling molecules in the PRS. The comparison of the lipid composition of animals under stressed and unstresed conditions could pinpoint at possible signaling lipids in the PRS.

Organellar stress response pathways are essential to maintain cellular functions. Accordingly, the mitochondrial and endoplasmic reticulum unfolded protein responses are induced in several diseases. Both stress response pathways have been shown to be conserved from *C. elegans* to mammals. To study the physiological relevance of the peroxisomal retrograde signaling for humans, it would be necessary to show that it is also conserved. Peroxisomal diseases are caused by mutations in peroxisomal proteins. For example, the Zellweger syndrome is caused by a defect in peroxisomal biogenesis due to mutations in peroxins (reviewed in [Waterham and Ebberink, 2012]). Since the PRS is induced in the *prx-5* loss of function mutant, studying the PRS in patient cell lines could contribute to our understanding of the pathology of the Zellweger syndrome caused by a mutation in PEX5.

In the past decade, peroxisomes have emerged as important factors in the immune response and inflammation. Peroxisomal metabolites play a central role in the modulation of the immune response (reviwed in [Di Cara et al., 2019]). The PRS also displays a link between peroxisomal metabolism and the innate immune response in *C. elegans*. Further investigation of the role of the PRS in immune function could offer new opportunities to find novel therapeutic targets to treat infections.

A

TABLES FOR RNA-SEQ ANALYSIS

Table A.1: Gene set enrichment analysis of KEGG pathways in *prx-5(RNAi)* samples compared to *tag-208(RNAi)* control samples.

Pathway	Description	p-value	Enrichment
cel04146	Peroxisome	0.0000	2.03
cel03050	Proteasome	0.0000	-2.32
cel03040	Spliceosome	0.0000	-2.34
cel03010	Ribosome	0.0000	-2.96
cel04142	Lysosome	0.0000	1.94
cel03008	Ribosome biogenesis in eukaryotes	0.0000	-2.15
cel00970	Aminoacyl-tRNA biosynthesis	0.0000	-2.00
cel04140	Autophagy	0.0000	1.81
cel00980	Metabolism of xenobiotics by cytochrome P450	0.0000	1.79
cel00830	Retinol metabolism	0.0000	1.77
cel02010	ABC transporters	0.0014	1.75
cel00062	Fatty acid elongation	0.0000	1.81
cel00982	Drug metabolism	0.0012	1.77
cel03018	RNA degradation	0.0000	-1.91
cel00053	Ascorbate and aldarate metabolism	0.0028	1.71
cel00600	Sphingolipid metabolism	0.0040	1.71
cel03020	RNA polymerase	0.0033	-1.88
cel00860	Porphyrin and chlorophyll metabolism	0.0086	1.65
cel03030	DNA replication	0.0000	-1.76

Table A.2: KEGG pathway enrichment analysis using DAVID of genes significantly changed (FDR$<$0.05 and $\log_2$(fold change) $\geq$1 or $\log_2$(fold change) $\leq$-1) upon knock-down of *prx-5*.

Pathway	Description	p-value	Enrichment
cel04146	Peroxisome	1.96E-15	7.27
cel04142	Lysosome	2.19E-13	5.76
cel01212	Fatty acid metabolism	1.72E-06	5.32
cel00982	Drug metabolism - cytochrome P450	4.64E-06	6.00
cel00071	Fatty acid degradation	3.76E-05	4.87
cel00980	Metabolism of xenobiotics by cytochrome P450	8.62E-05	5.66
cel01040	Biosynthesis of unsaturated fatty acids	6.43E-04	7.55
cel02010	ABC transporters	1.88E-03	6.14
cel00600	Sphingolipid metabolism	4.43E-03	4.24
cel00062	Fatty acid elongation	7.91E-03	5.84
cel00592	alpha-Linolenic acid metabolism	9.65E-03	8.18
cel00310	Lysine degradation	1.75E-02	3.78
cel00380	Tryptophan metabolism	5.27E-02	3.41
cel00480	Glutathione metabolism	5.61E-02	2.81
cel00650	Butanoate metabolism	6.78E-02	4.09

Table A.3: GO enrichment analysis of the domain biological process using GOrilla and REVIGO of genes significantly changed (FDR$<$0.05 and $\log_2$(fold change) $\geq$1 or $\log_2$(fold change) $\leq$-1) upon knock-down of *prx-5*.

GO Term	Description	p-value	Enrichment
GO:0006952	Defense response	1.05E-35	3.75
GO:0006955	Immune response	2.65E-30	4.27
GO:0002376	Immune system process	3.05E-30	4.22
GO:0051707	Response to other organism	6.03E-13	3.15
GO:0009607	Response to biotic stimulus	7.78E-13	3.13
GO:0006950	Response to stress	1.87E-12	1.80
GO:0051704	Multi-organism process	2.07E-11	2.80
GO:0006629	Lipid metabolic process	3.70E-10	2.04
GO:0050896	Response to stimulus	2.52E-09	1.59
GO:0009605	Response to external stimulus	1.28E-08	2.26
GO:0016042	Lipid catabolic process	5.75E-08	3.02
GO:0006631	Fatty acid metabolic process	1.16E-07	2.87
GO:0007031	Peroxisome organization	5.76E-06	7.47
GO:0072329	Monocarboxylic acid catabolic process	7.79E-06	3.56
GO:0032787	Monocarboxylic acid metabolic process	8.86E-06	2.28
GO:0044242	Cellular lipid catabolic process	8.98E-06	3.10
GO:0043574	Peroxisomal transport	1.58E-05	8.01
GO:0015919	Peroxisomal membrane transport	1.58E-05	8.01
GO:0019395	Fatty acid oxidation	1.82E-05	4.64
GO:0055114	Oxidation-reduction process	2.59E-05	1.61
GO:0097501	Stress response to metal ion	3.72E-05	5.34
GO:0016558	Protein import into peroxisome matrix	3.95E-05	8.90
GO:1990170	Stress response to cadmium ion	1.27E-04	7.63
GO:0042338	Cuticle development involved in collagen and cuticulin-based cuticle molting cycle	1.90E-04	4.00
GO:0046686	Response to cadmium ion	3.31E-04	4.67
GO:1905952	Regulation of lipid localization	5.28E-04	3.56
GO:0016119	Carotene metabolic process	8.19E-04	10.68
GO:0042214	Terpene metabolic process	8.19E-04	10.68
GO:0006876	Cellular cadmium ion homeostasis	9.82E-04	7.12
GO:0055073	Cadmium ion homeostasis	9.82E-04	7.12

Table A.4: *C. elegans* peroxisomal proteins. Proteins were included if they met at least one of the following criteria: (i) The protein has been described to be a *C. elegans* peroxisomal protein in the literature (see reference). (ii) The protein has a clear PTS1 sequence (PTS prediction score >0 [Neuberger et al., 2003]) or a PEX19 targeting prediction [Schluter et al., 2010] in *C. elegans*. (iii) The mammalian homolog is localized to peroxisomes.

Protein	Reference	PTS predictor	PEX19 targeting	C-terminus	Mammalian homolog
ACL-7	[Schluter et al., 2010]	1.523		AKL	Homolog of human GNPAT
ACOX-1.1	[Gilst et al., 2005]	9.735		SKL	Homolog of human ACOX1
ACOX-1.2	[Gilst et al., 2005]	6.263		AKL	Homolog of human ACOX1
ACOX-1.3	[Gilst et al., 2005]	6.263		AKL	Homolog of human ACOX1
ACOX-1.4	[Gilst et al., 2005]	1.416		AKL	Homolog of human ACOX1
ACOX-1.5	[Gilst et al., 2005]	13.629		SKL	Homolog of human ACOX1
ACOX-1.6	[Schluter et al., 2010]	10.065		SKL	Homolog of human ACOX1
ACOX-3	[Schluter et al., 2010]	2.460	0.019	SKL	Homolog of human ACOX3
ACS-14		0.439		AKL	Homolog of human ACSF2
ACS-7	[Zhou et al., 2018]	5.256		AKL	Homolog of human ACSF2
ADS-1	[Schluter et al., 2010]	5.871		CKL	Homolog of human AGPS
AGXT-1	[Schluter et al., 2010]	-74.585		KSK	Homolog of human AGXT
ALH-4	[Schluter et al., 2010]	-49.897		NLH	Homolog of members of the human ALDH family
B0334.3	[Schluter et al., 2010]	10.061		SKM	Homolog of human HACL1
B0395.3	[Schluter et al., 2010]	4.427		SKL	Homolog of human CRAT
C15B12.1	[Schluter et al., 2010]	-5.166		SKI	Homolog of human PIPOX
C24A3.4	[Schluter et al., 2010]	10.760	0.026	SKL	Homolog of human AMACR
C37H5.13	[Schluter et al., 2010]	-7.913	0.090	PKV	Homolog of human ACOT8
CTL-2	[Togo et al., 2000]	-9.292		SHI	Homolog of human CAT
DAAO-1	[Schluter et al., 2010]	9.250		SKL	Homolog of human DDO-1
DAF-22	[Butcher et al., 2009]	-0.963		SKI	Homolog of human SCPx
DHS-18	[Schluter et al., 2010]	12.664		SKL	Homolog of human HSDL2
DHS-28	[Schluter et al., 2010]	9.394		SKL	Homolog of human MFE2

Table A.4 continued from previous page

Protein	Reference	PTS predictor	PEX19 targeting	C-terminus	Mammalian homolog
DRP-1	[Schluter et al., 2010]	-91.195		QVW	Homolog of human DRP1
ECH-3	[Gilst et al., 2005]	4.646		SKL	Homolog of human ECHS1
ECH-8	[Gilst et al., 2005]	5.513		AKL	Homolog of human EHHADH
ECH-9	[Gilst et al., 2005]	15.869		SKL	Homolog of human EHHADH
F18F11.1	[Schluter et al., 2010]				Homolog of human PXMP4
F25E2.3	[Schluter et al., 2010]	-45.614	0.072	PAK	Homolog of human ACOT8
F32D8.13	[Schluter et al., 2010]	-9.930		DKL	Homolog of human PMVK
F41E6.5	[Schluter et al., 2010]	-83.548		EIF	Homolog of human HAO1
F44E7.4	[Schluter et al., 2010]	-8.202		SKY	Homolog of rat IDE
F53C11.3	[Gurvitz et al., 2000]	8.457		SKL	Homolog of human DECR1
FARD-1	[Schluter et al., 2010]	-39.527		QKS	Homolog of human FAR1
FIS-1					Homolog of human FIS1
FIS-2	[Schluter et al., 2010]				Homolog of human FIS1
GSTK-1		7.975		SKL	Homolog of human GSTK1
IDH-1	[Schluter et al., 2010]	-59.157		QAH	Homolog of human IDH1/PICD
IDI-1	[Schluter et al., 2010]	-50.272		KLH	Homolog of rat IDI1
LONP-2	[Schluter et al., 2010]	9.851		AKL	Homolog of human LONP2
MAOC-1	[Zhou et al., 2018]	-13.146		SKL	Functional homolog of human MFE2
MIRO-1					Homolog of human MIRO1
MLCD-1	[Schluter et al., 2010]	-48.204		DIF	Homolog of human MLYCD
MSPN-1					Homolog of mouse ATAD1
PMP-1	[Schluter et al., 2010]				Homolog of human ABCD3
PMP-2	[Schluter et al., 2010]				Homolog of human ABCD3

Table A.4 continued from previous page

Protein	Reference	PTS predictor	PEX19 targeting	C-terminus	Mammalian homolog
PMP-3	[Schluter et al., 2010]				Homolog of human ABCD4
PMP-4	[Schluter et al., 2010]				Homolog of human ABCD1
PMP-5	[Schluter et al., 2010]				Homolog of human ABCD4
PRX-1	[Petriv et al., 2002]				Homolog of human PEX1
PRX-10	[Thieringer et al., 2003]				Homolog of human PEX10
PRX-11	[Thieringer et al., 2003]				Homolog of human PEX11
PRX-12	[Petriv et al., 2002]		0.099		Homolog of human PEX12
PRX-13	[Petriv et al., 2002]				Homolog of human PEX13
PRX-14	[Petriv et al., 2002]				Homolog of human PEX14
PRX-19	[Petriv et al., 2002]				Homolog of human PEX19
PRX-3	[Petriv et al., 2002]				Homolog of human PEX3
PRX-5	[Petriv et al., 2002]				Homolog of human PEX5
PRX-6	[Petriv et al., 2002]				Homolog of human PEX6
T20B3.1	[Schluter et al., 2010]	-30.846		QKL	Homolog of human CROT
W03D8.8	[Schluter et al., 2010]	2.859		SKL	Homolog of human ACOT2
ZK550.6	[Schluter et al., 2010]	-0.376		SNL	Homolog of human PHYH

B

TABLES FOR PROTEOMIC ANALYSIS

Table B.1: Significantly changed proteins upon knock-down of *prx-5*. Proteins with a $\log_2$(fold change) value $\geq$1 (increased) or $\leq$-1 (decreased) and a p-value $<$0.05 were considered as significantly changed.

Protein	$\log_2$(fold change)	-$\log_{10}$(p-value)
Y38F2AR.9	-3.87	1.85
PUD-2.1	-2.23	1.33
ZC449.8	-2.08	1.70
CLEC-209	-2.06	1.66
IDA-1	-1.98	1.86
NUC-1	-1.87	2.09
T04F8.8	-1.83	1.43
PHO-7	-1.83	2.45
COX-17	-1.81	1.52
T13F3.6	-1.77	1.45
F15A4.6	-1.75	2.71
HKE-4.1	-1.71	1.58
K03B4.2	-1.71	1.67
Y73B6BL.31	-1.71	2.59
THOC-7	-1.67	2.36
NUO-3	-1.65	1.45
Y39B6A.42	-1.64	1.31
Y82E9BR.2	-1.63	1.89
IFY-1	-1.63	1.48
FLP-33	-1.60	1.59
GLY-9	-1.54	1.60
ATTF-6	-1.52	1.31
F32D1.7	-1.49	1.55
REC-8	-1.49	2.50
CPSF-4	-1.46	1.55
GLO-4	-1.44	2.22
COL-101	-1.39	1.31
FLP-26	-1.36	1.44
VIT-1	-1.32	2.41
C23H5.8	-1.28	1.63
C40H1.8	-1.26	1.87
DNJ-27	-1.26	2.09
VRP-1	-1.26	1.56
PRX-5	-1.24	1.37
MCP-1	-1.23	1.58
ZK470.2	-1.23	1.35
F29B9.8	-1.22	1.62
K09E4.2	-1.22	1.50
F17C11.11	-1.20	2.36
FARL-11	-1.19	1.82
CLEC-4	-1.17	1.40
RIC-3	-1.15	1.62

Table B.1 continued from previous page

Protein	$\log_2$(fold change)	-$\log_{10}$(p-value)
F54E4.3	-1.15	1.46
F11A5.9	-1.14	1.66
NSPD-5	-1.12	1.46
R13A5.10	-1.11	1.75
IRG-3	-1.11	1.31
HSP-25	-1.10	1.45
Y71F9AL.12	-1.08	1.45
C25A1.1	-1.08	1.37
ETHE-1	-1.06	1.64
HLH-28	-1.05	1.55
K02A11.4	-1.04	1.85
R08D7.7	-1.04	1.58
F26G1.5	-1.04	1.53
TAF-7.2	-1.02	1.36
SKR-17	-1.01	1.62
ACL-3	1.03	1.63
ACOX-1.5	2.68	1.81
ACOX-1.6	1.25	2.02
ACOX-3	2.88	4.42
ACS-7	1.16	1.64
ALH-5	1.01	1.53
AQP-7	3.07	4.13
ARF-1.1	1.30	1.43
ASD-1	1.53	2.02
ASP-12	3.24	2.99
ASP-3	1.72	2.16
ASP-6	1.46	1.97
ASP-8	1.70	2.14
B0205.13	3.04	3.62
B0303.11/B0303.12	1.59	1.53
BCMO-2	1.22	1.91
BTB-9	1.37	1.47
C08E8.4	2.15	2.48
C17H12.8	1.50	1.84
C24A3.4	1.46	2.12
CAH-6	1.18	1.42
CCCH-3	1.13	1.42
CDR-4	3.17	1.96
CEC-6	1.44	1.41
D2013.6	1.17	1.81
F08D12.7	1.18	1.44
F25H2.6	1.12	1.67
F36H12.4	1.28	1.69
F38A6.5	1.69	2.13
F45D11.15	1.30	2.06

Table B.1 continued from previous page

Protein	$\log_2$(fold change)	-$\log_{10}$(p-value)
F49E8.7	1.25	1.72
F53A3.7	1.08	1.45
F54D7.2	1.61	1.77
F57B10.5	1.01	1.65
F59B1.8	1.03	1.78
R10H10.3	2.45	3.34
T19A6.1	1.99	1.39
T21H3.1	3.03	2.38
T22C1.3	1.48	1.70
T28D9.4	1.34	2.08
T28H10.3	1.93	3.26
W10G11.19	1.06	1.31
Y25C1A.13	1.46	1.50
Y37H2A.14	2.17	3.58
Y41C4A.32	2.94	3.18
Y43F4B.7	1.09	1.57
Y43F8B.1	1.19	1.36
Y72A10A.1	1.39	1.51
Y80D3A.9	1.36	2.07
CLEC-63	2.92	2.98
CLEC-65	1.92	3.13
COL-157	1.36	1.36
CPR-4	2.80	2.17
CTL-1	2.16	1.50
CTL-2	1.62	1.91
CTSA-1	2.27	2.64
CTSA-2	1.34	1.59
DHS-18	2.22	2.44
DHS-28	2.70	1.38
DIC-1	1.10	1.40
DOD-19	1.90	1.78
DPM-1	1.03	1.33
ECH-7	1.47	1.75
EFL-2	1.06	1.58
EMB-8	1.37	1.52
F42H10.6	1.24	1.33
F53C11.3	1.87	1.45
FBXA-90	1.60	2.26
FLP-34	1.76	1.46
GBA-1	1.54	2.13
GRL-4	1.51	1.33
GSTK-1	1.00	1.37
HACD-1	2.04	1.41
HRG-2	2.79	2.84
HRG-7	1.37	1.74

Table B.1 continued from previous page

Protein	$\log_2$(fold change)	-$\log_{10}$(p-value)
HUM-4	1.24	1.32
IRG-7	1.45	1.47
K12H4.7	1.47	1.37
LACT-3	2.54	2.58
LEC-2	2.09	1.32
LYS-8	1.71	1.75
MADF-11	1.03	1.50
MAOC-1	3.17	1.91
NOL-10	1.52	1.78
OGA-1	1.17	1.39
PBO-1	1.42	1.33
PCYT-2.1	1.65	1.66
PGP-9	1.13	1.33
PIS-1	1.11	1.41
PMP-4	1.97	1.99
RABX-5	1.78	2.41
RDE-2	1.65	1.56
RET-1	1.18	1.32
RIOK-3	1.40	1.50
SGK-1	1.05	1.37
SMG-7	1.34	1.31
SNF-11	1.13	1.62
SOD-3	1.04	1.44
SODH-1	3.11	2.27
SPTL-2	1.76	2.07
SPV-1	1.20	1.79
SUMV-1	1.39	1.46
T16H12.4	1.21	1.93
TAG-280	1.28	1.47
TBB-6	3.04	2.89
TRPA-1	1.45	1.67
TRXR-1	1.13	1.35
TTLL-5	1.15	1.41
TTYH-1	1.63	2.22
UGT-16	3.04	3.36
UGT-18	2.17	1.88
UGT-19	1.60	1.89
UGT-2	1.06	1.41
UGT-21	1.83	2.69
UGT-31	1.31	1.48
UGT-62	3.41	1.80
UNC-101	1.03	1.46
UNC-26	2.18	1.62
Y48A6B.9	1.73	1.94
ZK550.6	2.86	2.41

Table B.2: GO enrichment analysis using GOrilla and REVIGO of proteins significantly changed ($p<0.05$ and $\log_2$(fold change) ≥ 1 or $\log_2$(fold change) ≤ -1) upon knock-down of *prx-5*.

GO domain	GO Term	Description	p-value	Enrichment
Biological process	GO:0006629	Lipid metabolic process	1.29E-05	3.01
	GO:0006955	Immune response	2.11E-05	4.60
	GO:0002376	Immune system process	2.88E-05	4.46
	GO:0044255	Cellular lipid metabolic process	5.73E-05	3.04
	GO:0044242	Cellular lipid catabolic process	7.39E-05	5.58
	GO:0019395	Fatty acid oxidation	1.10E-04	7.54
	GO:0006952	Defense response	1.37E-04	3.50
	GO:0072329	Monocarboxylic acid catabolic process	6.53E-04	5.51
	GO:0034394	Protein localization to cell surface	6.99E-04	37.68
	GO:0015812	Gamma-aminobutyric acid transport	6.99E-04	37.68
	GO:0055088	Lipid homeostasis	9.28E-04	14.13
Molecular Function	GO:0016758	Transferase activity. Transferring hexosyl groups	1.63E-05	5.23
	GO:0016757	Transferase activity. Transferring glycosyl groups	2.11E-05	4.60
	GO:0004190	Aspartic-type endopeptidase activity	2.96E-05	12.56
	GO:0070001	Aspartic-type peptidase activity	2.96E-05	12.56
	GO:0003997	Acyl-CoA oxidase activity	3.45E-04	18.84
	GO:0016634	Oxidoreductase activity. Acting on the CH-CH group of donors. Oxygen as acceptor	5.91E-04	16.15
Cellular component	GO:0042579	Microbody	5.35E-07	8.69
	GO:0005777	Peroxisome	1.90E-05	7.99

BIBLIOGRAPHY

[Aksam et al., 2007] Aksam, E. B., Koek, A., Jourdan, S., Veenhuis, M., and van der Klei, I. J. (2007). A peroxisomal Lon protease and peroxisome degradation by autophagy play key roles in vitality of *Hansenula polymorpha* cells. *Autophagy*, 3(2):96–105.

[Almanza et al., 2019] Almanza, A., Carlesso, A., Chintha, C., Creedican, S., Doultsinos, D., Leuzzi, B., Luís, A., McCarthy, N., Montibeller, L., More, S., et al. (2019). Endoplasmic reticulum stress signalling – from basic mechanisms to clinical applications. *The FEBS journal*, 286(2):241–278.

[Altun et al., 2020] Altun, Z., Herndon, L., Wolkow, C., Crocker, C., Lints, R., and Hall, D., editors (2002-2020). *WormAtlas*. http://www.wormatlas.org.

[Angermüller et al., 1987] Angermüller, S., Bruder, G., Völkl, A., Wesch, H., and Fahimi, H. D. (1987). Localization of xanthine oxidase in crystalline cores of peroxisomes. a cytochemical and biochemical study. *European journal of cell biology*, 45(1):137–144.

[Aoyama et al., 1998] Aoyama, T., Peters, J. M., Iritani, N., Nakajima, T., Furihata, K., Hashimoto, T., and Gonzalez, F. J. (1998). Altered constitutive expression of fatty acid-metabolizing enzymes in mice lacking the peroxisome proliferator-activated receptor α (PPARα). *Journal of Biological Chemistry*, 273(10):5678–5684.

[Artyukhin et al., 2018] Artyukhin, A. B., Zhang, Y. K., Akagi, A. E., Panda, O., Sternberg, P. W., and Schroeder, F. C. (2018). Metabolomic "Dark Matter" Dependent on Peroxisomal beta-oxidation in *Caenorhabditis elegans*. *J. Am. Chem. Soc.*, 140(8):2841–2852.

[Baes et al., 1997] Baes, M., Gressens, P., Baumgart, E., Carmeliet, P., Casteels, M., Fransen, M., Evrard, P., Fahimi, D., Declercq, P. E., Collen, D., van Veldhoven, P. P., and Mannaerts, G. P. (1997). A mouse model for zellweger syndrome. *Nature Genetics*, 17(1):49–57.

[Baker et al., 2012] Baker, B. M., Nargund, A. M., Sun, T., and Haynes, C. M. (2012). Protective coupling of mitochondrial function and protein synthesis via the eIF2alpha kinase GCN-2. *PLOS Genetics*, 8(6):e1002760.

[Baroy et al., 2015] Baroy, T., Koster, J., Strømme, P., Ebberink, M. S., Misceo, D., Ferdinandusse, S., Holmgren, A., Hughes, T., Merckoll, E., Westvik, J., Woldseth, B., Walter, J., Wood, N., Tvedt, B., Stadskleiv, K., Wanders, R. J. A., Waterham, H. R., and Frengen, E. (2015). A novel type of rhizomelic chondrodysplasia punctata, RCDP5, is caused by loss of the PEX5 long isoform. *Human Molecular Genetics*, 24(20):5845–5854.

[Bartoszewska et al., 2012] Bartoszewska, M., Williams, C., Kikhney, A., Opalinski, L., van Roermund, C. W. T., de Boer, R., Veenhuis, M., and van der Klei, I. J. (2012).

Peroxisomal proteostasis involves a lon family protein that functions as protease and chaperone. *The Journal of biological chemistry*, 287(22733816):27380–27395.

[Benedetti et al., 2006] Benedetti, C., Haynes, C. M., Yang, Y., Harding, H. P., and Ron, D. (2006). Ubiquitin-like protein 5 positively regulates chaperone gene expression in the mitochondrial unfolded protein response. *Genetics*, 174(1):229.

[Bennett et al., 2014] Bennett, C. F., Vander Wende, H., Simko, M., Klum, S., Barfield, S., Choi, H., Pineda, V. V., and Kaeberlein, M. (2014). Activation of the mitochondrial unfolded protein response does not predict longevity in *Caenorhabditis elegans*. *Nature communications*, 5(24662282):3483–3483.

[Berendse et al., 2016] Berendse, K., Engelen, M., Ferdinandusse, S., Majoie, C. B. L. M., Waterham, H. R., Vaz, F. M., Koelman, J. H. T. M., Barth, P. G., Wanders, R. J. A., and Poll-The, B. T. (2016). Zellweger spectrum disorders: clinical manifestations in patients surviving into adulthood. *Journal of inherited metabolic disease*, 39(26287655):93–106.

[Bout et al., 1991] Bout, A., Franse, M. M., Collins, J., Blonden, L., Tager, J. M., and Benne, R. (1991). Characterization of the gene encoding human peroxisomal 3-oxoacyl-CoA thiolase (ACAA). No large DNA rearrangement in a thiolase-deficient patient. *Biochimica et Biophysica Acta (BBA) - Gene Structure and Expression*, 1090(1):43–51.

[Braverman et al., 1998] Braverman, N., Dodt, G., Gould, S. J., and Valle, D. (1998). An isoform of Pex5p, the human PTS1 receptor, is required for the import of PTS2 proteins into peroxisomes. *Human Molecular Genetics*, 7(8):1195–1205.

[Braverman et al., 1997] Braverman, N., Steel, G., Obie, C., Moser, A., Moser, H., Gould, S. J., and Valle, D. (1997). Human Pex7 encodes the peroxisomal PTS2 receptor and is responsible for rhizomelic chondrodysplasia punctata. *Nature genetics*, 15(4):369.

[Brenner, 1974] Brenner, S. (1974). The genetics of *Caenorhabditis elegans*. *Genetics*, 77(4366476):71–94.

[Brites et al., 2009] Brites, P., Mooyer, P. A. W., el Mrabet, L., Waterham, H. R., and Wanders, R. J. A. (2009). Plasmalogens participate in very-long-chain fatty acid-induced pathology. *Brain*, 132(2):482–492.

[Brown et al., 1999] Brown, M. R., Miller, F J, J., Li, W. G., Ellingson, A. N., Mozena, J. D., Chatterjee, P., Engelhardt, J. F., Zwacka, R. M., Oberley, L. W., Fang, X., Spector, A. A., and Weintraub, N. L. (1999). Overexpression of human catalase inhibits proliferation and promotes apoptosis in vascular smooth muscle cells. *Circulation research*, 85(10488055):524–533.

[Buchert et al., 2014] Buchert, R., Tawamie, H., Smith, C., Uebe, S., Innes, A. M., Al Hallak, B., Ekici, A. B., Sticht, H., Schwarze, B., Lamont, R. E., Parboosingh, J. S., Bernier, F. P., and Abou Jamra, R. (2014). A peroxisomal disorder of severe intellectual disability, epilepsy, and cataracts due to fatty acyl-coa reductase 1 deficiency. *American journal of human genetics*, 95(25439727):602–610.

[Butcher et al., 2007] Butcher, R. A., Fujita, M., Schroeder, F. C., and Clardy, J. (2007). Small-molecule pheromones that control dauer development in *Caenorhabditis elegans*. *Nature Chemical Biology*, 3(7):420–422.

[Butcher et al., 2009] Butcher, R. A., Ragains, J. R., Li, W., Ruvkun, G., Clardy, J., and Mak, H. Y. (2009). Biosynthesis of the *Caenorhabditis elegans* dauer pheromone. *Proceedings of the National Academy of Sciences of the United States of America*, 106(19174521):1875–1879.

[Chang et al., 2015] Chang, H. Y., Lee, H.-N., Kim, W., and Surh, Y.-J. (2015). Docosahexaenoic acid induces m2 macrophage polarization through peroxisome proliferator-activated receptor γ activation. *Life Sciences*, 120:39–47.

[Chang et al., 2017] Chang, J. T., Kumsta, C., Hellman, A. B., Adams, L. M., and Hansen, M. (2017). Spatiotemporal regulation of autophagy during *Caenorhabditis elegans* aging. *eLife*, 6(28675140):e18459.

[Chen et al., 2011] Chen, B., Retzlaff, M., Roos, T., and Frydman, J. (2011). Cellular strategies of protein quality control. *Cold Spring Harbor perspectives in biology*, 3(21746797):a004374–a004374.

[Cho et al., 2013] Cho, U., Zimmerman, S. M., Chen, L.-c., Owen, E., Kim, J. V., Kim, S. K., and Wandless, T. J. (2013). Rapid and tunable control of protein stability in *[*Caenorhabditis elegans using a small molecule. *PLoS One*, 8(8):e72393.

[Chávez et al., 2009] Chávez, V., Mohri-Shiomi, A., and Garsin, D. A. (2009). Ce-Duox1/BLI-3 generates reactive oxygen species as a protective innate immune mechanism in *Caenorhabditis elegans*. *Infection and immunity*, 77(19687201):4983–4989.

[Chávez et al., 2007] Chávez, V., Mohri-Shiomi, A., Maadani, A., Vega, L. A., and Garsin, D. A. (2007). Oxidative stress enzymes are required for DAF-16-mediated immunity due to generation of reactive oxygen species by *Caenorhabditis elegans*. *Genetics*, 176(17483415):1567–1577.

[Coppa et al., 2020] Coppa, A., Guha, S., Fourcade, S., Parameswaran, J., Ruiz, M., Moser, A. B., Schlüter, A., Murphy, M. P., Lizcano, J. M., Miranda-Vizuete, A., et al. (2020). The peroxisomal fatty acid transporter abcd1/pmp-4 is required in the c. elegans hypodermis for axonal maintenance: A worm model for adrenoleukodystrophy. *Free Radical Biology and Medicine*.

[Corsi et al., 2015] Corsi, A. K., Wightman, B., and A, C. M. (2015). *Transparent window into biology: a primer on Caenorhabditis elegans*. WormBook.

[Cuppen et al., 2003] Cuppen, E., van der Linden, A. M., Jansen, G., and Plasterk, R. H. A. (2003). Proteins interacting with *Caenorhabditis elegans* gα subunits. *Comparative and functional genomics*, 4(18629017):479–491.

[Danpure and Jennings, 1986] Danpure, C. J. and Jennings, P. R. (1986). Peroxisomal alanine: glyoxylate aminotransferase deficiency in primary hyperoxaluria type I. *FEBS Letters*, 201(1):20–34.

[Danpure et al., 1994] Danpure, C. J., Jennings, P. R., Fryer, P., Purdue, P. E., and Allsop, J. (1994). Primary hyperoxaluria type 1: Genotypic and phenotypic heterogeneity. *Journal of Inherited Metabolic Disease*, 17(4):487–499.

[Dasgupta et al., 2019] Dasgupta, M., Shashikanth, M., Bojanala, N., Gupta, A., Javed, S., and Singh, V. (2019). Nuclear hormone receptor NHR-49 shapes immunometabolic response of *Caenorhabditis elegans* to *Enterococcus faecalis infection*. *bioRxiv*, page 549907.

[De Duve and Baudhuin, 1966] De Duve, C. A. B. P. and Baudhuin, P. (1966). Peroxisomes (microbodies and related particles). *Physiological reviews*, 46(2):323–357.

[Delille et al., 2010] Delille, H. K., Agricola, B., Guimaraes, S. C., Borta, H., Lüers, G. H., Fransen, M., and Schrader, M. (2010). Pex11pβ-mediated growth and division of mammalian peroxisomes follows a maturation pathway. *Journal of Cell Science*, 123(16):2750.

[Deosaran et al., 2013] Deosaran, E., Larsen, K. B., Hua, R., Sargent, G., Wang, Y., Kim, S., Lamark, T., Jauregui, M., Law, K., Lippincott-Schwartz, J., Brech, A., Johansen, T., and Kim, P. K. (2013). NBR1 acts as an autophagy receptor for peroxisomes. *Journal of Cell Science*, 126(4):939.

[Devchand et al., 1996] Devchand, P. R., Keller, H., Peters, J. M., Vazquez, M., Gonzalez, F. J., and Wahli, W. (1996). The PPARα-leukotriene b4 pathway to inflammation control. *Nature*, 384(6604):39–43.

[Di Cara et al., 2019] Di Cara, F., Andreoletti, P., Trompier, D., Vejux, A., Bülow, M. H., Sellin, J., Lizard, G., Cherkaoui-Malki, M., and Savary, S. (2019). Peroxisomes in immune response and inflammation. *International journal of molecular sciences*, 20(31398943):3877.

[Di Cara et al., 2017] Di Cara, F., Sheshachalam, A., Braverman, N. E., Rachubinski, R. A., and Simmonds, A. J. (2017). Peroxisome-mediated metabolism is required for immune response to microbial infection. *Immunity*, 47(1):93–106.e7.

[Distel et al., 1996] Distel, B., Erdmann, R., Gould, S. J., Blobel, G., Crane, D. I., Cregg, J. M., Dodt, G., Fujiki, Y., Goodman, J. M., Just, W. W., Kiel, J. A., Kunau, W. H., Lazarow, P. B., Mannaerts, G. P., Moser, H. W., Osumi, T., Rachubinski, R. A., Roscher, A., Subramani, S., Tabak, H. F., Tsukamoto, T., Valle, D., van der Klei, I., van Veldhoven, P. P., and Veenhuis, M. (1996). A unified nomenclature for peroxisome biogenesis factors. *The Journal of cell biology*, 135(1):1–3.

[Dowell et al., 1999] Dowell, P., Ishmael, J. E., Avram, D., Peterson, V. J., Nevrivy, D. J., and Leid, M. (1999). Identification of nuclear receptor corepressor as a peroxisome proliferator-activated receptor α interacting protein. *Journal of Biological Chemistry*, 274(22):15901–15907.

[Eden et al., 2009] Eden, E., Navon, R., Steinfeld, I., Lipson, D., and Yakhini, Z. (2009). Gorilla: a tool for discovery and visualization of enriched GO terms in ranked gene lists. *BMC Bioinformatics*, 10:48.

[Edgar et al., 2002] Edgar, R., Domrachev, M., and Lash, A. E. (2002). Gene expression omnibus: Ncbi gene expression and hybridization array data repository. *Nucleic acids research*, 30(11752295):207–210.

[Ehrenborg and Krook, 2009] Ehrenborg, E. and Krook, A. (2009). Regulation of skeletal muscle physiology and metabolism by peroxisome proliferator-activated receptor δ. *Pharmacological reviews*, 61(3):373–393.

[Escorcia et al., 2018] Escorcia, W., Ruter, D. L., Nhan, J., and Curran, S. P. (2018). Quantification of lipid abundance and evaluation of lipid distribution in *Caenorhabditis elegans* by Nile Red and Oil Red O staining. *Journal of visualized experiments : JoVE*, (29553519):57352.

[Fan et al., 1996] Fan, C.-Y., Pan, J., Chu, R., Lee, D., Kluckman, K. D., Usuda, N., Singh, I., Yeldandi, A. V., Rao, M. S., Maeda, N., et al. (1996). Targeted disruption of the peroxisomal fatty acyl-coa oxidase gene: Generation of a mouse model of pseudoneonatal adrenoleukodystrophy a. *Annals of the New York Academy of Sciences*, 804(1):530–541.

[Fang et al., 2004] Fang, Y., Morrell, J. C., Jones, J. M., and Gould, S. J. (2004). Pex3 functions as a Pex19 docking factor in the import of class I peroxisomal membrane proteins. *The Journal of cell biology*, 164(15007061):863–875.

[Farmer et al., 2013] Farmer, L. M., Rinaldi, M. A., Young, P. G., Danan, C. H., Burkhart, S. E., and Bartel, B. (2013). Disrupting autophagy restores peroxisome function to an arabidopsis lon2 mutant and reveals a role for the lon2 protease in peroxisomal matrix protein degradation. *The Plant Cell*, 25(10):4085–4100.

[Ferdinandusse et al., 2000] Ferdinandusse, S., Denis, S., Clayton, P. T., Graham, A., Rees, J. E., Allen, J. T., McLean, B. N., Brown, A. Y., Vreken, P., Waterham, H. R., and Wanders, R. J. A. (2000). Mutations in the gene encoding peroxisomal α-methylacyl-coa racemase cause adult-onset sensory motor neuropathy. *Nature Genetics*, 24(2):188–191.

[Ferdinandusse et al., 2003] Ferdinandusse, S., Denis, S., Dacremont, G., and Wanders, R. J. A. (2003). Studies on the metabolic fate of n-3 polyunsaturated fatty acids. *Journal of Lipid Research*, 44(10):1992–1997.

[Ferdinandusse et al., 2007] Ferdinandusse, S., Denis, S., Hogenhout, E. M., Koster, J., van Roermund, C. W. T., IJlst, L., Moser, A. B., Wanders, R. J. A., and Waterham, H. R. (2007). Clinical, biochemical, and mutational spectrum of peroxisomal acyl-coenzyme a oxidase deficiency. *Hum. Mutat.*, 28(9):904–912.

[Ferdinandusse et al., 2006a] Ferdinandusse, S., Denis, S., Mooyer, P. A. W., Dekker, C., Duran, M., Soorani-Lunsing, R. J., Boltshauser, E., Macaya, A., Gärtner, J., Majoie, C. B. L. M., Barth, P. G., Wanders, R. J. A., and Poll-The, B. T. (2006a). Clinical and biochemical spectrum of d-bifunctional protein deficiency. *Ann Neurol.*, 59(1):92–104.

[Ferdinandusse et al., 2018] Ferdinandusse, S., Denis, S., van Roermund, C. W., Preece, M. A., Koster, J., Ebberink, M. S., Waterham, H. R., and Wanders, R. J. (2018). A novel case of ACOX2 deficiency leads to recognition of a third human peroxisomal

acyl-CoA oxidase. *Biochimica et Biophysica Acta (BBA) - Molecular Basis of Disease*, 1864(3):952–958.

[Ferdinandusse et al., 2017] Ferdinandusse, S., Falkenberg, K. D., Koster, J., Mooyer, P. A., Jones, R., van Roermund, C. W. T., Pizzino, A., Schrader, M., Wanders, R. J. A., Vanderver, A., and Waterham, H. R. (2017). Acbd5 deficiency causes a defect in peroxisomal very long-chain fatty acid metabolism. *J Med Genet*, 54(5):330.

[Ferdinandusse et al., 2014] Ferdinandusse, S., Jimenez-Sanchez, G., Koster, J., Denis, S., Van Roermund, C. W., Silva-Zolezzi, I., Moser, A. B., Visser, W. F., Gulluoglu, M., Durmaz, O., Demirkol, M., Waterham, H. R., Gökcay, G., Wanders, R. J. A., and Valle, D. (2014). A novel bile acid biosynthesis defect due to a deficiency of peroxisomal abcd3. *Hum Mol Genet*, 24(2):361–370.

[Ferdinandusse et al., 2006b] Ferdinandusse, S., Kostopoulos, P., Denis, S., Rusch, H., Overmars, H., Dillmann, U., Reith, W., Haas, D., Wanders, R. J. A., Duran, M., and Marziniak, M. (2006b). Mutations in the gene encoding peroxisomal sterol carrier protein x (scpx) cause leukencephalopathy with dystonia and motor neuropathy. *American journal of human genetics*, 78(16685654):1046–1052.

[Fiorese et al., 2016] Fiorese, C. J., Schulz, A. M., Lin, Y.-F., Rosin, N., Pellegrino, M. W., and Haynes, C. M. (2016). The transcription factor ATF5 mediates a mammalian mitochondrial UPR. *Current biology : CB*, 26(15):2037–2043.

[Folick et al., 2015] Folick, A., Oakley, H. D., Yu, Y., Armstrong, E. H., Kumari, M., Sanor, L., Moore, D. D., Ortlund, E. A., Zechner, R., and Wang, M. C. (2015). Aging. Lysosomal signaling molecules regulate longevity in *Caenorhabditis elegans*. *Science (New York, N.Y.)*, 347(25554789):83–86.

[Forman et al., 1997] Forman, B. M., Chen, J., and Evans, R. M. (1997). Hypolipidemic drugs, polyunsaturated fatty acids, and eicosanoids are ligands for peroxisome proliferator-activated receptors α and δ. *Proceedings of the National Academy of Sciences*, 94(9):4312–4317.

[Fox, John and Weisberg, Sanford, 2019] Fox, John and Weisberg, Sanford (2019). *An R companion to applied regression*. Sage, Thousand Oaks CA, third edition.

[Francisco et al., 2013] Francisco, T., Rodrigues, T. A., Freitas, M. O., Grou, C. P., Carvalho, A. F., Sá-Miranda, C., Pinto, M. P., and Azevedo, J. E. (2013). A cargo-centered perspective on the PEX5 receptor-mediated peroxisomal protein import pathway. *Journal of Biological Chemistry*, 288(40):29151–29159.

[Fransen et al., 1995] Fransen, M., Brees, C., Baumgart, E., Vanhooren, J. C. T., Baes, M., Mannaerts, G. P., and Van Veldhoven, P. P. (1995). Identification and characterization of the putative human peroxisomal C-terminal targeting signal import receptor. *Journal of Biological Chemistry*, 270(13):7731–7736.

[Fransen et al., 1998] Fransen, M., Terlecky, S. R., and Subramani, S. (1998). Identification of a human PTS1 receptor docking protein directly required for peroxisomal protein import. *Proceedings of the National Academy of Sciences*, 95(14):8087–8092.

[Fredens et al., 2011] Fredens, J., Engholm-Keller, K., Giessing, A., Pultz, D., Larsen, M. R., Hojrup, P., Moller-Jensen, J., and Faergeman, N. J. (2011). Quantitative proteomics by amino acid labeling in *C. elegans*. *Nat Methods*, 8(10):845–7.

[Freitas et al., 2011] Freitas, M. O., Francisco, T., Rodrigues, T. A., Alencastre, I. S., Pinto, M. P., Grou, C. P., Carvalho, A. F., Fransen, M., Sá-Miranda, C., and Azevedo, J. E. (2011). PEX5 protein binds monomeric catalase blocking its tetramerization and releases it upon binding the n-terminal domain of PEX4. *The Journal of biological chemistry*, 286(21976670):40509–40519.

[Frishberg et al., 2014] Frishberg, Y., Zeharia, A., Lyakhovetsky, R., Bargal, R., and Belostotsky, R. (2014). Mutations in hao1 encoding glycolate oxidase cause isolated glycolic aciduria. *J Med Genet*, 51(8):526.

[Frøkjaer-Jensen et al., 2012] Frøkjaer-Jensen, C., Davis, M. W., Ailion, M., and Jorgensen, E. M. (2012). Improved MOS1-mediated transgenesis in *C. elegans*. *Nature methods*, 9(2):117–118.

[Frøkjaer-Jensen et al., 2014] Frøkjaer-Jensen, C., Davis, M. W., Sarov, M., Taylor, J., Flibotte, S., LaBella, M., Pozniakovsky, A., Moerman, D. G., and Jorgensen, E. M. (2014). Random and targeted transgene insertion in *Caenorhabditis elegans* using a modified MOS1 transposon. *Nature Methods*, 11:529.

[Ghenea et al., 2001] Ghenea, S., Takeuchi, M., Motoyama, J., Sasamoto, K., Kunau, W.-H., Kamiryo, T., and Bun-ya, M. (2001). The cDNA Sequence and Expression of the AAA-family Peroxin Genes ¡i¿pex-1¡/i¿ and ¡i¿pex-6¡/i¿ from the Nematode *Caenorhabditis elegans*. *Zoological Science*, 18(5):675–681.

[Gilst et al., 2005] Gilst, M. R. V., Hadjivassiliou, H., Jolly, A., and Yamamoto, K. R. (2005). Nuclear hormone receptor NHR-49 controls fat consumption and fatty acid composition in *C. elegans*. *PLOS Biology*, 3(2):e53.

[Golden and Riddle, 1982] Golden, J. and Riddle, D. (1982). A pheromone influences larval development in the nematode *Caenorhabditis elegans*. *Science*, 218(4572):578–580.

[Golden and Riddle, 1985] Golden, J. W. and Riddle, D. L. (1985). A gene affecting production of the *Caenorhabditis elegans* dauer-inducing pheromone. *Molecular and General Genetics MGG*, 198(3):534–536.

[Goto-Yamada et al., 2014] Goto-Yamada, S., Mano, S., Nakamori, C., Kondo, M., Yamawaki, R., Kato, A., and Nishimura, M. (2014). Chaperone and protease functions of Lon protease 2 modulate the peroxisomal transition and degradation with autophagy. *Plant Cell Physiol*, 55(3):482–96.

[Gould et al., 1989] Gould, S. J., Keller, G. A., Hosken, N., Wilkinson, J., and Subramani, S. (1989). A conserved tripeptide sorts proteins to peroxisomes. *The Journal of cell biology*, 108(2654139):1657–1664.

[Gouveia et al., 2000] Gouveia, A. M. M., Reguenga, C., Oliveira, M. E. M., Sá-Miranda, C., and Azevedo, J. E. (2000). Characterization of peroxisomal Pex5p from rat liver: Pex5p in the Pex5p-Pex14p membrane complex is a transmembrane protein. *Journal of Biological Chemistry*, 275(42):32444–32451.

[Govaerts et al., 1982] Govaerts, L., Monnens, L., Tegelaers, W., Trijbels, F., and van Raay-Selten, A. (1982). Cerebro-hepato-renal syndrome of zellweger: clinical symptoms and relevant laboratory findings in 16 patients. *European journal of pediatrics*, 139(2):125–128.

[Gronemeyer et al., 2013] Gronemeyer, T., Wiese, S., Ofman, R., Bunse, C., Pawlas, M., Hayen, H., Eisenacher, M., Stephan, C., Meyer, H. E., Waterham, H. R., Erdmann, R., Wanders, R. J., and Warscheid, B. (2013). The proteome of human liver peroxisomes: identification of five new peroxisomal constituents by a label-free quantitative proteomics survey. *PloS one*, 8(23460848):e57395–e57395.

[Grou et al., 2008] Grou, C. P., Carvalho, A. F., Pinto, M. P., Wiese, S., Piechura, H., Meyer, H. E., Warscheid, B., Sá-Miranda, C., and Azevedo, J. E. (2008). Members of the E2D (UbcH5) family mediate the ubiquitination of the conserved cysteine of Pex5p, the peroxisomal import receptor. *Journal of Biological Chemistry*, 283(21):14190–14197.

[Grou et al., 2012] Grou, C. P., Francisco, T., Rodrigues, T. A., Freitas, M. O., Pinto, M. P., Carvalho, A. F., Domingues, P., Wood, S. A., Rodríguez-Borges, J. E., Sá-Miranda, C., Fransen, M., and Azevedo, J. E. (2012). Identification of ubiquitin-specific protease 9X (Usp9X) as a deubiquitinase acting on ubiquitin-peroxin 5 (Pex5) thioester conjugate. *Journal of Biological Chemistry*, 287(16):12815–12827.

[Gurvitz et al., 2000] Gurvitz, A., Langer, S., Piskacek, M., Hamilton, B., Ruis, H., and Hartig, A. (2000). Predicting the function and subcellular location of *Caenorhabditis elegans* proteins similar to *Saccharomyces cerevisiae* beta-oxidation enzymes. *Yeast*, 17(3):188–200.

[Hadžić et al., 2012] Hadžić, N., Bull, L. N., Clayton, P. T., and Knisely, A. S. (2012). Diagnosis in bile acid-coa: amino acid n-acyltransferase deficiency. *World journal of gastroenterology*, 18(22783059):3322–3326.

[Hahm et al., 2011] Hahm, J. H., Kim, S., and Paik, Y. K. (2011). GPA-9 is a novel regulator of innate immunity against *Escherichia coli* foods in adult *Caenorhabditis elegans*. *Aging Cell*, 10(2):208–19.

[Hashimoto and Hayashi, 1987] Hashimoto, F. and Hayashi, H. (1987). Significance of catalase in peroxisomal fatty acyl-CoA beta-oxidation. *Biochimica et biophysica acta*, 921(1):142–150.

[Haynes et al., 2007] Haynes, C. M., Petrova, K., Benedetti, C., Yang, Y., and Ron, D. (2007). Clpp mediates activation of a mitochondrial unfolded protein response in *C. elegans*. *Developmental Cell*, 13(4):467–480.

[Haynes et al., 2010] Haynes, C. M., Yang, Y., Blais, S. P., Neubert, T. A., and Ron, D. (2010). The matrix peptide exporter HAF-1 signals a mitochondrial UPR by activating the transcription factor ZC376.7 in *C. elegans*. *Molecular cell*, 37(20188671):529–540.

[Heymans et al., 1983] Heymans, H. S. A., Schutgens, R. B. H., Tan, R., van den Bosch, H., and Borst, P. (1983). Severe plasmalogen deficiency in tissues of infants without peroxisomes (Zellweger syndrome). *Nature*, 306(5938):69–70.

[Hiebler et al., 2014] Hiebler, S., Masuda, T., Hacia, J. G., Moser, A. B., Faust, P. L., Liu, A., Chowdhury, N., Huang, N., Lauer, A., Bennett, J., Watkins, P. A., Zack, D. J., Braverman, N. E., Raymond, G. V., and Steinberg, S. J. (2014). The pex1-g844d mouse: a model for mild human zellweger spectrum disorder. *Molecular genetics and metabolism*, 111(24503136):522–532.

[Hoeven et al., 2011] Hoeven, R. v. d., McCallum, K. C., Cruz, M. R., and Garsin, D. A. (2011). Ce-Duox1/BLI-3 generated reactive oxygen species trigger protective SKN-1 activity via p38 MAPK signaling during infection in *C. elegans*. *PLoS pathogens*, 7(22216003):e1002453–e1002453.

[Hollister et al., 2013] Hollister, K. A., Conner, E. S., Zhang, X., Spell, M., Bernard, G. M., Patel, P., de Carvalho, A. C., Butcher, R. A., and Ragains, J. R. (2013). Ascaroside activity in *Caenorhabditis elegans* is highly dependent on chemical structure. *Bioorg Med Chem*, 21(18):5754–69.

[Hope, Ryan M., 2013] Hope, Ryan M. (2013). *Rmisc: Rmisc: Ryan miscellaneous*. R package version 1.5.

[Hostetler et al., 2009] Hostetler, H. A., McIntosh, A. L., Atshaves, B. P., Storey, S. M., Payne, H. R., Kier, A. B., and Schroeder, F. (2009). L-FABP directly interacts with PPARalpha in cultured primary hepatocytes. *Journal of lipid research*, 50(19289416):1663–1675.

[Hou et al., 2014] Hou, N. S., Gutschmidt, A., Choi, D. Y., Pather, K., Shi, X., Watts, J. L., Hoppe, T., and Taubert, S. (2014). Activation of the endoplasmic reticulum unfolded protein response by lipid disequilibrium without disturbed proteostasis *in vivo*. *Proceedings of the National Academy of Sciences of the United States of America*, 111:E2271–E2280.

[Huang et al., 2009a] Huang, D. W., Sherman, B. T., and Lempicki, R. A. (2009a). Bioinformatics enrichment tools: paths toward the comprehensive functional analysis of large gene lists. *Nucleic acids research*, 37(19033363):1–13.

[Huang et al., 2009b] Huang, D. W., Sherman, B. T., and Lempicki, R. A. (2009b). Systematic and integrative analysis of large gene lists using david bioinformatics resources. *Nature Protocols*, 4(1):44–57.

[Huang and Miller, 1991] Huang, X. and Miller, W. (1991). A time-efficient, linear-space local similarity algorithm. *Advances in Applied Mathematics*, 12(3):337–357.

[Hunter et al., 1997] Hunter, T., Bannister, W. H., and Hunter, G. J. (1997). Cloning, expression, and characterization of two manganese superoxide dismutases from *Caenorhabditis elegans*. *Journal of Biological Chemistry*, 272(45):28652–28659.

[Igarashi et al., 1976] Igarashi, M., Schaumburg, H. H., Powers, J., Kishimoto, Y., Koilodny, E., and Suzuki, K. (1976). Fatty acid abnormality in adrenoleukodystrophy. *Journal of Neurochemistry*, 26(4):851–860.

[Ivashchenko et al., 2011] Ivashchenko, O., Van Veldhoven, P. P., Brees, C., Ho, Y.-S., Terlecky, S. R., and Fransen, M. (2011). Intraperoxisomal redox balance in mammalian cells: oxidative stress and interorganellar cross-talk. *Molecular biology of the cell*, 22(21372177):1440–1451.

[Iwata et al., 2006] Iwata, J.-i., Ezaki, J., Komatsu, M., Yokota, S., Ueno, T., Tanida, I., Chiba, T., Tanaka, K., and Kominami, E. (2006). Excess peroxisomes are degraded by autophagic machinery in mammals. *Journal of Biological Chemistry*, 281(7):4035–4041.

[Jansen and Wanders, 2006] Jansen, G. A. and Wanders, R. J. (2006). Alpha-oxidation. *Biochimica et Biophysica Acta (BBA) - Molecular Cell Research*, 1763(12):1403–1412. Peroxisomes: Morphology, Function, Biogenesis and Disorders.

[Jansen et al., 1997] Jansen, G. A., Wanders, R. J. A., Watkins, P. A., and Mihalik, S. J. (1997). Phytanoyl-coenzyme a hydroxylase deficiency – the enzyme defect in refsum's disease. *N Engl J Med*, 337(2):133–134.

[Jansen and van der Klei, 2019] Jansen, R. L. M. and van der Klei, I. J. (2019). The peroxisome biogenesis factors Pex3 and Pex19: multitasking proteins with disputed functions. *FEBS Letters*, 593(5):457–474.

[Jiang et al., 1997] Jiang, L. L., Kurosawa, T., Sato, M., Suzuki, Y., and Hashimoto, T. (1997). Physiological role of D-3-hydroxyacyl-CoA dehydratase/D-3-hydroxyacyl-CoA dehydrogenase bifunctional protein. *The Journal of Biochemistry*, 121(3):506–513.

[Jones et al., 2004] Jones, J. M., Morrell, J. C., and Gould, S. J. (2004). Pex19 is a predominantly cytosolic chaperone and import receptor for class 1 peroxisomal membrane proteins. *The Journal of Cell Biology*, 164(1):57–67.

[Joo et al., 2010] Joo, H.-J., Kim, K.-Y., Yim, Y.-H., Jin, Y.-X., Kim, H., Kim, M.-Y., and Paik, Y.-K. (2010). Contribution of the peroxisomal ACOX gene to the dynamic balance of daumone production in *Caenorhabditis elegans*. *Journal of Biological Chemistry*, 285(38):29319–29325.

[Jovaisaite et al., 2014] Jovaisaite, V., Mouchiroud, L., and Auwerx, J. (2014). The mitochondrial unfolded protein response, a conserved stress response pathway with implications in health and disease. *The Journal of experimental biology*, 217:137–43.

[Kamath and Ahringer, 2003] Kamath, R. S. and Ahringer, J. (2003). Genome-wide rnai screening in *Caenorhabditis elegans*. *Methods*, 30(4):313–321.

[Kanehisa and Sato, 2020] Kanehisa, M. and Sato, Y. (2020). Kegg mapper for inferring cellular functions from protein sequences. *Protein Science*, 29(1):28–35.

[Keller et al., 1991] Keller, G. A., Warner, T. G., Steimer, K. S., and Hallewell, R. A. (1991). Cu,Zn superoxide dismutase is a peroxisomal enzyme in human fibroblasts and hepatoma cells. *Proceedings of the National Academy of Sciences*, 88(16):7381–7385.

[Keller et al., 1993] Keller, H., Dreyer, C., Medin, J., Mahfoudi, A., Ozato, K., and Wahli, W. (1993). Fatty acids and retinoids control lipid metabolism through activation of peroxisome proliferator-activated receptor-retinoid X receptor heterodimers. *Proceedings of the National Academy of Sciences of the United States of America*, 90(8384714):2160–2164.

[Kikuchi et al., 2004] Kikuchi, M., Hatano, N., Yokota, S., Shimozawa, N., Imanaka, T., and Taniguchi, H. (2004). Proteomic analysis of rat liver peroxisome: presence of peroxisome-specific isozyme of Lon protease. *The Journal of biological chemistry*, 279:421–428.

[Kim et al., 2002] Kim, D. H., Feinbaum, R., Alloing, G., Emerson, F. E., Garsin, D. A., Inoue, H., Tanaka-Hino, M., Hisamoto, N., Matsumoto, K., Tan, M.-W., and Ausubel, F. M. (2002). A conserved p38 MAP kinase pathway in *Caenorhabditis elegans* innate immunity. *Science*, 297(5581):623–626.

[Kim, 2017] Kim, P. (2017). Peroxisome Biogenesis: A union between two organelles. *Current Biology*, 27(7):R271–R274.

[Kim and Hettema, 2015] Kim, P. K. and Hettema, E. H. (2015). Multiple pathways for protein transport to peroxisomes. *Journal of molecular biology*, 427(25681696):1176–1190.

[Kliewer et al., 1997] Kliewer, S. A., Sundseth, S. S., Jones, S. A., Brown, P. J., Wisely, G. B., Koble, C. S., Devchand, P., Wahli, W., Willson, T. M., Lenhard, J. M., and Lehmann, J. M. (1997). Fatty acids and eicosanoids regulate gene expression through direct interactions with peroxisome proliferator-activated receptors α and γ. *Proceedings of the National Academy of Sciences*, 94(9):4318–4323.

[Kobayashi et al., 2007] Kobayashi, S., Tanaka, A., and Fujiki, Y. (2007). Fis1, Dlp1, and Pex11p coordinately regulate peroxisome morphogenesis. *Experimental Cell Research*, 313(8):1675–1686.

[Koch and Brocard, 2012] Koch, J. and Brocard, C. (2012). Pex11 proteins attract Mff and human Fis1 to coordinate peroxisomal fission. *J. Cell Sci.*, 125(16):3813.

[Koch et al., 2016] Koch, J., Feichtinger, R. G., Freisinger, P., Pies, M., Schrödl, F., Iuso, A., Sperl, W., Mayr, J. A., Prokisch, H., and Haack, T. B. (2016). Disturbed mitochondrial and peroxisomal dynamics due to loss of mff causes leigh-like encephalopathy, optic atrophy and peripheral neuropathy. *Journal of Medical Genetics*, 53(4):270–278.

[Koepke et al., 2008] Koepke, J. I., Wood, C. S., Terlecky, L. J., Walton, P. A., and Terlecky, S. R. (2008). Progeric effects of catalase inactivation in human cells. *Toxicology and applied pharmacology*, 232(1):99–108.

[Köhler et al., 2015] Köhler, F., Müller-Rischart, A. K., Conradt, B., and Rolland, S. G. (2015). The loss of LRPPRC function induces the mitochondrial unfolded protein response. *Aging*, 7(26412102):701–717.

[Lametschwandtner et al., 1998] Lametschwandtner, G., Brocard, C., Fransen, M., Van Veldhoven, P., Berger, J., and Hartig, A. (1998). The difference in recognition of terminal tripeptides as peroxisomal targeting signal 1 between yeast and human is due to different affinities of their receptor Pex5p to the cognate signal and to residues adjacent to it. *Journal of Biological Chemistry*, 273(50):33635–33643.

[Langmead et al., 2009] Langmead, B., Trapnell, C., Pop, M., and Salzberg, S. L. (2009). Ultrafast and memory-efficient alignment of short dna sequences to the human genome. *Genome Biology*, 10(3):R25.

[Lee et al., 2014] Lee, A., Asahina, K., Okamoto, T., Kawaguchi, K., Kostsin, D. G., Kashiwayama, Y., Takanashi, K., Yazaki, K., Imanaka, T., and Morita, M. (2014). Role of NH2-terminal hydrophobic motif in the subcellular localization of ATP-binding cassette protein subfamily D: common features in eukaryotic organisms. *Biochemical and Biophysical Research Communications*, 453(3):612–618.

[Lee et al., 2017] Lee, R. Y., Howe, K. L., Harris, T. W., Arnaboldi, V., Cain, S., Chan, J., Chen, W. J., Davis, P., Gao, S., Grove, C., Kishore, R., Muller, H.-M., Nakamura, C., Nuin, P., Paulini, M., Raciti, D., Rodgers, F., Russell, M., Schindelman, G., Tuli, M. A., Van Auken, K., Wang, Q., Williams, G., Wright, A., Yook, K., Berriman, M., Kersey, P., Schedl, T., Stein, L., and Sternberg, P. W. (2017). Wormbase 2017: molting into a new stage. *Nucleic Acids Research*, 46(D1):D869–D874.

[Lee et al., 2013] Lee, S. H., Wong, R. R., Chin, C. Y., Lim, T. Y., Eng, S. A., Kong, C., Ijap, N. A., Lau, M. S., Lim, M. P., Gan, Y. H., He, F. L., Tan, M. W., and Nathan, S. (2013). Burkholderia pseudomallei suppresses *caenorhabditis elegans* immunity by specific degradation of a GATA transcription factor. *Proc Natl Acad Sci U S A*, 110(37):15067–72.

[Li et al., 2002] Li, X., Baumgart, E., Dong, G.-X., Morrell, J. C., Jimenez-Sanchez, G., Valle, D., Smith, K. D., and Gould, S. J. (2002). Pex11alpha is required for peroxisome proliferation in response to 4-phenylbutyrate but is dispensable for peroxisome proliferator-activated receptor alpha-mediated peroxisome proliferation. *Molecular and cellular biology*, 22(12417726):8226–8240.

[Liang et al., 2010] Liang, B., Ferguson, K., Kadyk, L., and Watts, J. L. (2010). The role of nuclear receptor NHR-64 in fat storage regulation in *Caenorhabditis elegans*. *PloS one*, 5(3):e9869.

[Liao et al., 2019] Liao, Y., Wang, J., Jaehnig, E. J., Shi, Z., and Zhang, B. (2019). WebGestalt 2019: gene set analysis toolkit with revamped UIs and APIs. *Nucleic acids research*, 47(31114916):W199–W205.

[Lismont et al., 2015] Lismont, C., Nordgren, M., Van Veldhoven, P. P., and Fransen, M. (2015). Redox interplay between mitochondria and peroxisomes. *Frontiers in cell and developmental biology*, 3:35.

[Liu et al., 2014] Liu, Y., Samuel, B. S., Breen, P. C., and Ruvkun, G. (2014). Caenorhabditis elegans pathways that surveil and defend mitochondria. *Nature*, 508(24695221):406–410.

[Liu et al., 2016] Liu, Y., Sellegounder, D., and Sun, J. (2016). Neuronal GPCR OCTR-1 regulates innate immunity by controlling protein synthesis in *Caenorhabditis elegans*. *Sci Rep*, 6:36832.

[López-Erauskin et al., 2013] López-Erauskin, J., Galino, J., Ruiz, M., Cuezva, J. M., Fabregat, I., Cacabelos, D., Boada, J., Martínez, J., Ferrer, I., Pamplona, R., Villarroya, F., Portero-Otín, M., Fourcade, S., and Pujol, A. (2013). Impaired mitochondrial oxidative phosphorylation in the peroxisomal disease X-linked adrenoleukodystrophy. *hmg*, 22(16):3296–3305.

[Macala et al., 1983] Macala, L. J., Yu, R. K., and Ando, S. (1983). Analysis of brain lipids by high performance thin-layer chromatography and densitometry. *Journal of Lipid Research*, 24(9):1243–1250.

[Mak et al., 2006] Mak, H. Y., Nelson, L. S., Basson, M., Johnson, C. D., and Ruvkun, G. (2006). Polygenic control of *Caenorhabditis elegans* fat storage. *Nature Genetics*, 38(3):363–368.

[Mao et al., 2019] Mao, K., Ji, F., Breen, P., Sewell, A., Han, M., Sadreyev, R., and Ruvkun, G. (2019). Mitochondrial dysfunction in *C. elegans* activates mitochondrial relocalization and nuclear hormone receptor-dependent detoxification genes. *Cell metabolism*, 29(5):1182–1191.

[Martinus et al., 1996] Martinus, R. D., Garth, G. P., Webster, T. L., Cartwright, P., Naylor, D. J., Høj, P. B., and Hoogenraad, N. J. (1996). Selective induction of mitochondrial chaperones in response to loss of the mitochondrial genome. *European Journal of Biochemistry*, 240(1):98–103.

[Mast et al., 2011] Mast, F. D., Li, J., Virk, M. K., Hughes, S. C., Simmonds, A. J., and Rachubinski, R. A. (2011). A Drosophila model for the Zellweger spectrum of peroxisome biogenesis disorders. *Disease models & mechanisms*, 4(21669930):659–672.

[Matsumoto et al., 2003] Matsumoto, N., Tamura, S., Furuki, S., Miyata, N., Moser, A., Shimozawa, N., Moser, H. W., Suzuki, Y., Kondo, N., and Fujiki, Y. (2003). Mutations in novel peroxin gene pex26 that cause peroxisome-biogenesis disorders of complementation group 8 provide a genotype-phenotype correlation. *The American Journal of Human Genetics*, 73(2):233–246.

[Matsuzaki and Fujiki, 2008] Matsuzaki, T. and Fujiki, Y. (2008). The peroxisomal membrane protein import receptor Pex3p is directly transported to peroxisomes by a novel Pex19p- and Pex16p-dependent pathway. *The Journal of Cell Biology*, 183(7):1275–1286.

[Melber and Haynes, 2018] Melber, A. and Haynes, C. M. (2018). UPRmt regulation and output: a stress response mediated by mitochondrial-nuclear communication. *Cell Research*, 28(3):281–295.

[Mello et al., 1991] Mello, C. C., Kramer, J. M., Stinchcomb, D., and Ambros, V. (1991). Efficient gene transfer in *C.elegans*: extrachromosomal maintenance and integration of transforming sequences. *The EMBO journal*, 10(12):3959–3970.

[Miranda-Vizuete and Veal, 2017] Miranda-Vizuete, A. and Veal, E. A. (2017). *Caenorhabditis elegans* as a model for understanding ROS function in physiology and disease. *Redox biology*, 11(28193593):708–714.

[Miyata and Fujiki, 2005] Miyata, N. and Fujiki, Y. (2005). Shuttling mechanism of peroxisome targeting signal type 1 receptor Pex5: ATP-independent import and ATP-dependent export. *Molecular and cellular biology*, 25(24):10822–10832.

[Mosser et al., 1993] Mosser, J., Douar, A.-M., Sarde, C.-O., Kioschis, P., Feil, R., Moser, H., Poustka, A.-M., Mandel, J.-L., and Aubourg, P. (1993). Putative x-linked

adrenoleukodystrophy gene shares unexpected homology with abc transporters. *Nature*, 361(6414):726–730.

[Motley et al., 1997] Motley, A. M., Hettema, E. H., Hogenhout, E. M., Brites, P., ten Asbroek, A. L. M. A., Wijburg, F. A., Baas, F., Heijmans, H. S., Tabak, H. F., Wanders, R. J. A., and Distel, B. (1997). Rhizomelic chondrodysplasia punctata is a peroxisomal protein targeting disease caused by a non-functional pts2 receptor. *Nature Genetics*, 15(4):377–380.

[Motley et al., 2000] Motley, A. M., Hettema, E. H., Ketting, R., Plasterk, R., and Tabak, H. F. (2000). *Caenorhabditis elegans* has a single pathway to target matrix proteins to peroxisomes. *EMBO reports*, 1(1):40–46.

[Mukai and Fujiki, 2006] Mukai, S. and Fujiki, Y. (2006). Molecular mechanisms of import of peroxisome-targeting signal type 2 (PTS2) proteins by PTS2 receptor Pex7p and PTS1 receptor Pex5pL. *Journal of Biological Chemistry*, 281(49):37311–37320.

[Nandakumar and Tan, 2008] Nandakumar, M. and Tan, M.-W. (2008). Gamma-linolenic and stearidonic acids are required for basal immunity in caenorhabditis elegans through their effects on p38 MAP kinase activity. *PLOS Genetics*, 4(11):e1000273.

[Nargund et al., 2012] Nargund, A. M., Pellegrino, M. W., Fiorese, C. J., Baker, B. M., and Haynes, C. M. (2012). Mitochondrial import efficiency of ATFS-1 regulates mitochondrial UPR activation. *Science (New York, N.Y.)*, 337(6094):587–590.

[Neuberger et al., 2003] Neuberger, G., Maurer-Stroh, S., Eisenhaber, B., Hartig, A., and Eisenhaber, F. (2003). Prediction of peroxisomal targeting signal 1 containing proteins from amino acid sequence. *Journal of Molecular Biology*, 328(3):581–592.

[Novikoff and Novikoff, 1973] Novikoff, A. B. and Novikoff, P. M. (1973). Microperoxisomes. *Journal of Histochemistry & Cytochemistry*, 21(11):963–966.

[Ofman et al., 1998] Ofman, R., Hettema, E. H., Hogenhout, E. M., Caruso, U., Muijsers, A. O., and Wanders, R. J. A. (1998). Acyl-coa: Dihydroxyacetonephosphate acyltransferase: Cloning of the human cdna and resolution of the molecular basis in rhizomelic chondrodysplasia punctata type 2. *Hum Mol Genet*, 7(5):847–853.

[Okumoto et al., 2011] Okumoto, K., Misono, S., Miyata, N., Matsumoto, Y., Mukai, S., and Fujiki, Y. (2011). Cysteine ubiquitination of PTS1 receptor Pex5p regulates Pex5p recycling. *Traffic*, 12(8):1067–1083.

[Okumoto et al., 2014] Okumoto, K., Noda, H., and Fujiki, Y. (2014). Distinct modes of ubiquitination of peroxisome-targeting signal type 1 (PTS1) receptor Pex5p regulate PTS1 protein import. *Journal of Biological Chemistry*, 289(20):14089–14108.

[Omi et al., 2008] Omi, S., Nakata, R., Okamura-Ikeda, K., Konishi, H., and Taniguchi, H. (2008). Contribution of peroxisome-specific isoform of Lon protease in sorting PTS1 proteins to peroxisomes. *The Journal of Biochemistry*, 143(5):649–660.

[O'Rourke et al., 2009] O'Rourke, E. J., Soukas, A. A., Carr, C. E., and Ruvkun, G. (2009). *C. elegans* major fats are stored in vesicles distinct from lysosome-related organelles. *Cell metabolism*, 10(5):430–435.

[Otera and Fujiki, 2012] Otera, H. and Fujiki, Y. (2012). Pex5p imports folded tetrameric catalase by interaction with Pex13p. *Traffic*, 13(10):1364–1377.

[Palosaari and Hiltunen, 1990] Palosaari, P. M. and Hiltunen, J. K. (1990). Peroxisomal bifunctional protein from rat liver is a trifunctional enzyme possessing 2-enoyl-CoA hydratase, 3-hydroxyacyl-CoA dehydrogenase, and delta 3, delta 2-enoyl-CoA isomerase activities. *J Biol Chem*, 265(5):2446–9.

[Pathare et al., 2012] Pathare, P. P., Lin, A., Bornfeldt, K. E., Taubert, S., and Van Gilst, M. R. (2012). Coordinate regulation of lipid metabolism by novel nuclear receptor partnerships. *PLOS Genetics*, 8(4):e1002645.

[Pedersen and Gustafsson, 1980] Pedersen, J. I. and Gustafsson, J. (1980). Conversion of 3α,7α,12α-trihydroxy-5β-cholestanoic acid into cholic acid by rat liver peroxisomes. *FEBS Letters*, 121(2):345–348.

[Peeters et al., 2015] Peeters, A., Shinde, A. B., Dirkx, R., Smet, J., De Bock, K., Espeel, M., Vanhorebeek, I., Vanlander, A., Van Coster, R., Carmeliet, P., et al. (2015). Mitochondria in peroxisome-deficient hepatocytes exhibit impaired respiration, depleted dna, and PGC-1α independent proliferation. *Biochimica et Biophysica Acta (BBA)-Molecular Cell Research*, 1853(2):285–298.

[Pellegrino et al., 2014] Pellegrino, M. W., Nargund, A. M., Kirienko, N. V., Gillis, R., Fiorese, C. J., and Haynes, C. M. (2014). Mitochondrial UPR-regulated innate immunity provides resistance to pathogen infection. *Nature*, 516(7531):414–417.

[Perez-Riverol et al., 2019] Perez-Riverol, Y., Csordas, A., Bai, J., Bernal-Llinares, M., Hewapathirana, S., Kundu, D. J., Inuganti, A., Griss, J., Mayer, G., Eisenacher, M., Pérez, E., Uszkoreit, J., Pfeuffer, J., Sachsenberg, T., Yilmaz, S., Tiwary, S., Cox, J., Audain, E., Walzer, M., Jarnuczak, A. F., Ternent, T., Brazma, A., and Vizcaíno, J. A. (2019). The pride database and related tools and resources in 2019: improving support for quantification data. *Nucleic acids research*, 47(D1):D442–D450.

[Peters, Gjalt-Jorn Ygram, 2017] Peters, Gjalt-Jorn Ygram (2017). Diamond plots: a tutorial to introduce a visualisation tool that facilitates interpretation and comparison of multiple sample estimates while respecting their inaccuracy. *PsyArXiv*.

[Petriv et al., 2002] Petriv, O. I., Pilgrim, D. B., Rachubinski, R. A., and Titorenko, V. I. (2002). RNA interference of peroxisome-related genes in *C. elegans*: a new model for human peroxisomal disorders. *Physiological Genomics*, 10(2):79–91.

[Petriv and Rachubinski, 2004] Petriv, O. I. and Rachubinski, R. A. (2004). Lack of peroxisomal catalase causes a progeric phenotype in *Caenorhabditis elegans*. *Journal of Biological Chemistry*, 279(19):19996–20001.

[Pinto et al., 2006] Pinto, M. P., Grou, C. P., Alencastre, I. S., Oliveira, M. E., Sá-Miranda, C., Fransen, M., and Azevedo, J. E. (2006). The import competence of a peroxisomal membrane protein is determined by Pex19p before the docking step. *Journal of Biological Chemistry*, 281(45):34492–34502.

[Pohlert, Thorsten, 2014] Pohlert, Thorsten (2014). *The pairwise multiple comparison of mean ranks package (PMCMR)*. R package.

[Pujol et al., 2001] Pujol, N., Link, E. M., Liu, L. X., Kurz, C. L., Alloing, G., Tan, M.-W., Ray, K. P., Solari, R., Johnson, C. D., and Ewbank, J. J. (2001). A reverse genetic analysis of components of the Toll signaling pathway in *Caenorhabditis elegans*. *Current Biology*, 11(11):809–821.

[Pukkila-Worley et al., 2014] Pukkila-Worley, R., Feinbaum, R. L., McEwan, D. L., Conery, A. L., and Ausubel, F. M. (2014). The evolutionarily conserved mediator subunit MDT-15/MED15 links protective innate immune responses and xenobiotic detoxification. *PLoS pathogens*, 10(24875643):e1004143–e1004143.

[R Core Team, 2019] R Core Team (2019). *R: a language and environment for statistical computing*. R Foundation for Statistical Computing, Vienna, Austria.

[Reddy and Chu, 1996] Reddy, J. K. and Chu, R. (1996). Peroxisome proliferator-induced pleiotropic responses: Pursuit of a phenomenon. *Annals of the New York Academy of Sciences*, 804(1):176–201.

[Rhodin, 1954] Rhodin, J. (1954). *Correlation of ultrastructure organization and function in normal and experimentally treated proximal convoluted tubule cells of the mouse kidney*. PhD thesis, Karolinska Institute Stockholm.

[Rolland et al., 2019] Rolland, S. G., Schneid, S., Schwarz, M., Rackles, E., Fischer, C., Haeussler, S., Regmi, S. G., Yeroslaviz, A., Habermann, B., Mokranjac, D., Lambie, E., and Conradt, B. (2019). Compromised mitochondrial protein import acts as a signal for UPRmt. *Cell Reports*, 28(7):1659–1669.e5.

[Rosewich et al., 2005] Rosewich, H., Ohlenbusch, A., and Gärtner, J. (2005). Genetic and clinical aspects of zellweger spectrum patients with pex1 mutations. *Journal of medical genetics*, 42(16141001):e58–e58.

[Rual et al., 2004] Rual, J.-F., Ceron, J., Koreth, J., Hao, T., Nicot, A.-S., Hirozane-Kishikawa, T., Vandenhaute, J., Orkin, S. H., Hill, D. E., van den Heuvel, S., and Vidal, M. (2004). Toward improving *Caenorhabditis elegans* phenome mapping with an orfeome-based RNAi library. *Genome research*, 14(10B):2162–2168.

[Rueden et al., 2017] Rueden, C. T., Schindelin, J., Hiner, M. C., DeZonia, B. E., Walter, A. E., Arena, E. T., and Eliceiri, K. W. (2017). Imagej2: ImageJ for the next generation of scientific image data. *BMC Bioinformatics*, 18(1):529.

[Sasaki and Yoshida, 2015] Sasaki, K. and Yoshida, H. (2015). Organelle autoregulation—stress responses in the ER, golgi, mitochondria and lysosome. *The Journal of Biochemistry*, 157(4):185–195.

[Schindelin et al., 2012] Schindelin, J., Arganda-Carreras, I., Frise, E., Kaynig, V., Longair, M., Pietzsch, T., Preibisch, S., Rueden, C., Saalfeld, S., Schmid, B., Tinevez, J.-Y., White, D. J., Hartenstein, V., Eliceiri, K., Tomancak, P., and Cardona, A. (2012). Fiji: an open-source platform for biological-image analysis. *Nature Methods*, 9:676.

[Schluter et al., 2010] Schluter, A., Real-Chicharro, A., Gabaldon, T., Sanchez-Jimenez, F., and Pujol, A. (2010). Peroxisomedb 2.0: an integrative view of the global peroxisomal metabolome. *Nucleic Acids Research*, 38:D800–5.

[Shapira et al., 2006] Shapira, M., Hamlin, B. J., Rong, J., Chen, K., Ronen, M., and Tan, M.-W. (2006). A conserved role for a gata transcription factor in regulating epithelial innate immune responses. *Proceedings of the National Academy of Sciences of the United States of America*, 103(16968778):14086–14091.

[Shaye and Greenwald, 2011] Shaye, D. D. and Greenwald, I. (2011). Ortholist: a compendium of *C. elegans* genes with human orthologs. *PloS one*, 6(21647448):e20085–e20085.

[Sim and Hibberd, 2016] Sim, S. and Hibberd, M. L. (2016). *Caenorhabditis elegans* susceptibility to gut *Enterococcus faecalis* infection is associated with fat metabolism and epithelial junction integrity. *BMC microbiology*, 16(26769134):6–6.

[Simmer et al., 2003] Simmer, F., Moorman, C., Van Der Linden, A. M., Kuijk, E., Van Den Berghe, P. V., Kamath, R. S., Fraser, A. G., Ahringer, J., and Plasterk, R. H. (2003). Genome-wide RNAi of *C. elegans* using the hypersensitive rrf-3 strain reveals novel gene functions. *PLoS biology*, 1(1):e12.

[Simonsen et al., 2012] Simonsen, K. T., Gallego, S. F., Faergeman, N. J., and Kallipolitis, B. H. (2012). Strength in numbers: "omics" studies of *C. elegans* innate immunity. *Virulence*, 3(23076279):477–484.

[Siraki et al., 2002] Siraki, A. G., Pourahmad, J., Chan, T. S., Khan, S., and O'Brien, P. J. (2002). Endogenous and endobiotic induced reactive oxygen species formation by isolated hepatocytes. *Free Radical Biology and Medicine*, 32(1):2–10.

[Srinivasan et al., 2008a] Srinivasan, J., Kaplan, F., Ajredini, R., Zachariah, C., Alborn, H. T., Teal, P. E. A., Malik, R. U., Edison, A. S., Sternberg, P. W., and Schroeder, F. C. (2008a). A blend of small molecules regulates both mating and development in *Caenorhabditis elegans*. *Nature*, 454:1115.

[Srinivasan et al., 2012] Srinivasan, J., von Reuss, S. H., Bose, N., Zaslaver, A., Mahanti, P., Ho, M. C., O'Doherty, O. G., Edison, A. S., Sternberg, P. W., and Schroeder, F. C. (2012). A modular library of small molecule signals regulates social behaviors in *Caenorhabditis elegans*. *PLoS Biol*, 10(1):e1001237.

[Srinivasan et al., 2008b] Srinivasan, S., Sadegh, L., Elle, I. C., Christensen, A. G. L., Faergeman, N. J., and Ashrafi, K. (2008b). Serotonin regulates *C. elegans* fat and feeding through independent molecular mechanisms. *Cell Metabolism*, 7(6):533–544.

[Steinberg et al., 1999] Steinberg, S. J., Wang, S. J., Kim, D. G., Mihalik, S. J., and Watkins, P. A. (1999). Human very-long-chain acyl-CoA synthetase: cloning, topography, and relevance to branched-chain fatty acid metabolism. *Biochem Biophys Res Commun*, 257(2):615–21.

[Stiernagle, 2006] Stiernagle, T. (2006). *Maintenance of C. elegans*, volume 11. WormBook.

[Sugiura et al., 2017] Sugiura, A., Mattie, S., Prudent, J., and McBride, H. M. (2017). Newly born peroxisomes are a hybrid of mitochondrial and ER-derived pre-peroxisomes. *Nature*, 542:251.

[Supek et al., 2011] Supek, F., Bosnjak, M., Skunca, N., and Smuc, T. (2011). REVIGO summarizes and visualizes long lists of gene ontology terms. *PLoS One*, 6(7):e21800.

[Swinkels et al., 1991] Swinkels, B., Gould, S., Bodnar, A., Rachubinski, R., and Subramani, S. (1991). A novel, cleavable peroxisomal targeting signal at the amino-terminus of the rat 3-ketoacyl-CoA thiolase. *The EMBO Journal*, 10(11):3255–3262.

[Szklarczyk et al., 2019] Szklarczyk, D., Gable, A. L., Lyon, D., Junge, A., Wyder, S., Huerta-Cepas, J., Simonovic, M., Doncheva, N. T., Morris, J. H., Bork, P., Jensen, L. J., and Mering, C. V. (2019). String v11: protein-protein association networks with increased coverage, supporting functional discovery in genome-wide experimental datasets. *Nucleic Acids Res*, 47(D1):D607–D613.

[Takahara, 1952] Takahara, S. (1952). Progressive oral gangrene probably due to lack of catalase in the blood (acatalasaemia): Report of nine cases. *The Lancet*, 260(6745):1101–1104.

[Tan et al., 1999] Tan, M. W., Mahajan-Miklos, S., and Ausubel, F. M. (1999). Killing of *Caenorhabditis elegans* by *Pseudomonas aeruginosa* used to model mammalian bacterial pathogenesis. *Proceedings of the National Academy of Sciences of the United States of America*, 96(9892699):715–720.

[Taub et al., 1999] Taub, J., Lau, J. F., Ma, C., Hahn, J. H., Hoque, R., Rothblatt, J., and Chalfie, M. (1999). A cytosolic catalase is needed to extend adult lifespan in *C. elegans* daf-C and clk-1 mutants. *Nature*, 399(6732):162–166.

[Taubert et al., 2006] Taubert, S., Van Gilst, M. R., Hansen, M., and Yamamoto, K. R. (2006). A mediator subunit, MDT-15, integrates regulation of fatty acid metabolism by NHR-49-dependent and -independent pathways in *C. elegans*. *Genes Dev*, 20(9):1137–49.

[Teske et al., 2013] Teske, B. F., Fusakio, M. E., Zhou, D., Shan, J., McClintick, J. N., Kilberg, M. S., and Wek, R. C. (2013). CHOP induces activating transcription factor 5 (ATF5) to trigger apoptosis in response to perturbations in protein homeostasis. *MBoC*, 24(15):2477–2490.

[Thieringer et al., 2003] Thieringer, H., Moellers, B., Dodt, G., Kunau, W.-H., and Driscoll, M. (2003). Modeling human peroxisome biogenesis disorders in the nematode *Caenorhabditis elegans*. *Journal of Cell Science*, 116(9):1797–1804.

[Timmons and Fire, 1998] Timmons, L. and Fire, A. (1998). Specific interference by ingested dsRNA. *Nature*, 395(6705):854–854.

[Togo et al., 2000] Togo, S. H., Maebuchi, M., Yokota, S., Bun-ya, M., Kawahara, A., and Kamiryo, T. (2000). Immunological detection of alkaline-diaminobenzidine-negativeperoxisomes of the nematode *Caenorhabditis elegans*. *European Journal of Biochemistry*, 267(5):1307–1312.

[Troemel et al., 2006] Troemel, E. R., Chu, S. W., Reinke, V., Lee, S. S., Ausubel, F. M., and Kim, D. H. (2006). P38 MAPK regulates expression of immune response genes and contributes to longevity in *C. elegans*. *PLoS genetics*, 2(11):e183.

[Tugwood et al., 1992] Tugwood, J. D., Issemann, I., Anderson, R. G., Bundell, K. R., McPheat, W. L., and Green, S. (1992). The mouse peroxisome proliferator activated receptor recognizes a response element in the 5' flanking sequence of the rat acyl CoA oxidase gene. *The EMBO journal*, 11(2):433–439.

[van Roermund et al., 2014] van Roermund, C. W. T., IJlst, L., Wagemans, T., Wanders, R. J. A., and Waterham, H. R. (2014). A role for the human peroxisomal half-transporter ABCD3 in the oxidation of dicarboxylic acids. *Biochimica et Biophysica Acta (BBA) - Molecular and Cell Biology of Lipids*, 1841(4):563–568.

[van Roermund et al., 2011] van Roermund, C. W. T., Visser, W. F., IJlst, L., Waterham, H. R., and Wanders, R. J. A. (2011). Differential substrate specificities of human ABCD1 and ABCD2 in peroxisomal fatty acid β-oxidation. *Biochimica et Biophysica Acta (BBA) - Molecular and Cell Biology of Lipids*, 1811(3):148–152.

[Van Veldhoven and Baes, 2013] Van Veldhoven, P. and Baes, M. (2013). Peroxisome deficient invertebrate and vertebrate animal models. *Frontiers in Physiology*, 4:335.

[Van Veldhoven et al., 1991] Van Veldhoven, P. P., Brees, C., and Mannaerts, G. P. (1991). D-aspartate oxidase, a peroxisomal enzyme in liver of rat and man. *Biochimica et Biophysica Acta (BBA) - General Subjects*, 1073(1):203–208.

[Vanhove et al., 1993] Vanhove, G. F., Van Veldhoven, P. P., Fransen, M., Denis, S., Eyssen, H. J., Wanders, R. J., and Mannaerts, G. P. (1993). The CoA esters of 2-methyl-branched chain fatty acids and of the bile acid intermediates di- and trihydroxycoprostanic acids are oxidized by one single peroxisomal branched chain acyl-CoA oxidase in human liver and kidney. *J Biol Chem*, 268(14):10335–44.

[Vijayan et al., 2017] Vijayan, V., Srinu, T., Karnati, S., Garikapati, V., Linke, M., Kamalyan, L., Mali, S. R., Sudan, K., Kollas, A., Schmid, T., Schulz, S., Spengler, B., Weichhart, T., Immenschuh, S., and Baumgart-Vogt, E. (2017). A new immunomodulatory role for peroxisomes in macrophages activated by the TLR4 ligand lipopolysaccharide. *J. Immunol.*, 198(6):2414.

[Vilarinho et al., 2016] Vilarinho, S., Sari, S., Mazzacuva, F., Bilgüvar, K., Esendagli-Yilmaz, G., Jain, D., Akyol, G., Dalgiç, B., Günel, M., Clayton, P. T., and Lifton, R. P. (2016). Acox2 deficiency: A disorder of bile acid synthesis with transaminase elevation, liver fibrosis, ataxia, and cognitive impairment. *Proceedings of the National Academy of Sciences*, 113(40):11289–11293.

[Viswakarma et al., 2010] Viswakarma, N., Jia, Y., Bai, L., Vluggens, A., Borensztajn, J., Xu, J., and Reddy, J. K. (2010). Coactivators in PPAR-regulated gene expression. *PPAR Research*, 2010:21.

[von Reuss et al., 2012] von Reuss, S. H., Bose, N., Srinivasan, J., Yim, J. J., Judkins, J. C., Sternberg, P. W., and Schroeder, F. C. (2012). Comparative metabolomics reveals biogenesis of ascarosides, a modular library of small-molecule signals in *C. elegans*. *Journal of the American Chemical Society*, 134(3):1817–1824.

[Walbrecq et al., 2015] Walbrecq, G., Wang, B., Becker, S., Hannotiau, A., Fransen, M., and Knoops, B. (2015). Antioxidant cytoprotection by peroxisomal peroxiredoxin-5. *Free Radical Biology and Medicine*, 84:215–226.

[Walton, 2012] Walton, P. (2012). Effects of peroxisomal catalase inhibition on mitochondrial function. *Frontiers in Physiology*, 3:108.

[Walton et al., 2017] Walton, P. A., Brees, C., Lismont, C., Apanasets, O., and Fransen, M. (2017). The peroxisomal import receptor PEX5 functions as a stress sensor, retaining catalase in the cytosol in times of oxidative stress. *Biochimica et Biophysica Acta (BBA) - Molecular Cell Research*, 1864(10):1833–1843.

[Wanders, 2018] Wanders, R. J. (2018). Peroxisomal disorders: Improved laboratory diagnosis, new defects and the complicated route to treatment. *Molecular and cellular probes*, 40:60–69.

[Wanders et al., 1997] Wanders, R. J., Denis, S., Wouters, F., Wirtz, K. W., and Seedorf, U. (1997). Sterol carrier protein X (ScpX) is a peroxisomal branched-chain beta-ketothiolase specifically reacting with 3-oxo-pristanoyl-CoA: a new, unique role for scpx in branched-chain fatty acid metabolism in peroxisomes. *Biochem Biophys Res Commun*, 236(3):565–9.

[Wanders et al., 1989] Wanders, R. J. A., Romeyn, G. J., Schutgens, R. B. H., and Tager, J. M. (1989). L-pipecolate oxidase: a distinct peroxisomal enzyme in man. *Biochemical and Biophysical Research Communications*, 164(1):550–555.

[Wanders et al., 2016] Wanders, R. J. A., Waterham, H. R., and Ferdinandusse, S. (2016). Metabolic interplay between peroxisomes and other subcellular organelles including mitochondria and the endoplasmic reticulum. *Frontiers in Cell and Developmental Biology*, 3:83.

[Wang et al., 2013] Wang, B., Van Veldhoven, P. P., Brees, C., Rubio, N., Nordgren, M., Apanasets, O., Kunze, M., Baes, M., Agostinis, P., and Fransen, M. (2013). Mitochondria are targets for peroxisome-derived oxidative stress in cultured mammalian cells. *Free Radical Biology and Medicine*, 65:882–894.

[Wang et al., 2011] Wang, M. C., Min, W., Freudiger, C. W., Ruvkun, G., and Xie, X. S. (2011). Rnai screening for fat regulatory genes with srs microscopy. *Nature methods*, 8(21240281):135–138.

[Wangler et al., 2018] Wangler, M. F., Hubert, L., Donti, T. R., Ventura, M. J., Miller, M. J., Braverman, N., Gawron, K., Bose, M., Moser, A. B., Jones, R. O., Rizzo, W. B., Sutton, V. R., Sun, Q., Kennedy, A. D., and Elsea, S. H. (2018). A metabolomic map of zellweger spectrum disorders reveals novel disease biomarkers. *Genetics in Medicine*, 20(10):1274–1283.

[Waterham and Ebberink, 2012] Waterham, H. R. and Ebberink, M. S. (2012). Genetics and molecular basis of human peroxisome biogenesis disorders. *Biochimica et Biophysica Acta (BBA) - Molecular Basis of Disease*, 1822(9):1430–1441. Metabolic Functions and Biogenesis of Peroxisomes in Health and Disease.

[Waterham et al., 2007] Waterham, H. R., Koster, J., van Roermund, C. W. T., Mooyer, P. A. W., Wanders, R. J. A., and Leonard, J. V. (2007). A lethal defect of mitochondrial and peroxisomal fission. *N Engl J Med*, 356(17):1736–1741.

[Watkins et al., 2007] Watkins, P. A., Maiguel, D., Jia, Z., and Pevsner, J. (2007). Evidence for 26 distinct acyl-coenzyme A synthetase genes in the human genome. *Journal of Lipid Research*, 48(12):2736–2750.

[Weir et al., 2017a] Weir, H. J., Yao, P., Huynh, F. K., Escoubas, C. C., Goncalves, R. L., Burkewitz, K., Laboy, R., Hirschey, M. D., and Mair, W. B. (2017a). Dietary restriction and AMPK increase lifespan via mitochondrial network and peroxisome remodeling. *Cell metabolism*, 26(29107506):884–896.e5.

[Weir et al., 2017b] Weir, N. R., Kamber, R. A., Martenson, J. S., Denic, V., and Hegde, R. S. (2017b). The AAA protein Msp1 mediates clearance of excess tail-anchored proteins from the peroxisomal membrane. *eLife*, 6:e28507.

[Wicks et al., 2001] Wicks, S. R., Yeh, R. T., Gish, W. R., Waterston, R. H., and Plasterk, R. H. A. (2001). Rapid gene mapping in *Caenorhabditis elegans* using a high density polymorphism map. *Nature Genetics*, 28(2):160–164.

[Wiesinger et al., 2015] Wiesinger, C., Eichler, F. S., and Berger, J. (2015). The genetic landscape of x-linked adrenoleukodystrophy: inheritance, mutations, modifier genes, and diagnosis. *The application of clinical genetics*, 8(25999754):109–121.

[Wong et al., 2007] Wong, D., Bazopoulou, D., Pujol, N., Tavernarakis, N., and Ewbank, J. J. (2007). Genome-wide investigation reveals pathogen-specific and shared signatures in the response of *Caenorhabditis elegans* to infection. *Genome Biol*, 8(9):R194.

[Xu et al., 2011] Xu, M., Joo, H.-J., and Paik, Y.-K. (2011). Novel functions of lipid-binding protein 5 in *Caenorhabditis elegans* fat metabolism. *The Journal of biological chemistry*, 286(32):28111–28118.

[Yokota et al., 2008] Yokota, S., Haraguchi, C. M., and Oda, T. (2008). Induction of peroxisomal Lon protease in rat liver after di-(2-ethylhexyl)phthalate treatment. *Histochemistry and cell biology*, 129:73–83.

[Yokota et al., 2002] Yokota, S., Togo, S. H., Maebuchi, M., Bun-ya, M., Haraguchi, C. M., and Kamiryo, T. (2002). Peroxisomes of the nematode *Caenorhabditis elegans*: distribution and morphological characteristics. *Histochemistry and Cell Biology*, 118(4):329–336.

[Yoneda et al., 2004] Yoneda, T., Benedetti, C., Urano, F., Clark, S. G., Harding, H. P., and Ron, D. (2004). Compartment-specific perturbation of protein handling activates genes encoding mitochondrial chaperones. *Journal of Cell Science*, 117(18):4055–4066.

[Yunger et al., 2017] Yunger, E., Safra, M., Levi-Ferber, M., Haviv-Chesner, A., and Henis-Korenblit, S. (2017). Innate immunity mediated longevity and longevity induced by germ cell removal converge on the C-type lectin domain protein IRG-7. *PLoS Genet*, 13(2):e1006577.

[Zhang et al., 2010] Zhang, S. O., Box, A. C., Xu, N., Le Men, J., Yu, J., Guo, F., Trimble, R., and Mak, H. Y. (2010). Genetic and dietary regulation of lipid droplet expansion in *Caenorhabditis elegans*. *Proceedings of the National Academy of Sciences*, 107(10):4640–4645.

[Zhang et al., 2016] Zhang, X., Li, K., Jones, R. A., Bruner, S. D., and Butcher, R. A. (2016). Structural characterization of acyl-CoA oxidases reveals a direct link between pheromone biosynthesis and metabolic state in *Caenorhabditis elegans*. *Proceedings of the National Academy of Sciences of the United States of America*, 113(36):10055–10060.

[Zhang et al., 2018] Zhang, X., Wang, Y., Perez, D. H., Jones Lipinski, R. A., and Butcher, R. A. (2018). Acyl-CoA oxidases fine-tune the production of ascaroside pheromones with specific side chain lengths. *ACS Chemical Biology*, 13(4):1048–1056.

[Zhou et al., 2012] Zhou, B., Yang, L., Li, S., Huang, J., Chen, H., Hou, L., Wang, J., Green, C. D., Yan, Z., Huang, X., Kaeberlein, M., Zhu, L., Xiao, H., Liu, Y., and Han, J.-D. J. (2012). Midlife gene expressions identify modulators of aging through dietary interventions. *Proc Natl Acad Sci USA*, 109(19):E1201.

[Zhou et al., 2008] Zhou, D., Palam, L. R., Jiang, L., Narasimhan, J., Staschke, K. A., and Wek, R. C. (2008). Phosphorylation of eIF2 directs ATF5 translational control in response to diverse stress conditions. *Journal of Biological Chemistry*, 283(11):7064–7073.

[Zhou et al., 2018] Zhou, Y., Wang, Y., Zhang, X., Bhar, S., Jones Lipinski, R. A., Han, J., Feng, L., and Butcher, R. A. (2018). Biosynthetic tailoring of existing ascaroside pheromones alters their biological function in *C. elegans*. *eLife*, 7:e33286.